https://ntrs.nasa.gov/search.jsp?R=19850014910 2020-03-20T18:24:21+00:00Z

General Disclaimer

One or more of the Following Statements may affect this Document

- This document has been reproduced from the best copy furnished by the organizational source. It is being released in the interest of making available as much information as possible.

- This document may contain data, which exceeds the sheet parameters. It was furnished in this condition by the organizational source and is the best copy available.

- This document may contain tone-on-tone or color graphs, charts and/or pictures, which have been reproduced in black and white.

- This document is paginated as submitted by the original source.

- Portions of this document are not fully legible due to the historical nature of some of the material. However, it is the best reproduction available from the original submission.

Produced by the NASA Center for Aerospace Information (CASI)

(NASA-TM-86200) CALCULATIONS OF MICROWAVE BRIGHTNESS TEMPERATURE OF ROUGH SOIL SURFACES: BARE FIELD (NASA) 88 p
HC A05/MF A01 CSCL 08M
N85-23221
Unclas
G3/43 14698

NASA

Technical Memorandum 86200

CALCULATIONS OF MICROWAVE BRIGHTNESS TEMPERATURE OF ROUGH SOIL SURFACES: BARE FIELD

Thomas J. Schmugge
James R. Wang
Tsan Mo

March 1985

National Aeronautics and
Space Administration

Goddard Space Flight Center
Greenbelt, Maryland 20771

CALCULATIONS OF MICROWAVE BRIGHTNESS TEMPERATURE OF ROUGH SOIL SURFACES: BARE FIELD

Thomas J. Schmugge and James R. Wang
NASA/Goddard Space Flight Center
Greenbelt, Maryland 20771

Tsan Mo
Computer Sciences Corporation
Beltsville, Maryland 20705

ABSTRACT

A model for simulating the remotely sensed microwave brightness temperatures of soils with rough surfaces is developed. The surface emissivity of the soil media is calculated from one minus its reflectivity, which is obtained by integration of the bistatic scattering coefficients for rough soil surfaces. The soil brightness temperature is obtained from the product of the surface emissivity and the effective soil temperature which is calculated with measured soil moisture profiles and soil temperature profiles at various soil depths. The roughness of a soil surface is characterized by two parameters, the surface height standard deviation σ and its horizontal correlation length ℓ. The model calculations are compared to the measured angular variations of the polarized brightness temperatures at both L-band (1.4 GHZ) and C-band (5 GHz) frequencies. A nonlinear least-squares fitting method is used to match the model calculations with the data, and the best-fit results produce the parameter values of σ and ℓ that best characterize the surface roughness. The effect of rough surface shadowing is also incorporated into the model by introducing a shadowing function $S(\theta)$, which represents the probability that a point on a rough surface is not shadowed by other parts of the surface. The model results for horizontal polarization are in excellent agreement with the data, both qualitatively and quantitatively. For vertical polarization, some discrepancies exist between the calculations and data. Possible causes of the discrepancy are discussed. The calculations show that the effect of surface shadowing is important at large incident angles for rough surfaces. Best-fit parameter values of $k\sigma$ show qualitative correlation with the measured surface roughness.

PRECEDING PAGE BLANK NOT FILMED

TABLE OF CONTENTS

PRECEDING PAGE BLANK NOT FILMED

LIST OF ILLUSTRATIONS

Figure

LIST OF TABLES

Table

SECTION 1 - INTRODUCTION

Recent interest in remote sensing with microwave sensors has attracted attention on the interaction of radiation with natural and agricultural soil surfaces. Many theoretical models [1-16] have been developed to simulate the remotely sensed data obtained from airborne/spaceborne radiometers and scatterometers. These model calculations and data have demonstrated that the active and passive sensors are sensitive to changes in the soil dielectric properties, surface roughness, and vegetation covers over soil surfaces. Analysis of either passive or active microwave data involves many parameters, values of which are usually difficult to obtain over large areas of either natural or agricultural fields. The parameters are the dielectric properties, surface roughness and vegetation cover. Theoretical simulation of the data can help us to understand the interaction of the microwave radiation with the soil media.

In recent studies [6, 9], Mo et al. have successfully modeled the measured angular distribution of radar backscattering coefficients of vegetation-covered fields, using a rough surface scattering model with a Gaussian distribution of surface height. The model results [6, 9] demonstrate that excellent agreement between the calculations and the airborne scatterometer data can be achieved by a nonlinear least-squares fitting process and that the parameter values which characterize the surface roughness and the vegetation canopy may also be extracted from the calculated results that best match the data. This same scattering model can also be employed to calculate the surface emissivity which is the measured quantity in passive remote sensing.

In this study, the bistatic scattering coefficients of the rough surface scattering model (corrected for the surface shadowing effect) are integrated to obtain the reflectivity at the air-soil interface and then the surface emissivity is calculated from one minus this reflectivity. The brightness temperature of a soil medium is then obtained from the product of the surface emissivity and the effective soil temperature. The results are compared to the data collected by Wang et al. [17] from truck-mounted radiometers at the frequencies 1.4 GHz (L-band) and 5 GHz (C-band). For a bare field, the calculation involves two surface parameters, the surface height standard deviation σ and its correlation length ℓ. A nonlinear least-squares fitting method is used to obtain the best-fit parameter values of σ and ℓ, which can produce the brightness temperatures that best match the angular variations of the measured brightness temperatures.

We present a systematic analysis of a large collection of measured brightness temperatures. Our main objective is to test the scattering model on a large data base representative of a wide range of surface roughness condition and soil moisture content, by reproducing the measured angular variation of the soil brightness temperatures.

Section 2 gives a brief description of the basic model and formulas used in the calculations. The model calculation results and the best-fit parameter values are presented in Section 3. A discussion of these results and parameters is given in Section 4. Appendix A contains the formulas of polarization coefficients. Comparisons for each set of the data and best-fit results are presented graphically in Appendix B.

SECTION 2 - THE MODEL

The thermal emission model used in this study is based on the Kirchhoff method for solving the rough-surface scattering of electromagnetic waves [18]. Detailed description of this method and theoretical derivation of the bistatic scattering coefficients have been given by Fung and Eom [2], by Ulaby et al. [5], and by Tsang and Newton [10], respectively.

The observed brightness temperature $T_p(\theta)$, for a rough surface of soil media having a complex dielectric constant ϵ, at an angle θ from the nadir direction can be expressed by,

$$T_p(\theta) = [1 - R_p(\theta)]\, T_e \qquad (1)$$

where T_e is the effective temperature of the soil media and $R_p(\theta)$ is the reflectivity of the rough surface. The letter p (= H or V) is the polarization index, representing either the horizontal or the vertical polarization.

The rough surface reflectivity $R_p(\theta)$ consists of a coherent component $R_{coh}(\theta)$ and an incoherent component $R_{inc}(\theta)$,

$$R_p(\theta) = R_{coh}(\theta) + R_{inc}(\theta) \qquad (2)$$

Both $R_{coh}(\theta)$ and $R_{inc}(\theta)$ can be obtained from the integration of the bistatic scattering coefficients of the rough surface [5].

If the roughness of a surface is characterized by the two parameters: the surface height standard deviation σ and

the correlation length ℓ, then the two components in Equation (2) can be written as [2,5],

$$R_p(\theta) = |R_{pp}|^2 \exp(-h\cos^2\theta) + \frac{1}{4\pi\cos\theta} \sum_{q=H,V} \int_{\text{hemi-sphere}} \sigma_{qpi}(\Omega,\Omega_s)\,d\Omega_s \quad (3)$$

where $h = 4k^2\sigma^2$ (k is the wavenumber) and $|R_{pp}|^2$ is the reflectivity of a smooth surface. The quantity $\sigma_{qpi}(\Omega,\Omega_s)$ is the incoherent bistatic scattering coefficient from the incident direction $\Omega = (\theta,\phi)$ and polarization p scattered into the outgoing direction $\Omega_s = (\theta_s,\phi_s)$ and polarization q.

The incoherent bistatic scattering coefficient σ_{qpi} in Equation (3) depends on the statistical properties of a rough surface: the surface height standard deviation and its correlation length of the height distribution. Models for σ_{qpi} have been developed by many investigators [2, 5, 10, 18, 19] for both Gaussian and non-Gaussian surface statistics. For mathematical simplicity, the Gaussian form of correlation function has been widely used in the calculation of bistatic scattering coefficient. In this study, we assume a Gaussian correlation function $\rho(\xi) = \exp(-\xi^2/\ell^2)$ for a rough soil surface, where ξ is a distance on the surface. Then it can be shown that the incoherent component of the bistatic scattering coefficient can be expressed in terms of the two surface parameters, σ and ℓ [2, 5],

$$\sigma_{qpi}(\Omega,\Omega_s) = \frac{(k\ell)^2}{4}\left[|a_o|^2 - \frac{2}{q_z}\mathrm{Re}(a_o a^*)(q_x\cos\phi + q_y\sin\phi)\right] M \quad (4)$$

where a^* is the complex conjugate of a and

$$M = \exp(-q_z^2\,\sigma^2) \sum_{n=1}^{\infty} \frac{(q_z\sigma)^{2n}}{n!n} \exp\left[-\frac{(q_x^2 + q_y^2)\ell^2}{4n}\right] \quad (5)$$

and

$$q_x = k(\sin\theta_s \cos\phi_s - \sin\theta\cos\phi)$$
$$q_y = k(\sin\theta_s \sin\phi_s - \sin\theta\sin\phi) \qquad (6)$$
$$q_z = k(\cos\theta_s + \cos\theta)$$

The quantities a_o and a in Equation (4) are polarization-dependent coefficients. Explicit formulas for these polarization coefficients under HH, VH, VV and HV polarization states can be found in [2] and [5]. For convenience of reference, these polarization coefficients are listed in Appendix A. Since the quantity a_o is proportional to R_{pp}, therefore σ_{qpi} will approach to zero if R_{pp} becomes vanishingly small, as in the case of the vertical polarization at large angles.

The formulas given in Equations [3] and [5] were derived without including the correction of shadowing effect of a rough surface scattering. The shadowing effect arises when part of a rough surface may be shadowed by other parts of the surface at a given look angle. It has been shown [20-23] that the shadowing effect is important for rough surfaces, particularly at large incident angles and that energy conservation would be violated if the shadowing effect were neglected.

However, this shadowing effect can be easily incorporated into the model by introducing a shadowing function $S(\theta)$, which is defined as the probability that a point on a rough surface is not shadowed by other parts of the surface. Since the effective surface area for scattering of waves is reduced if shadowing occurs, the reflectivity, $R_p(\theta)$ as defined in Equations (1) to (3), also decreased appropriately. To correct this shadowing effect, we replace

the quantity $R_p(\theta)$ by a modified reflectivity $R_p^s(\theta)$, which can be approximated by

$$R_p^s(\theta) = S(\theta)R_p(\theta) \tag{7}$$

where $R_p(\theta)$ is still defined by Equation (3). The shadowing function $S(\theta)$ has been studied by many investigators [20-23]. In this study, the function $S(\theta)$ given by Wagner [22] is used and it has the form,

$$S(\theta) = \frac{[1 + \mathrm{erf}(V)]\ (1 - e^{-B})}{2B} \tag{8}$$

where

$$V = \frac{\cot \theta}{2(\sigma/\ell)} \tag{9}$$

$$B = \frac{e^{-V^2} - \sqrt{\pi}\ V\ \mathrm{erfc}\ (V)}{2\sqrt{\pi}\ V} \tag{10}$$

and erf and erfc are the error function and error-function complement, respectively.

The shadow function $S(\theta)$ depends upon the surface slope $m = (\sigma/\ell)$ only, and Figure 1 shows $S(\theta)$ as a function of the angle θ for three values of $m = 0.1$, 0.5, and 1.0, respectively. These curves demonstrate that the shadowing function $S(\theta)$ has little effect on the scattering at small incident angles, but its effect becomes significant at large angles and as the slope of a rough surface increases.

Replacing $R_p(\theta)$ by $R_p^s(\theta)$ in Equation (1), one has the expression for the brightness temperature, including the shadowing effect,

$$T_p(\theta) = [1 - R_p^s(\theta)]T_e = e_p T_e \qquad (11)$$

where $e_p = 1-R_p^s(\theta)$ is the surface emissivity. Equation (11) will be used in this study to calculate the brightness temperature $T_H(\theta)$ and $T_V(\theta)$. The results are presented in the next section.

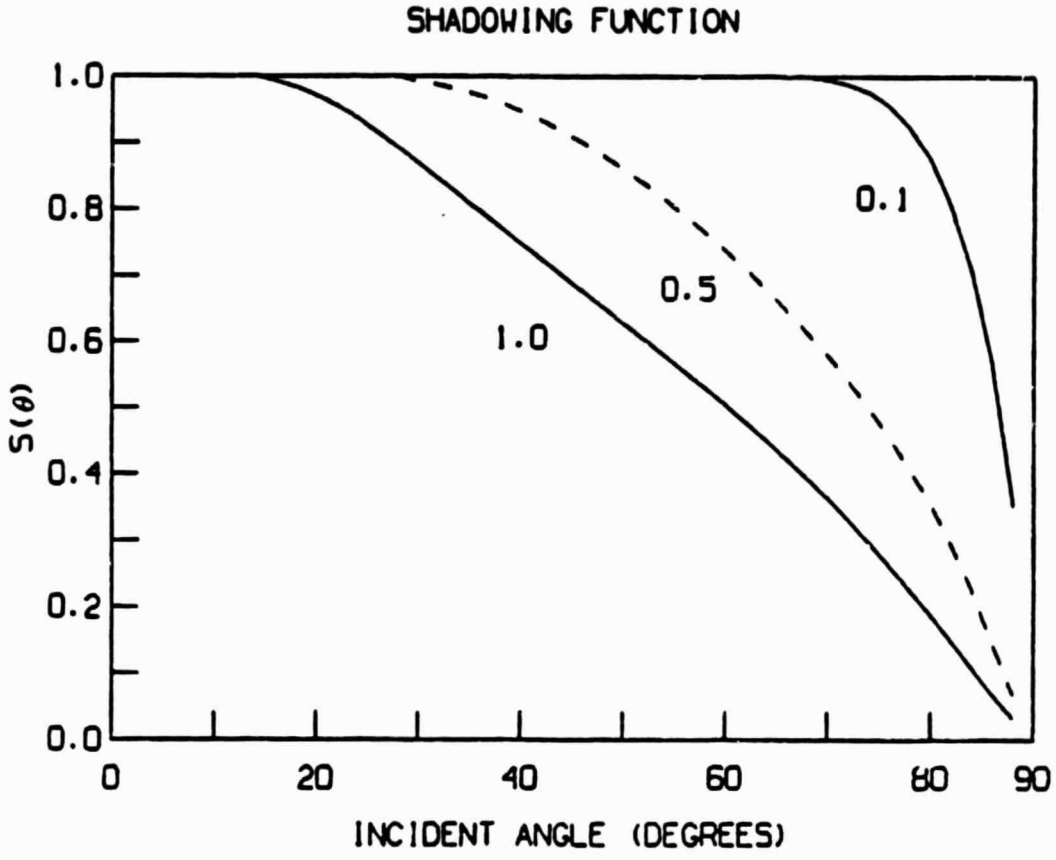

Figure 1. Shadowing Function $S(\theta)$ Versus Incident Angle θ. The function $S(\theta)$ is Defined in in Equation (8). The three curves correspond to three different σ/ℓ values (as labelled).

SECTION 3 - THE RESULTS

The radiometer data of brightness temperatures collected by Wang et al. [17] were used in this study to match the calculated results from the formulae, given in the previous section. These data at L-band (1.4 GHz) and C-band (5 GHz) frequencies were obtained with two truck-mounted radiometers in 1981 over three field plots of a test site at the USDA Beltsville Agricultural Research Center (BARC), Beltsville, Maryland. Angular distributions for both T_H and T_V were measured for incident angles from $\theta = 10^o$ to 70^o in 10^o steps. Soil moisture samples were taken within the four depth intervals of 0-0.5 cm, 0-2.5 cm, 2.5-5 cm, and 5-10 cm, while soil temperature profiles were taken at the depths of 1.25, 2.5, 7.5, and 15 cm, respectively.

The soil texture of one plot (identified as 121) is Elinsboro sandy loam consisting of 75% sand, 10% clay, and 15% silt, while those of other two plots (221 and 223) are silty loams with 34% sand, 24% clay, and 42% silt [17]. All three plots were bare fields with little vegetation cover during the period of data collection.

These ground truth data were used to calculate the soil dielectric constant ϵ [25], the effective soil temperatures, and the smooth surface reflectivities $|R_{pp}|^2$, which are needed in the model calculations. The surface condition for plot 121 was smooth, however, plots 221 and 223 were relatively rough and very rough, respectively. The surface roughness, which can be characterized by the two parameters σ and ℓ (the surface height standard deviation and correlation length), has significant effect on the observed and calculated brightness temperatures. In this section, the individual effect of each parameter will be demonstrated.

A nonlinear least-squares fitting method is used to match the theoretical model calculations with the data.

Angular distributions of measured brightness temperature were fitted with Equation (11) by varying the two parameters $k\sigma$ and $k\ell$. It is convenient to take the dimensionless quantities $k\sigma$ and $k\ell$, instead of σ and ℓ, as the adjustable parameter, because the wave number k always appears with σ and ℓ in the theoretical formulae. Before matching with the data, the calculated brightness temperatures for both T_H and T_V components were averaged over the beamwidth of the radiometer antenna gain patterns which were assumed in Gaussian form with 3-dB beamwidth of 13° for both L- and C-band frequencies [17].

Representative best-fit results and comparison to the data at both L- and C-bands are shown in Figures 2 to 4, respectively, for each of the field plots. In these figures, the solid and dashed curves represent the calculated results obtained with the best fit parameters for the T_H and T_V polarizations. The best-fit parameter values are listed at the top of each figure, and the soil moisture content (in weight-%) within the 0-2.5 cm surface layer is given on the lower part, together with the date (month/day/year) when the data were taken. The effective soil temperature T_e is also listed.

Figure 2 shows the best-fit results and comparison to the data collected from the smooth field plot 121 on July 22, 1981. The field was relatively dry and it had only 3.6% soil moisture content in the 2.5-cm surface layer. The L-band results are shown on the left part and the C-band on the right part of the figure. The results in Figure 2 demonstrate that the agreements between the calculations and the data are reasonably good, especially for the horizontally

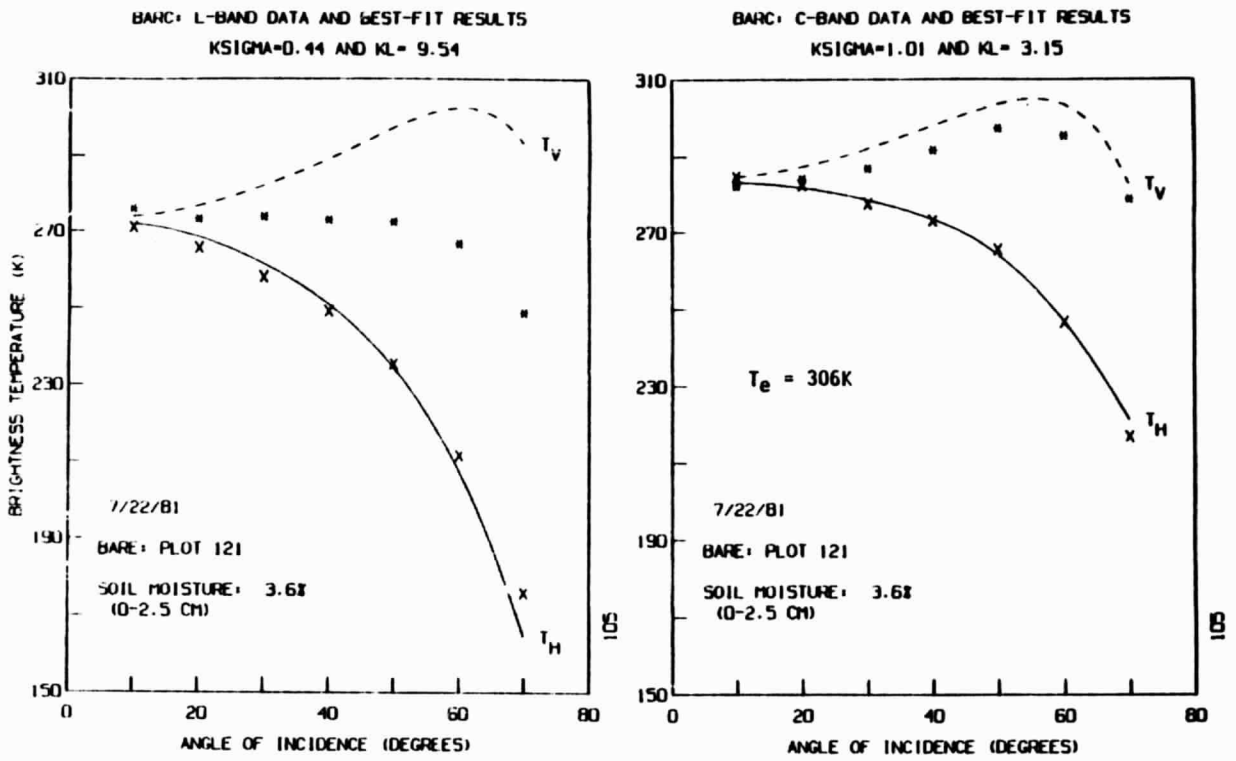

Figure 2. Comparison of Calculations and Measured Brightness Temperatures Over the Bare Field Plot 121

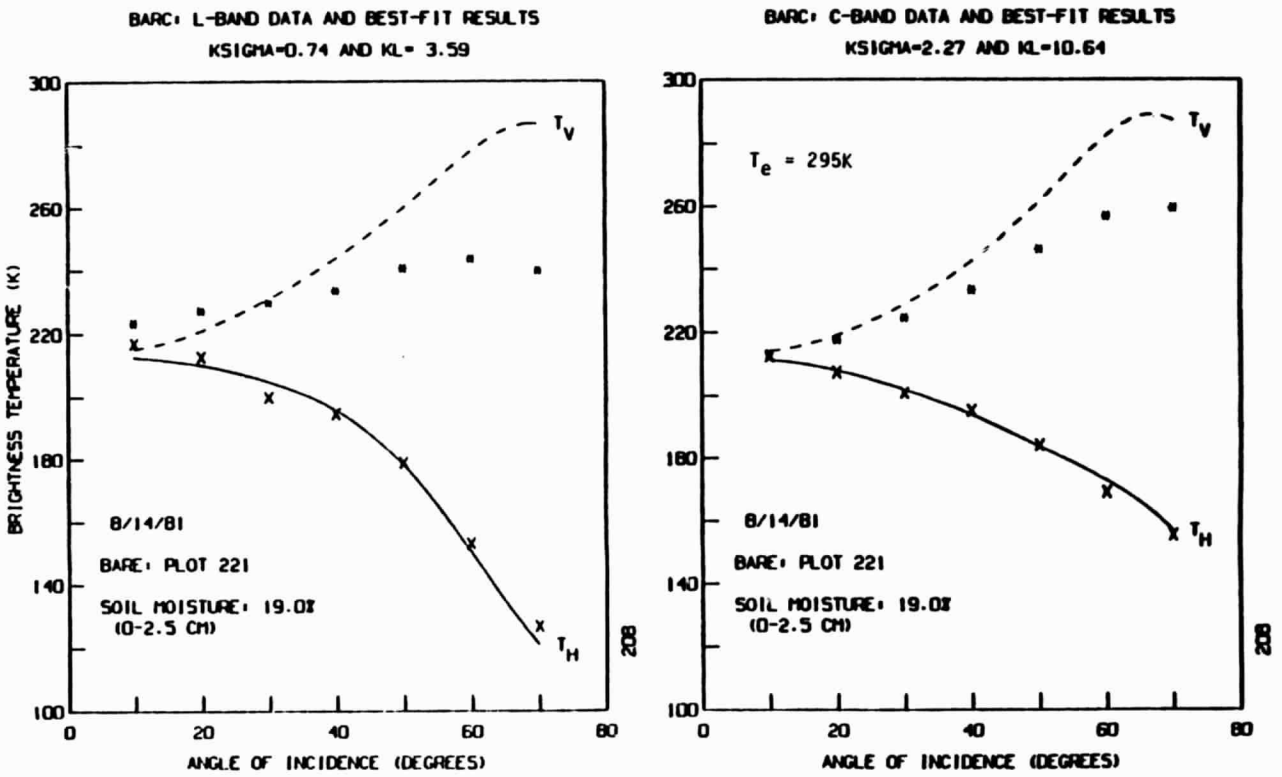

Figure 3. Comparison of Calculations and Measured Brightness Temperatures Over the Bare Field Plot 221

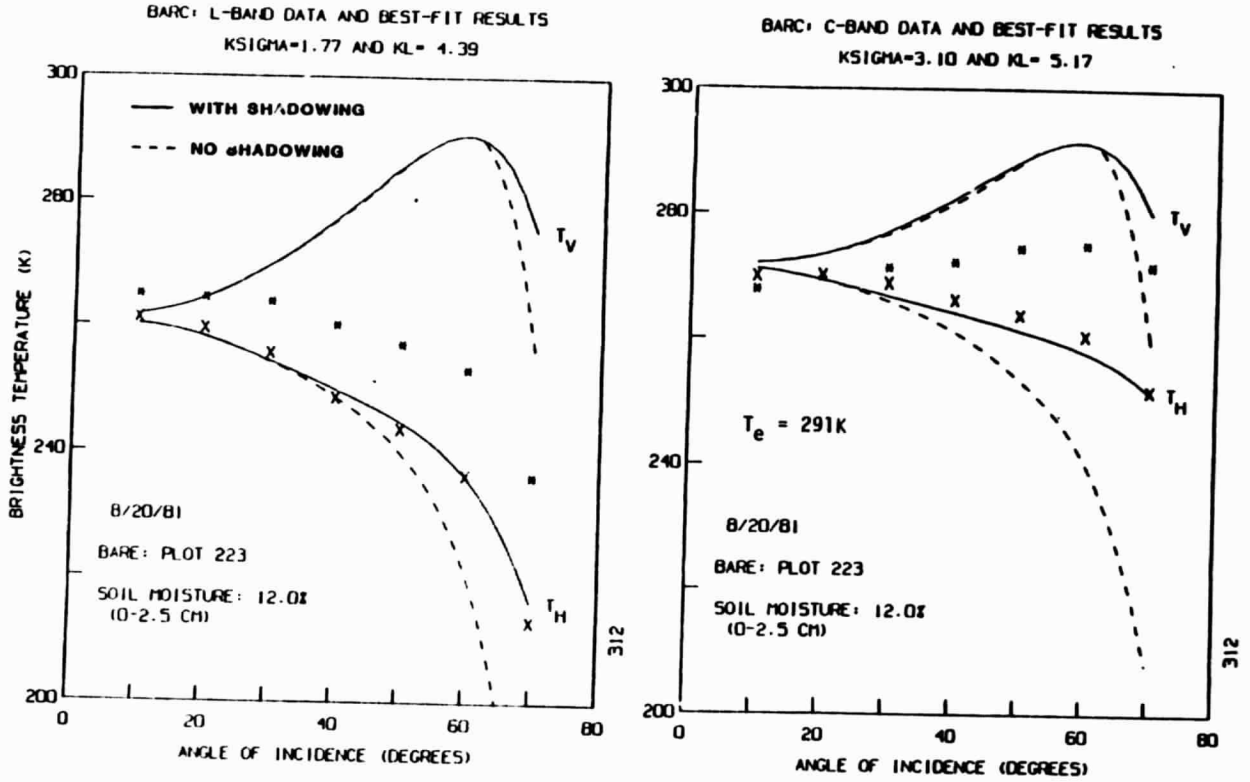

Figure 4. Comparison of Calculations and Measured Brightness Temperatures Over the Bare Field Plot 223. The Solid Curves are the Best Fits Including the Shadowing Effect, While the Dashed Ones Were Obtained Without the Shadowing Effect.

polarized brightness temperatures, which can be accurately reproduced at all incident angles.

However, the agreement for the vertical polarization is not as sood as the horizontal case, particularly for the large incidence angles. Also the differences are greater at L-band than at C-band. There are three causes for this discrepancy which we have considered. One is related to the Brewster's angle effect, the second is polarization mixing in the collected data, and the third is a possible calibration error in the L-band radiometer.

At Brewster's angle, which occurs around 60° for moist soils, both the smooth surface reflectivity $|R_{VV}|^2$ and the rough surface reflectivity $R_V(\theta)$ defined by Equation (3) vanish, and thus perhaps we are observing a limitation on the applicability of the Kirchhoff approximation when the reflectivity is very small.

Polarization mixing in the collected data might happen if the scattering surfaces were not smooth. The fact that the angular variations of the observed T_V component for the L-band case (Figures 2 and 3) follow the T_H data so closely may imply possible polarization mixing. For example, it can be shown [7] that if a 20% polarization mixing is assumed for the L-band case in Figure 2, the calculated T_V value at 70° would be 265K, instead of 290K as shown in Figure 2. However, the assumption of polarization mixing is not employed in this study, because other uncertainties may exist.

Calibration error of up to 7-8K could present in the L-band vertical polarization measurements at large incidence angles. This possible uncertainty in the measurements was pointed out in [24] when calibration of the microwave radiometers over a smooth water surface was described. It was observed there that the L-band vertically polarized

measurements always gave a higher brightness temperature at $\theta = 10^{\circ} - 20^{\circ}$ and a lower value at $\theta = 50^{\circ} - 70^{\circ}$, showing the same trend in the data presented in this study. This observed effect could be caused by a possible antenna side lobe looking far away from the main beam. At small θ, the side lobe would aim at the trees surrounding the water target, resulting in a higher brightness temperature. At large θ, it would look into the cold sky, resulting in a lower brightness temperature. The measurements over water surface at L-band horizontal polarization and at both polarizations of the C-band radiometer did not show the same phenomenon.

Typical best-fit results to the data collected over the field plot 221 are shown in Figure 3. The surface roughness of this plot is larger than that of plot 121 (see Figure 2), therefore the best-fit results provide larger values of $k\sigma$ than those given in Figure 2, as expected. Figure 3 shows that the angular distributions calculated with the best-fit parameters agree well with the measurements, particularly for the T_H components.

Figure 4 displays one set of the best fits to the data taken over the very rough field plot 223, which was plowed at the beginning of the data collection period. The data shown in Figure 4 have much smaller angular variations (particularly for the C-band case) than those of field plots 121 and 221, which had relatively smooth surfaces. The best-fit results, including the shadowing effect, are shown by the solid curves in Figure 4. It can be seen that the agreements between the calculated and measured T_H component are remarkably good, but the T_V components have discrepancies similar to those as appeared in Figure 2.

It is expected that the shadowing function $S(\theta)$, as shown in Figure 1, has significant effect on the brightness temperature in the case of very rough surface. This

shadowing effect is demonstrated in Figure 4 by the dashed curves, which are obtained by excluding the shadowing effect from the calculations. The $k\sigma$ and $k\ell$ values used in obtaining the solid and dashed curves in Figure 4 are identical. Comparison of the results in Figure 4 shows that the shadowing effect produces big changes in the calculated values of the brightness temperatures at large angles, while there are little noticeable changes in the results at angles less than 30° for the T_H component, and up to 60° for the T_V component. Varying the parameter $k\sigma$ or $k\ell$ to re-fit the data would not make up these big differences without destroying the best-fit results at the forward angles. The combined results in Figure 4 demonstrate that one can not ignore the shadowing effect in the modeling of microwave emissivity of rough soil surfaces particularly at angles greater than 30°. In addition, it has been shown that the energy-conservation principle would not hold in the reflecting and absorbing of incident waves at the interface of the scattering media, if the shadowing effect is omitted [5, 23].

The brightness temperature sensitivity to the variation of the individual surface roughness parameters is illustrated in Figure 5, where the solid curves are the best fits to the data. The dashed curves in Figure 5a were obtained by keeping $k\ell = 2.65$ at the best-fit value, but increasing the value of surface height standard deviation to $k\sigma = 1.64$ (which is 50% larger than the best-fit value). As one would expect for an increasingly rough surface, the larger $k\sigma$ value produces higher brightness temperatures. On the other hand, the dot-dashed curves in Figure 5a which were obtained with $k\sigma = 1.09$ (the best-fit value), and $k\ell = 3.97$ (50% larger than the best-fit value) show colder brightness temperatures.

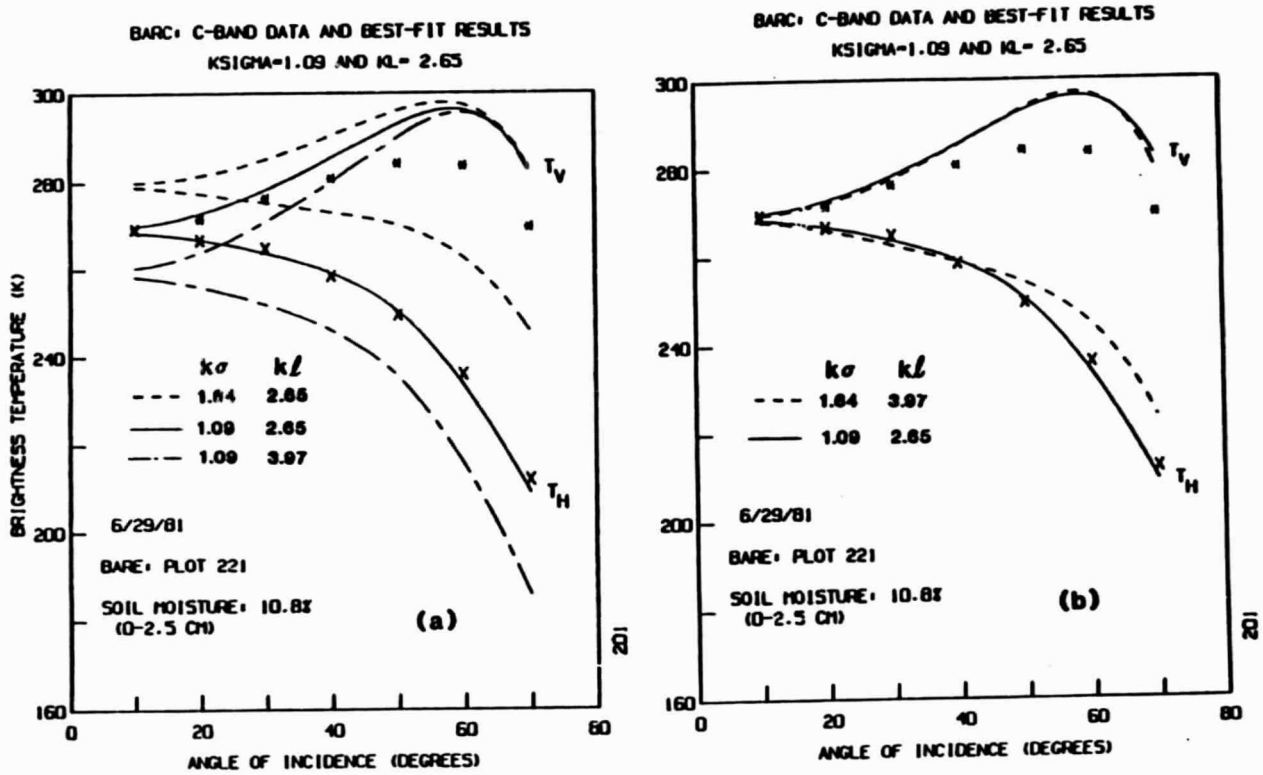

Figure 5. Sensitivity of the Brightness Temperatures to Variation of Surface Roughness Parameters. The Solid Curves are the Best Fits. (a) Results if the Parameter $k\sigma$ or $k\ell$ Were 50% Larger Than its Best Fit-Value. (b) Results if Both $k\sigma$ and $k\ell$ Were 50% Larger Than the Best-Fit Values.

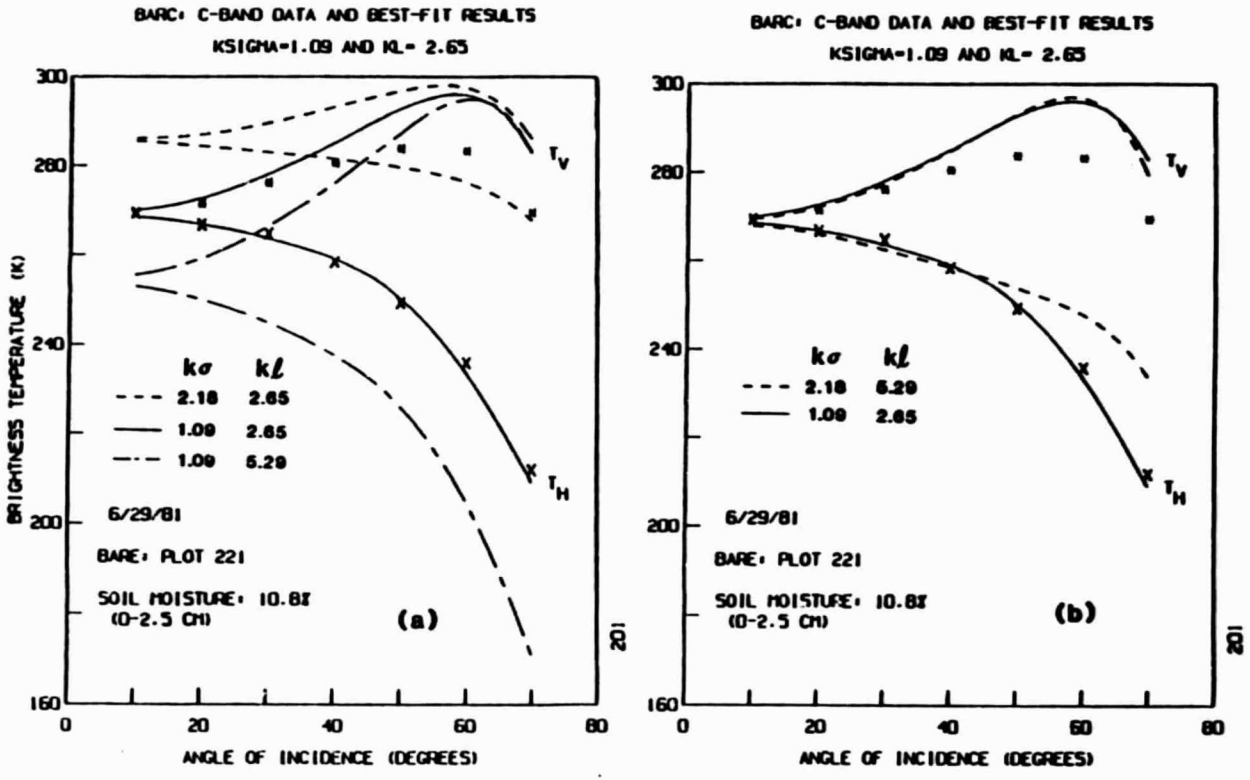

Figure 6. The Solid Curves are the Best Fits. (a) Results if the Parameter $k\sigma$ or $k\ell$ Were two Times its Best-Fit Value. (b) Results if Both $k\sigma$ and $k\ell$ Were Twice as Large as the Best-Fit Values.

Studying the results given in Figure 5a shows that the two parameters can be compensatory to each other in the non-linear least-squares fit to the data, and that the pair of best fit parameter values may be not unique, unless one of the parameters is pre-determined. However, the slope ratio $m = (k\sigma/k\ell)$ is probably more uniquely determined from best-fit results, as shown in Figure 5b where the dashed curves represent the effect of a 50% increment in both $k\sigma$ and $k\ell$. However, the slopes for the solid and dashed curves in Figure 5b remain constant (m=0.41). It can be seen from Figure 5b that the dashed curves approximately coincide with the best-fit results (the solid curves), except for the T_H component at angles greater tha. 50^o. These dashed curves could be considered in agreement with the data within experimental errors, although they were obtained with soil surface parameters which are 50 percent larger than the best-fit values.

Figure 6a presents the calculated results if either $k\sigma$ or $k\ell$ were twice their best-fit values and Figure 6b shows the results (the dashed curves) for both $k\sigma$ and $k\ell$ being twice as large as the best-fit values. Figure 6b demonstrates that there are large discrepancies between the calculated doubled value T_H results (the dashes) and the best fit curves at $\theta>50^o$.

Besides those shown in Figures 2 to 4, additional fits to the data were also performed. Totally, 90 sets of brightness temperature data (45 L-band and 45 C-band) have been satisfactorily fitted. The best-fit parameter values obtained from these fits are listed in Tables 1 and 2. The former contains the parameters for the data taken over field plot 121, and the latter gives the parameters for data from plots 221 and 223. The m values are also listed in these tables. The soil effective temperature (in K) and the measured soil moisture content within the surface 2.5-cm layer are given in the last two columns, respectively. Mean

Table 1. Best-fit parameters obtained from fits to the brightness temperature data collected over the bare field plot 121 (smooth). The slope is denoted by $m = (k\sigma/k\ell)$. The mean values of the parameter values are given in the bottom row.

Date	L-Band			C-Band			Plot	Effective Temperature (K)	Soil Moisture (wt-%)
	$k\sigma$	$k\ell$	m	$k\sigma$	$k\ell$	m			
6 24 81	0.71	2.50	0.28	0.94	1.82	0.52	121	308	5.4
7 13 81	1.07	5.90	0.18	0.74	1.74	0.42		309	5.5
7 14 81	0.87	5.11	0.17	0.82	2.22	0.37		309	4.5
7 21 81	0.11	19.07	0.01	0.04	7.24	0.01		308	9.5
7 22 81[a]	0.44	9.54	0.05	1.01	3.15	0.32		306	3.6
7 23 81	0.96	11.79	0.08	0.83	2.25	0.37		311	2.1
8 3 81	1.34	10.86	0.12	0.57	1.87	0.30		297	4.6
8 4 81	2.46	19.59	0.13	0.30	18.12	0.02		299	11.8
8 5 81	0.89	5.11	0.18	0.47	1.89	0.25		300	9.7
8 26 81	0.75	10.42	0.07	0.60	1.66	0.36		297	5.4
8 27 81	1.74	13.13	0.13	0.73	2.09	0.35		299	5.7
8 28 81	2.35	20.15	0.12	0.70	1.43	0.49		300	5.3
9 1 81	0.73	9.93	0.07	0.07	18.18	0.00		298	14.9
9 2 81	1.76	13.52	0.13	0.04	18.48	0.00		296	12.5
9 3 81	0.47	9.55	0.05	0.03	12.00	0.00		295	11.0
9 17 81	0.07	8.91	0.01	0.25	17.98	0.01		295	14.7
9 18 81	0.03	20.65	0.00	0.28	18.08	0.02		289	16.0
9 28 81	1.28	28.20	0.05	0.36	1.41	0.25		292	6.2
9 29 81	0.44	17.67	0.03	0.39	1.43	0.27		289	7.0
9 30 81	0.22	18.49	0.01	0.49	1.89	0.26		291	5.8
Mean	0.93	13.00	0.07	0.48	6.74	0.07			

a. Data are shown in Figure 2.

Table 2. Best-fit parameters obtained from fits to the brightness temperature data collected over the bare field plot 221 (medium rough) and plot 223 (very rough), respectively. The slope is denoted by $m = (k\sigma/k\ell)$. The mean values (for each plot) of the parameter values are listed at the bottom rows.

Date	L-Band			C-Band			Plot	Effective Temperature (K)	Soil Moisture (wt-%)
	$k\sigma$	$k\ell$	m	$k\sigma$	$k\ell$	m			
6 29 81	0.33	1.11	0.29	1.09	2.65	0.41	221	298	10.8
7 30 81	0.36	9.66	0.04	1.76	9.34	0.19		301	9.8
7 31 81	0.68	2.62	0.26	0.78	2.23	0.35		295	14.7
8 10 81	0.54	2.18	0.25	0.74	1.84	0.40		297	11.4
8 11 81	0.70	3.27	0.21	1.12	4.53	0.25		298	10.2
8 13 81	2.19	14.96	0.15	2.71	18.19	0.15		293	20.0
8 13 81	3.36	25.25	0.13	3.31	22.78	0.15		302	18.0
8 14 81[a]	0.74	3.59	0.21	2.27	10.64	0.21		295	19.0
8 14 81	1.99	14.47	0.14	2.07	8.66	0.24		306	15.4
8 17 81	0.69	3.19	0.22	2.61	11.43	0.23		290	17.5
8 18 81	0.60	2.72	0.22	0.98	2.33	0.42		295	14.1
8 19 81	0.35	1.24	0.28	1.03	3.32	0.31		291	12.4
8 20 81	3.33	27.23	0.12	0.87	2.55	0.34		291	10.5
Mean	1.22	8.58	0.14	1.62	7.73	0.21			
7 30 81	1.60	4.17	0.38	3.09	4.70	0.66	223	303	11.7
7 31 81	1.06	1.35	0.79	4.50	5.50	0.82		296	21.0
8 10 81	1.59	4.07	0.39	2.66	4.36	0.61		296	9.1
8 11 81	1.29	2.42	0.53	2.44	4.48	0.54		296	10.5
8 13 81	1.53	3.43	0.45	3.01	6.91	0.44		293	23.5
8 13 81	1.33	2.74	0.49	2.67	4.94	0.54		301	21.0
8 14 81	1.92	6.55	0.29	3.13	9.23	0.34		304	16.5
8 14 81	1.25	2.22	0.56	3.00	3.33	0.90		294	19.6
8 17 81	1.32	3.30	0.40	3.02	7.02	0.43		292	16.7
8 18 81	1.84	5.56	0.33	3.20	5.23	0.61		294	12.4
8 19 81	1.90	4.42	0.43	3.10	5.02	0.62		290	15.1
8 20 81[b]	1.77	4.39	0.40	3.10	5.17	0.60		291	12.0
Mean	1.53	3.72	0.41	3.07	5.50	0.56			

a. Data are shown in Figure 3.

b. Data are shown in Figure 4.

values of these parameters (in Tables 1 and 2) are listed at the bottom row for each field plot.

Comparisons for each of the best-fit results to the data are presented graphically in Appendix B.

Physically, the two surface roughness parameters σ and ℓ can be 'measured' from the surface height profiles. Table 3 gives a set of the measured values of σ and ℓ. These values of σ and ℓ were extracted from a group of photographs that recorded the surface height profiles during the data collection period. These photographic surface height profiles were digitized and used to calculate the σ and ℓ values, as listed in Table 3, which also contains the slope values from the best-fit results.

A typical surface height profile is shown in the upper part of Figure 7, which displays the surface height z as a function of the surface distance X from an arbitrary reference point (the origin). The z values in Figure 7 are relative to the mean height value, therefore the mean value of the z's is zero (i.e., $\langle z \rangle = 0$).

The lower part of Figure 7 shows the autocorrelation (or correlation) function for this profile. This function provides a measure of similarity of two surface heights separated by a spatial displacement X and was calculated according to the method given in [5].

The surface correlation length ℓ is defined as the displacement X at which the autocorrelation function is equal to $\rho(\ell)=e^{-1}$ ($= 0.37$). For example, the estimated value of correlation length from Figure 7 is $\ell = 4$ cm, as listed in Table 3.

The measured σ and ℓ values given in Table 3 only provide the conditions of the surface roughness for one day, while the data were collected over a period of three months.

Table 3. Measured values of surface height standard deviation σ and correlation length ℓ. The m represents the measured slope, while m_L and m_C denote the L- and C-band slope values from the best fit results, respectively.

Field ID	σ(cm)	ℓ(cm)	m	m_L	m_C	Surface Condition
121	0.24	4.0	0.06	0.07	0.07	Smooth
221	0.82	3.5	0.23	0.14	0.21	Medium rough
223	2.79	8.0	0.37	0.41	0.56	Very rough

$m \equiv \sigma/\ell$

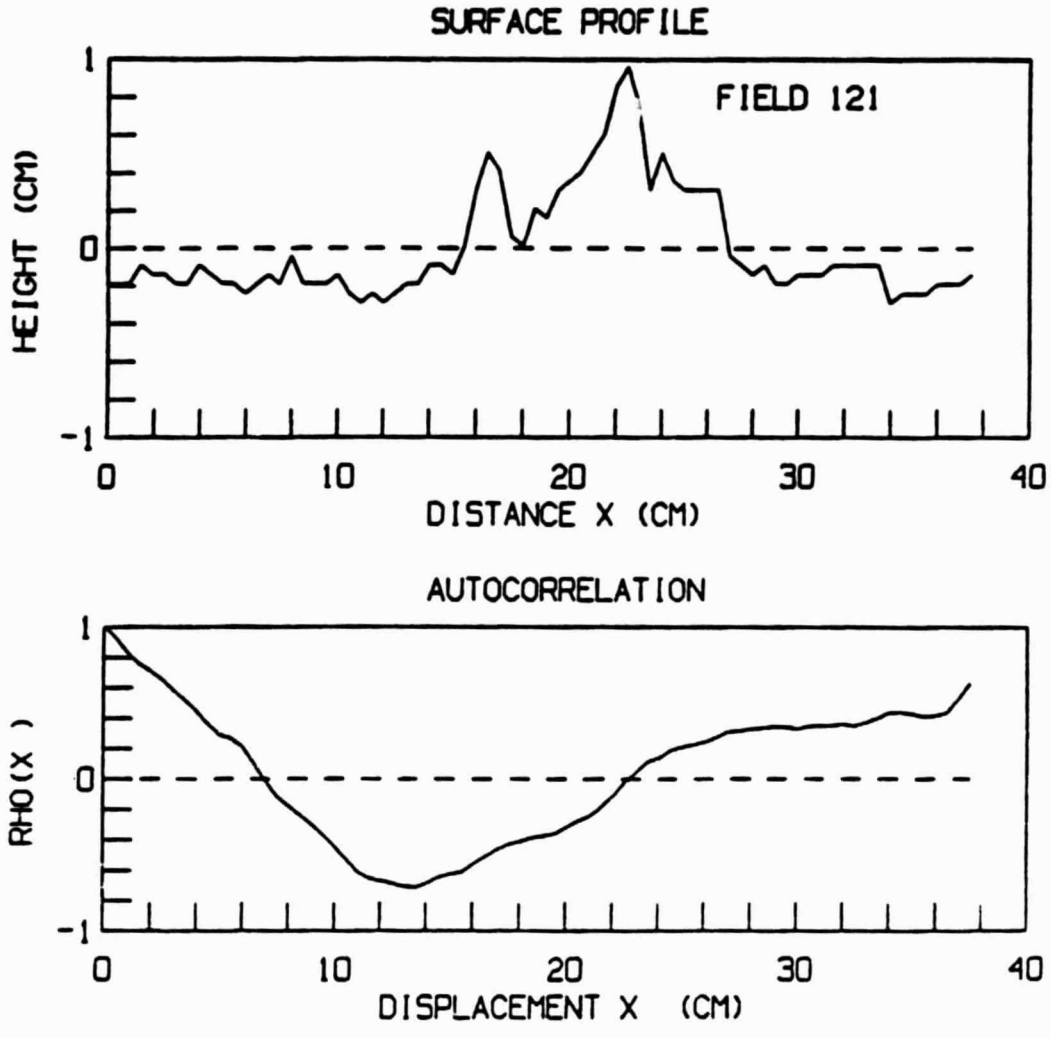

Figure 7. Surface height profile (upper part) and the corresponding autocorrelation function.

Therefore, one would not expect that these measured parameter values (in Table 3) agree well with the best-fit values (in Tables 1 and 2), which have large variations over the data-collection period.

These large variations in the best-fit values of the parameters, particularly during adjacent dates, are probably due to uncertainties in the measured soil moisture profiles, which are used to compute the soil dielectric constant and surface emissivity. For example, Table 2 gives the soil moistures (in 0-2.5 cm) for July 30 and 31, 1981 as 9.8% and 14.7%, respectively. However, the observed brightness temperatures on these two days exhibit approximately identical angular variations within experimental errors, as shown in Figure 8. Because of the difference in the soil moistures, best fits to the two sets of data lead to quite different numerical values for the parameters $k\sigma$ and $k\ell$, as listed in Table 2. This shows that the uncertainty in the soil moisture can introduce large variations in the best-fit values of the parameters.

To understand the effect of the uncertainty in the measured soil moisture on the best-fit values, we performed some simulation studies of the sensitivity of the $k\sigma$ and $k\ell$ determination to the soil moisture variations. The results are given Table 4, which lists the best-fit values that would result, if the measured soil moisture profile (for July 30, 1981) were arbitrarily increased by 10% to 50% over the measured value. Table 4 shows that the slope m increases as the soil moisture is increased, and that it approaches to the same value as of the adjacent day (July 31, 1981) as given in Table 2, when the soil moisture is increased by 50%, which makes the soil moisture profile on July 30 approximately equal to that of July 31, 1981.

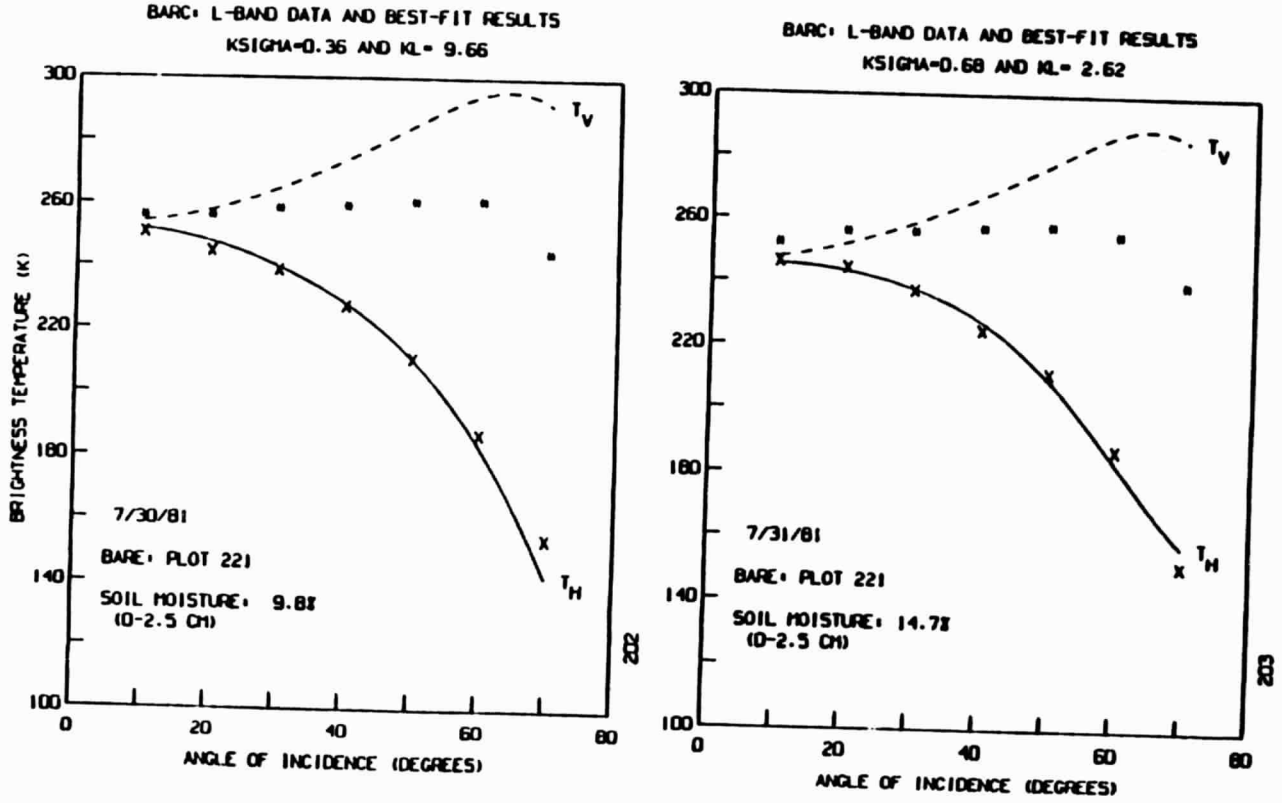

Figure 8. Effect of Soil Moisture on the Best-Fit Parameters. The Data for These Days are Approximately Identical Within Experimental Errors. The Large Difference in the Measured Soil Moistures Leads to Quite Different Values for the Best-Fit Parameters.

Table 4. Sensitivity Study of the Best-Fit Parameters to the Uncertainty in the Measured Soil Moisture. The Parameters Listed Below Were Obtained From the Best Fits to the Data Collected on July 30, 1981, if the Measured Soil Moisture Profile Were Increased by Δ = 10% to 50% Over its Measured Value. The increased Soil Moisture Values (in weight percent) are denoted by SM.

		L-Band			C-Band		
Δ (%)	SM	$k\sigma$	$k\ell$	m	$k\sigma$	$k\ell$	m
0	9.8	0.36	9.66	0.04	1.76	9.34	0.19
10	10.8	0.50	5.00	0.10	1.48	6.88	0.22
20	11.8	0.60	4.62	0.13	1.22	5.02	0.24
30	12.7	0.66	4.34	0.15	0.88	3.14	0.28
40	13.7	0.61	3.54	0.17	0.85	2.76	0.31
50	14.7	0.61	3.10	0.20	0.84	2.57	0.33

It is interesting to compare the mean values of the slope m (in Tables 1 and 2) to the measured m values in Table 3. It is believed that the m values can be more uniquely determined than the individual $k\sigma$ and $k\ell$ values (as described earlier). Table 1 shows that for plot 121, the mean value of m (defined as $k\sigma/k\ell$) is 0.07, while the corresponding measured one is 0.06 (see Table 3). The agreement in these two values is remarkable given the experimental uncertainties. Similar comparison of the mean m values for the other two field plots with the corresponding measured ones in Table 3 provide the same conclusion.

Some of the m values for L-band (in Tables 1 and 2) are smaller than those of C-band. Similar behavior was observed in the study of the radar backscattering coefficient [6]. The reason for this wavelength dependence of m values is not well known at the present time, although it may indicate that the parameters σ and ℓ are inadequate to completely specify the surface roughness. Further study of this problem is required.

SECTION 4 - SUMMARY AND DISCUSSION

We have developed a model for simulating the remotely sensed microwave brightness temperature of rough soil surfaces. The model is successfully applied to reproduce a series of measured angular distributions of polarized brightness temperature at both L-band and C-band frequencies. The model is based on the Kirchhoff approximation of electromagnetic wave scattering at a rough air-soil interface, and its bistatic scattering coefficients are integrated (over the scattered angles) to obtain the surface reflectivity $R_p^s(\theta)$, which also contains a correction factor of a shadowing function $S(\theta)$, that represents the probability of a point on a rough surface not being shadowed by other parts of the surface.

A nonlinear least-squares fitting method is used to obtain the best-fit surface roughness parameters, which can generate brightness temperatures that best match the data of the horizontal and vertical polarizations of the soil brightness temperatures. The best-fit results, as shown in Figures 2 to 4, demonstrate that the T_H component of the measured brightness temperatures can be satisfactorily reproduced at all angles. However, discrepancies exist for the T_V component, particularly at the L-band frequency. It is believed that some combinations of the reduced reflectivity at the Brewster angle, the uncertainties in the radiometer calibration performance, and polarization mixing contribute mostly to the discrepancies. Further investigation of this problem is required.

The best-fit $k\sigma$ values (as listed in Tables 1 and 2) are in qualitative agreement with the measured roughness of the soil surfaces of the three field plots. The mean $k\sigma$ values in Tables 1 and 2 indicate that the field plot 121

with the smoothest surface has the lowest $k\sigma$ values, and that the roughest plot 223 is associated with the largest $k\sigma$ values. Similarly, the mean m values in Tables 1 and 2 also correlate with the measured surface roughness, and in good agreement with the measurements (as listed in Table 3) within experimental errors.

Acknowledgment: We would like to thank P. O'Neill for providing the digitized data of the soil surface height profiles. Helpful discussion with B. J. Choudhury concerning the theoretical fits to the data is gracefully acknowledged. T. Mo is funded by NASA/Goddard Space Flight Center under contract NAS5-28188.

APPENDIX A

This appendix gives the polarization coefficients a_o and a which appear in Equations (4) and (5). The following formulas are taken from Reference [5].

HH-field:

$$a_o = -R_{HH} (\cos\theta + \cos\theta_s) \cos(\phi_s - \phi)$$

$$a = R_{HH} [\sin\theta_s - \sin\theta \cos(\phi_s - \phi)] - R_{HH\perp} (\cos\theta_s + \cos\theta) \cos(\phi_s - \phi)$$

VH-field:

$$a_o = -R_{HH} (1 + \cos\theta \cos\theta_s) \sin(\phi_s - \phi)$$

$$a = -[R_{HH} \sin\theta \cos\theta_s + R_{HH\perp} (1 + \cos\theta \cos\theta_s)] \sin(\phi_s - \phi)$$

VV-field:

$$a_o = R_{VV} (\cos\theta + \cos\theta_s) \cos(\phi_s - \phi)$$

$$a = R_{VV\perp} (\cos\theta_s + \cos\theta) \cos(\phi_s - \phi) - R_{VV} [\sin\theta_s - \sin\theta \cos(\phi_s - \phi)]$$

HV-field:

$$a_o = -R_{VV} (1 + \cos\theta \cos\theta\,\phi_s) \sin(\phi_s - \phi)$$

$$a = -[R_{VV} \sin\theta \cos\theta_s + R_{VV\perp} (1 + \cos\theta \cos\theta_s)] \sin(\phi_s - \phi)$$

where $|R_{PP}|^2$ represents the reflectivity of smooth surface with polarization PP(= HH or VV), and R_{PP1} is a component of the reflectivity. Formulas for R_{PP1}

expressed in terms of R_{pp} are given in References [2,5], and it can be shown that

$$R_{HH1} = -R_{HH} \frac{2 \sin \theta}{\cos \theta + \sqrt{\varepsilon - \sin^2 \theta}}$$

and

$$R_{VV1} = - \frac{(\varepsilon - 1) \sin \theta}{\varepsilon \cos \theta + \sqrt{\varepsilon - \sin^2 \theta}} + R_{VV} \frac{(\varepsilon + 1) \sin \theta}{\varepsilon \cos \theta + \sqrt{\varepsilon - \sin^2 \theta}}$$

where ε is the soil dielectric constant.

APPENDIX B

A complete set of the best-fit results and comparison with data are presented graphically in this appendix. Totally, it contains 90 nonlinear least-squares fits to the measured angular variations of brightness temperatures (consisting of 45 measurements each at L-band and C-band frequencies). The best-fit parameters are listed at the top of each graph, and are also given in Tables 1 and 2. The following notations apply to each figure:

1. The crosses (X) are the measured horizontal component of the brightness temperatures
2. The asterisks (*) are the measured vertical component of the brightness temperatures
3. The solid curve (labelled by T_H) represents the calculated horizontal component of brightness temperature
4. The dashed curve (labelled by T_V) denotes the calculated vertical component of brightness temperature.

The figures are arranged according to the field plots and data-collection dates. It appears in the following order:

Field Plot 121: Figures B-1 through B-20
Field Plot 221: Figures B-21 through B-33, and
Field Plot 223: Figures B-34 through B-45.

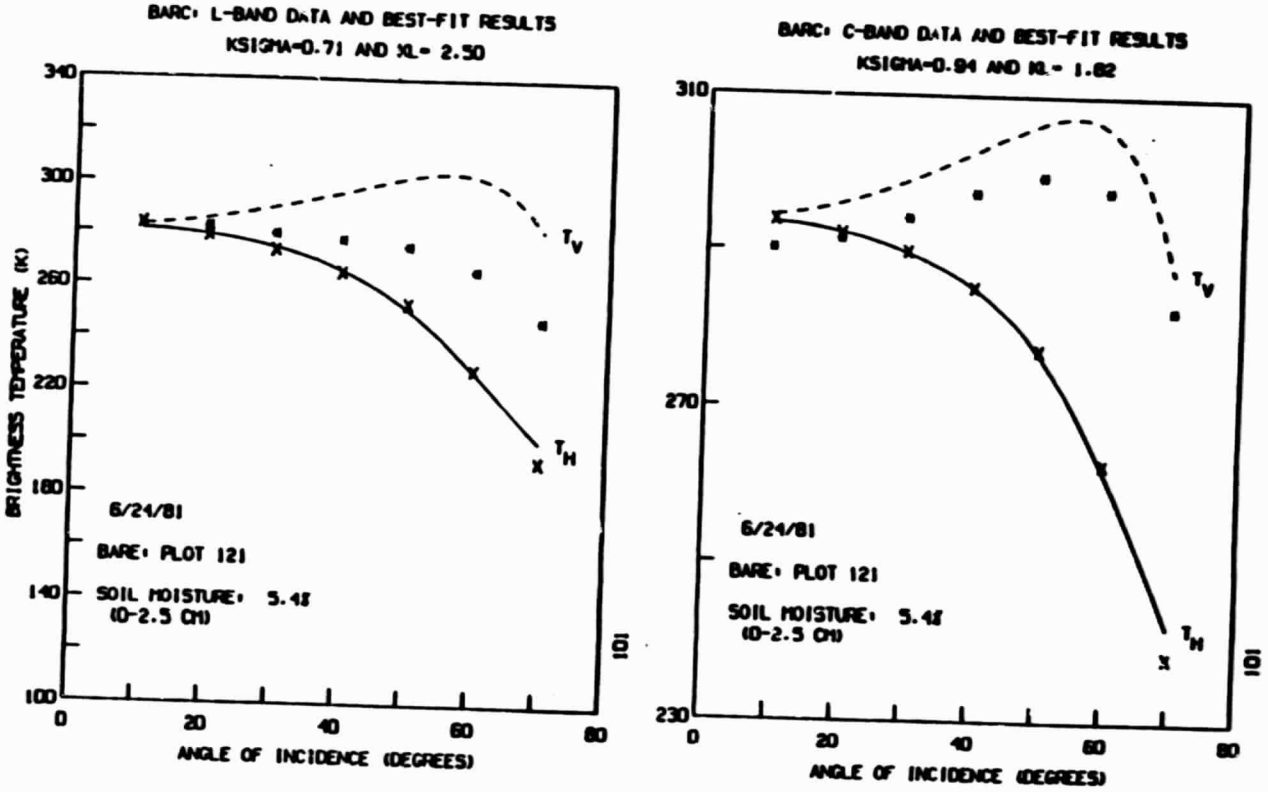
BARC: L-BAND DATA AND BEST-FIT RESULTS
KSIGMA=0.71 AND XL= 2.50
BRIGHTNESS TEMPERATURE (K)
340
300
260
220
180
140
100
0
20
40
60
80
ANGLE OF INCIDENCE (DEGREES)
T_V
T_H
6/24/81
BARE: PLOT 121
SOIL MOISTURE: 5.4%
(0-2.5 CM)
101
BARC: C-BAND DATA AND BEST-FIT RESULTS
KSIGMA=0.94 AND XL= 1.82
310
270
230
0
20
40
60
80
ANGLE OF INCIDENCE (DEGREES)
T_V
T_H
6/24/81
BARE: PLOT 121
SOIL MOISTURE: 5.4%
(0-2.5 CM)
101

Figure B-1

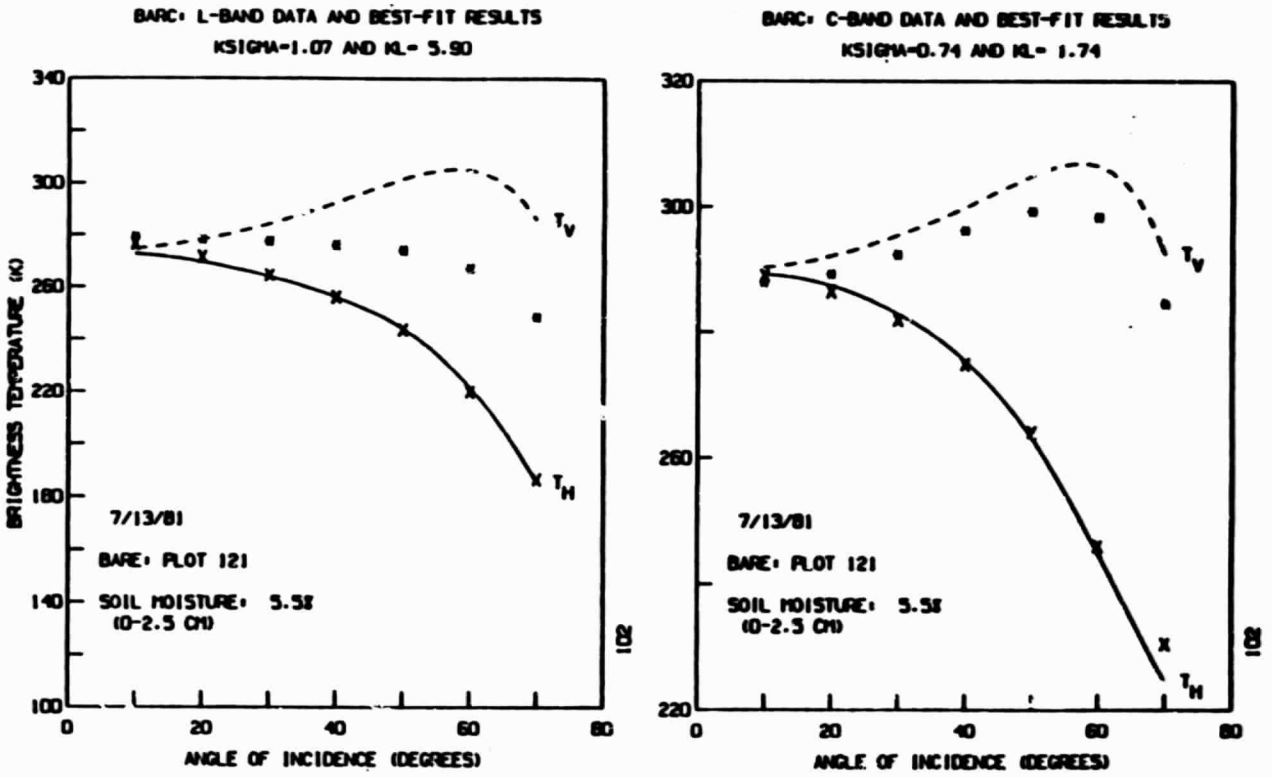
BARC: L-BAND DATA AND BEST-FIT RESULTS
KSIGMA=1.07 AND KL= 5.90
BRIGHTNESS TEMPERATURE (K)
340
300
260
220
180
140
100
0
20
40
60
80
ANGLE OF INCIDENCE (DEGREES)
T_V
T_H
7/13/81
BARE: PLOT 121
SOIL MOISTURE: 5.5%
(0-2.5 CM)
102
BARC: C-BAND DATA AND BEST-FIT RESULTS
KSIGMA=0.74 AND KL= 1.74
320
300
260
220
0
20
40
60
80
ANGLE OF INCIDENCE (DEGREES)
T_V
T_H
7/13/81
BARE: PLOT 121
SOIL MOISTURE: 5.5%
(0-2.5 CM)
102

Figure B-2

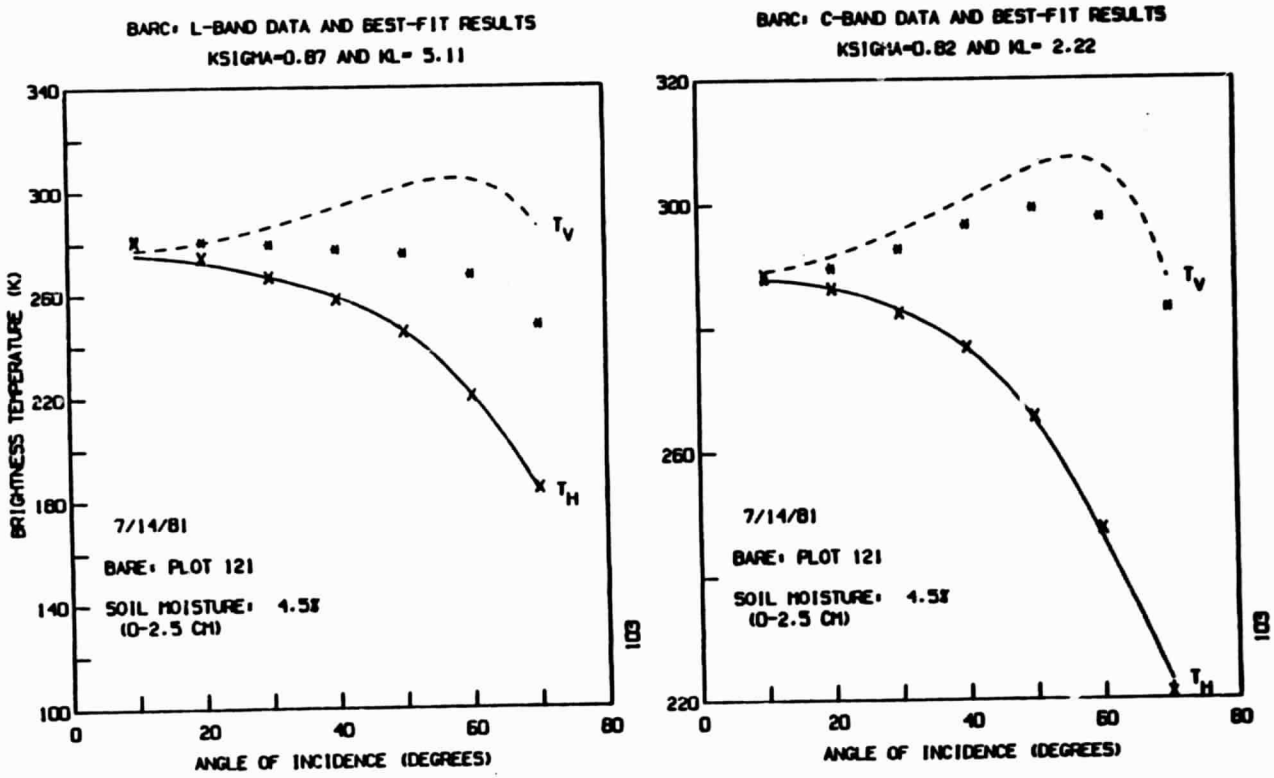
BARC: L-BAND DATA AND BEST-FIT RESULTS
KSIGMA=0.87 AND KL= 5.11
BRIGHTNESS TEMPERATURE (K)
ANGLE OF INCIDENCE (DEGREES)
T_V
T_H
7/14/81
BARE: PLOT 121
SOIL MOISTURE: 4.5%
(0-2.5 CM)
BARC: C-BAND DATA AND BEST-FIT RESULTS
KSIGMA=0.82 AND KL= 2.22
ANGLE OF INCIDENCE (DEGREES)
T_V
T_H
7/14/81
BARE: PLOT 121
SOIL MOISTURE: 4.5%
(0-2.5 CM)

Figure B-3

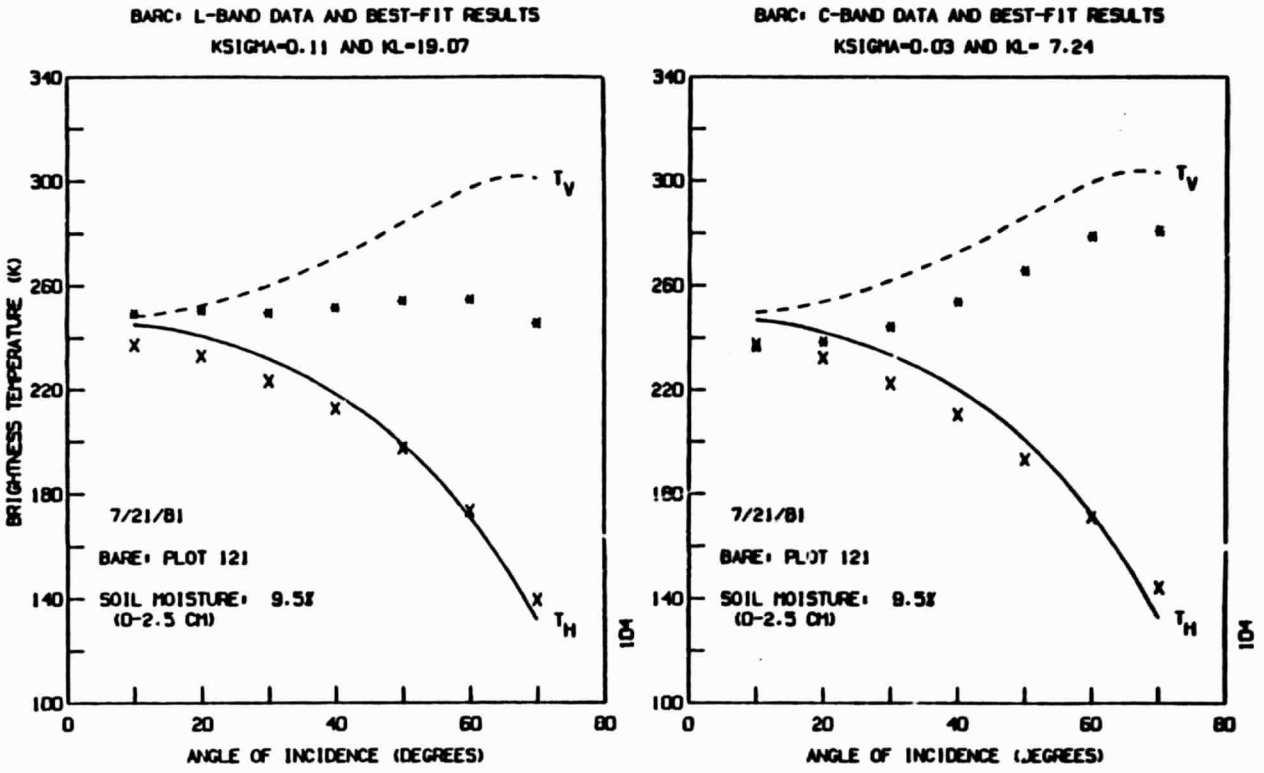
BARC: L-BAND DATA AND BEST-FIT RESULTS
KSIGMA=0.11 AND KL=19.07
BARC: C-BAND DATA AND BEST-FIT RESULTS
KSIGMA=0.03 AND KL= 7.24
BRIGHTNESS TEMPERATURE (K)
ANGLE OF INCIDENCE (DEGREES)
T_V
T_H
7/21/81
BARE: PLOT 121
SOIL MOISTURE: 9.5%
(0-2.5 CM)
100
140
180
220
260
300
340
0
20
40
60
80

Figure B-4

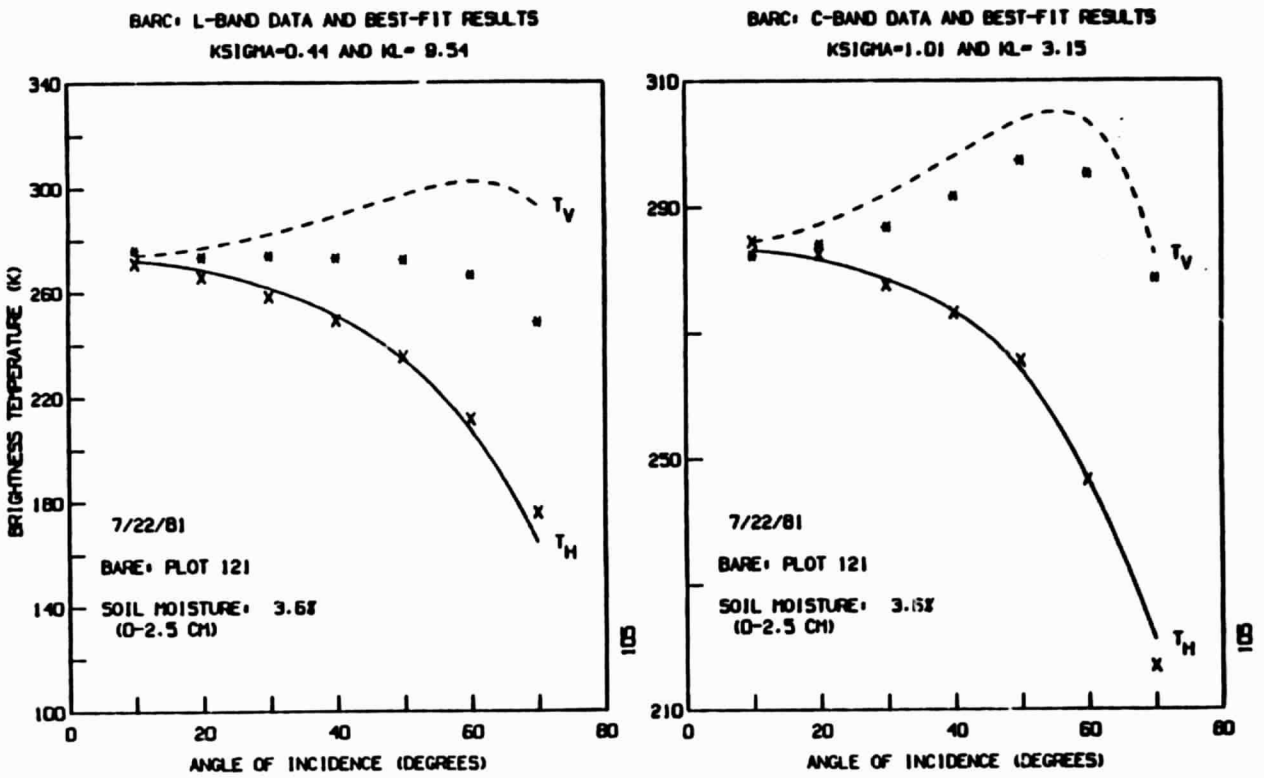
BARC: L-BAND DATA AND BEST-FIT RESULTS
KSIGMA=0.44 AND KL= 9.54
BRIGHTNESS TEMPERATURE (K)
340
300
260
220
180
140
100
0
20
40
60
80
ANGLE OF INCIDENCE (DEGREES)
T_V
T_H
7/22/81
BARE: PLOT 121
SOIL MOISTURE: 3.6%
(0-2.5 CM)
BARC: C-BAND DATA AND BEST-FIT RESULTS
KSIGMA=1.01 AND KL= 3.15
310
290
250
210
0
20
40
60
80
ANGLE OF INCIDENCE (DEGREES)
T_V
T_H
7/22/81
BARE: PLOT 121
SOIL MOISTURE: 3.6%
(0-2.5 CM)

Figure B-5

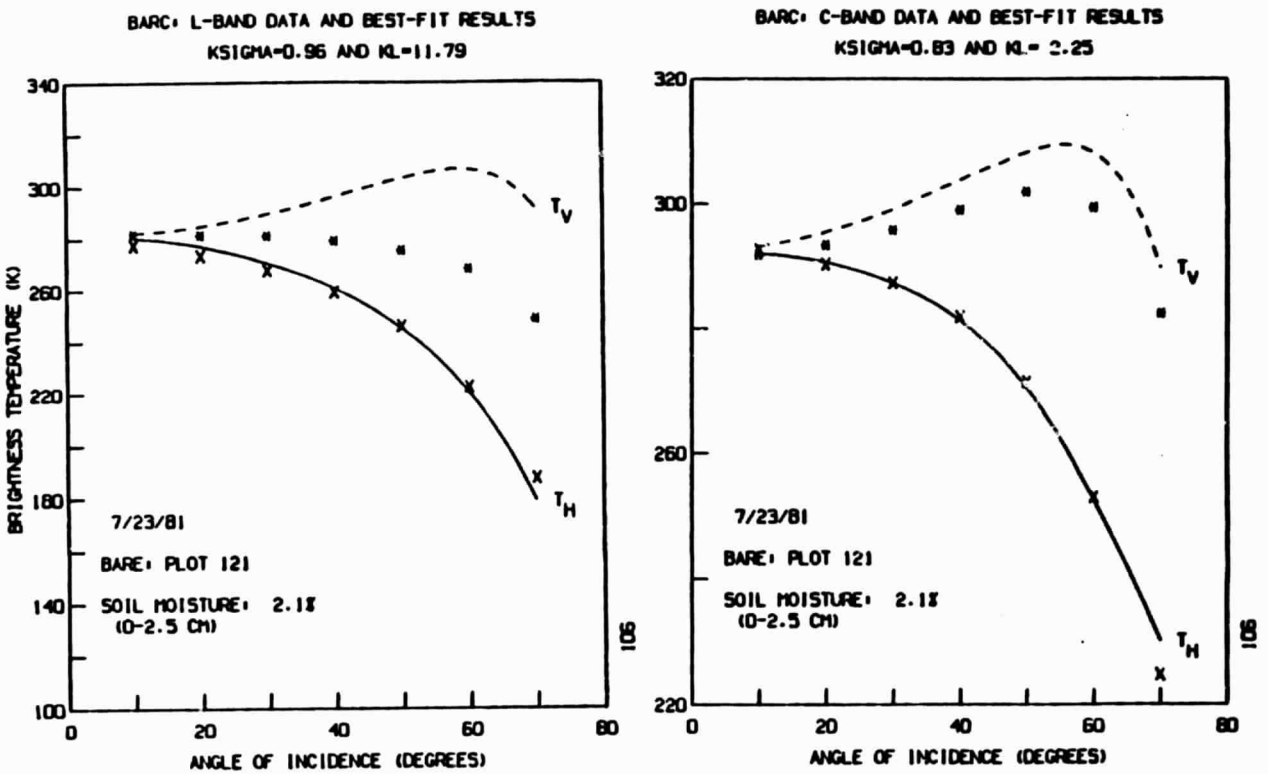
BARC: L-BAND DATA AND BEST-FIT RESULTS
KSIGMA=0.96 AND KL=11.79
BRIGHTNESS TEMPERATURE (K)
340
300
260
220
180
140
100
0
20
40
60
80
ANGLE OF INCIDENCE (DEGREES)
T_V
T_H
7/23/81
BARE: PLOT 121
SOIL MOISTURE: 2.1%
(0-2.5 CM)
BARC: C-BAND DATA AND BEST-FIT RESULTS
KSIGMA=0.83 AND KL= 2.25
320
300
260
220
0
20
40
60
80
ANGLE OF INCIDENCE (DEGREES)
T_V
T_H
7/23/81
BARE: PLOT 121
SOIL MOISTURE: 2.1%
(0-2.5 CM)

Figure B-6

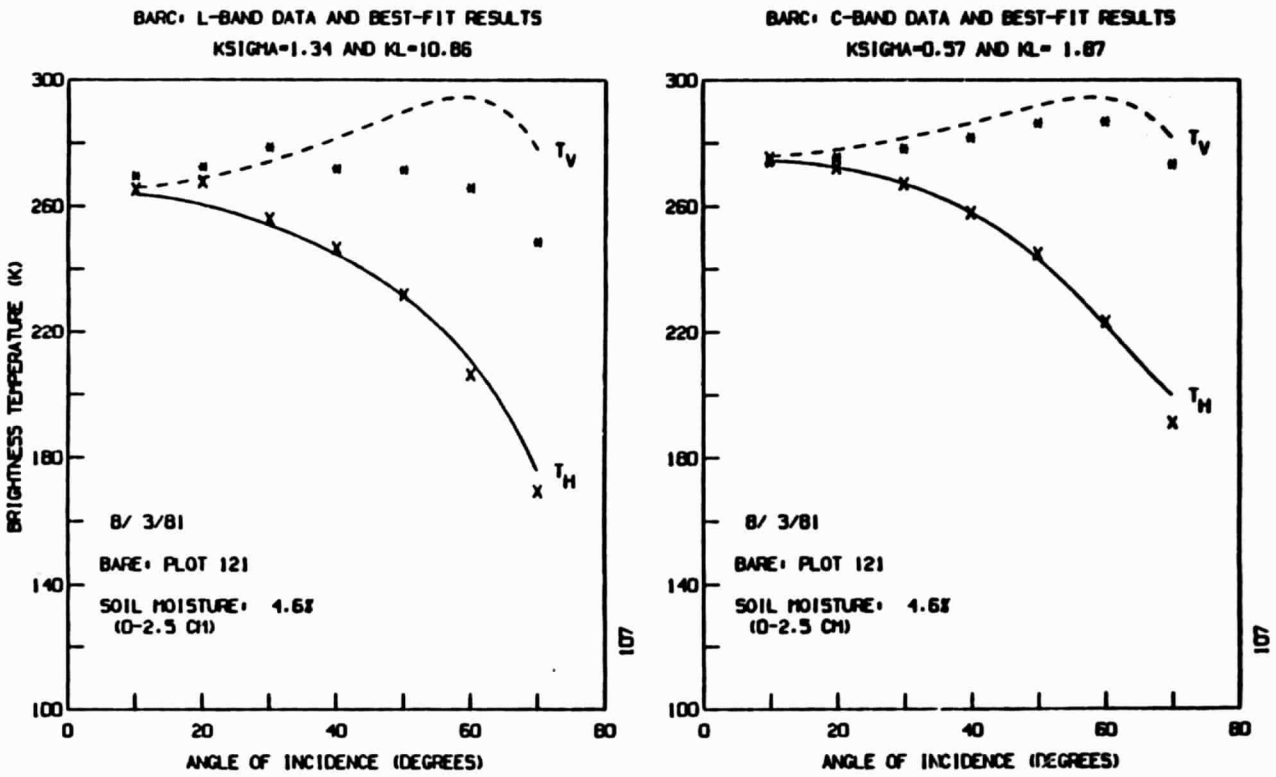
BARC: L-BAND DATA AND BEST-FIT RESULTS
KSIGMA=1.34 AND KL=10.86
BRIGHTNESS TEMPERATURE (K)
300
260
220
180
140
100
0
20
40
60
80
ANGLE OF INCIDENCE (DEGREES)
T_V
T_H
8/ 3/81
BARE: PLOT 121
SOIL MOISTURE: 4.6%
(0-2.5 CM)
107
BARC: C-BAND DATA AND BEST-FIT RESULTS
KSIGMA=0.57 AND KL= 1.87
300
260
220
180
140
100
0
20
40
60
80
ANGLE OF INCIDENCE (DEGREES)
T_V
T_H
8/ 3/81
BARE: PLOT 121
SOIL MOISTURE: 4.6%
(0-2.5 CM)
107

Figure B-7

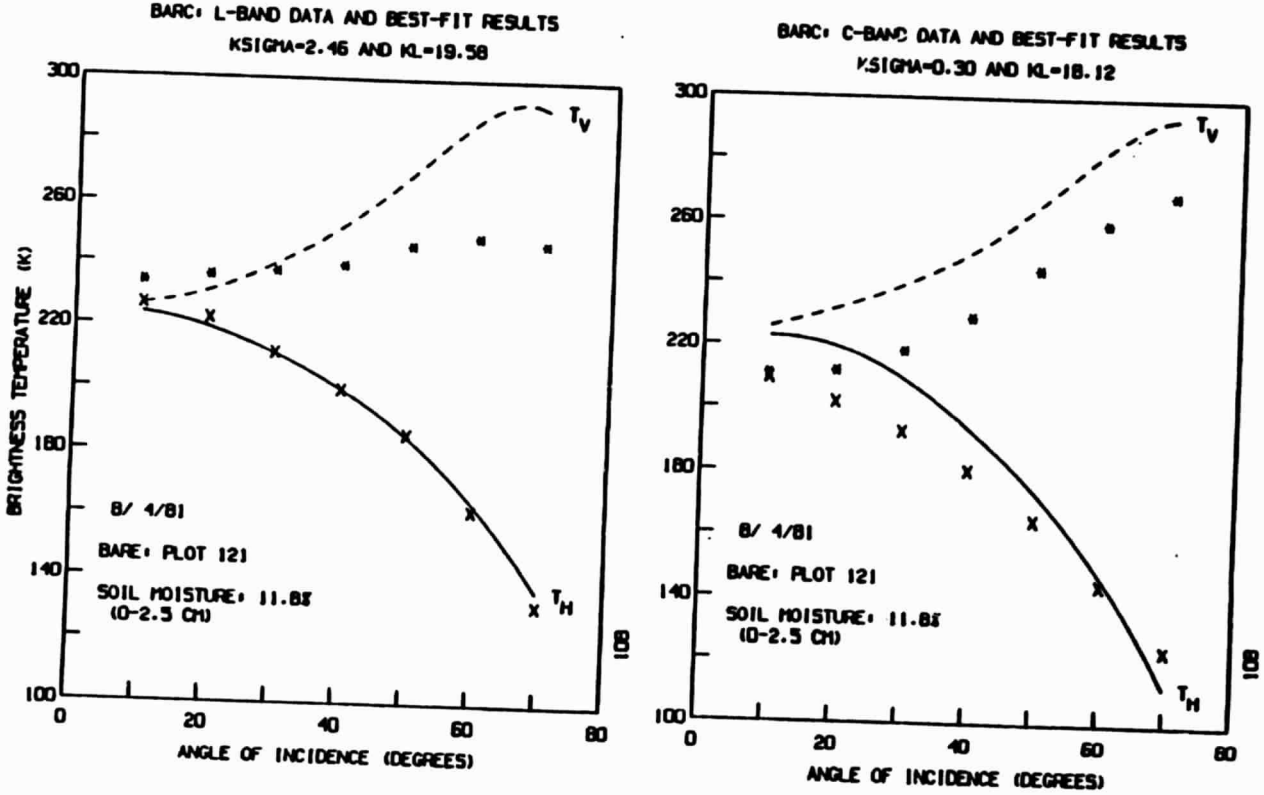
BARC: L-BAND DATA AND BEST-FIT RESULTS
KSIGMA=2.46 AND KL=19.58
BRIGHTNESS TEMPERATURE (K)
300
260
220
180
140
100
0
20
40
60
80
ANGLE OF INCIDENCE (DEGREES)
T_V
T_H
8/ 4/81
BARE: PLOT 121
SOIL MOISTURE: 11.8%
(0-2.5 CM)
BARC: C-BAND DATA AND BEST-FIT RESULTS
KSIGMA=0.30 AND KL=18.12
300
260
220
180
140
100
0
20
40
60
80
ANGLE OF INCIDENCE (DEGREES)
T_V
T_H
8/ 4/81
BARE: PLOT 121
SOIL MOISTURE: 11.8%
(0-2.5 CM)

Figure B-8

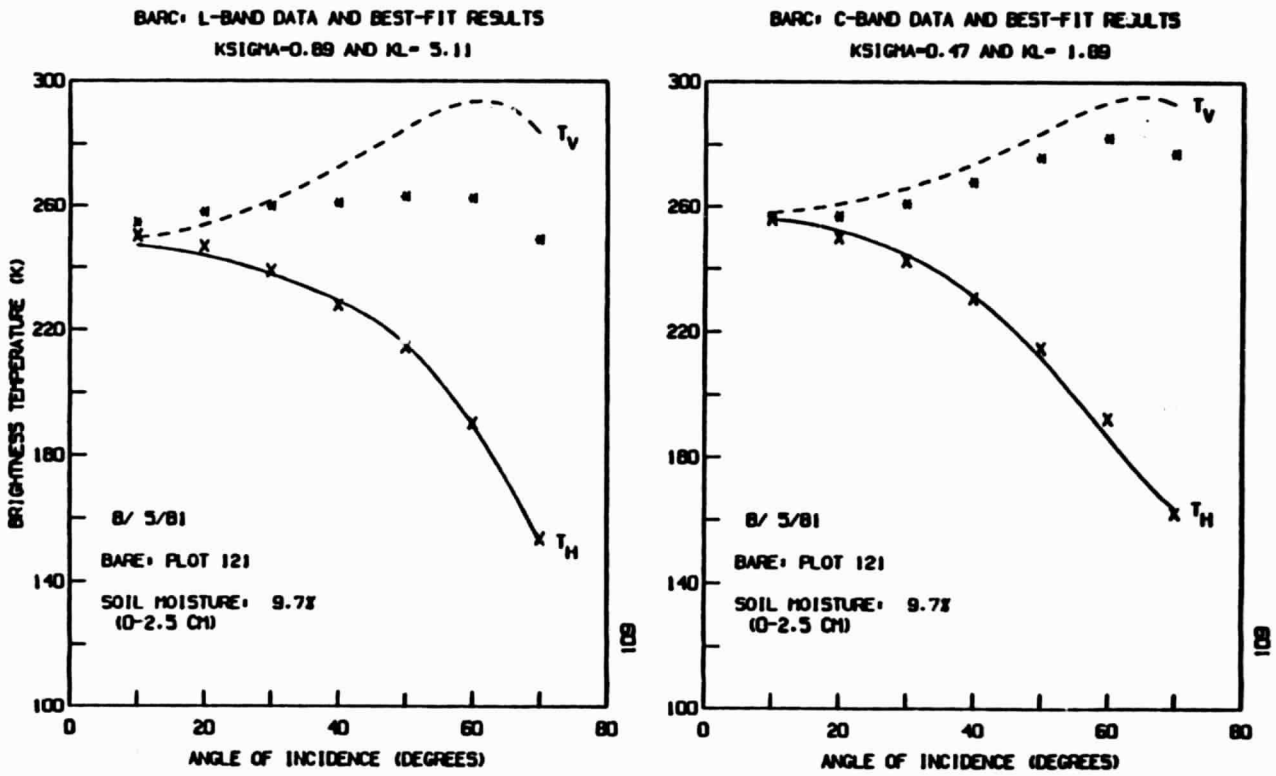
BARC: L-BAND DATA AND BEST-FIT RESULTS
KSIGMA=0.89 AND KL= 5.11
BRIGHTNESS TEMPERATURE (K)
ANGLE OF INCIDENCE (DEGREES)
T_V
T_H
8/ 5/81
BARE: PLOT 121
SOIL MOISTURE: 9.7%
(0-2.5 CM)
BARC: C-BAND DATA AND BEST-FIT RESULTS
KSIGMA=0.47 AND KL= 1.89
ANGLE OF INCIDENCE (DEGREES)
T_V
T_H
8/ 5/81
BARE: PLOT 121
SOIL MOISTURE: 9.7%
(0-2.5 CM)

Figure B-9

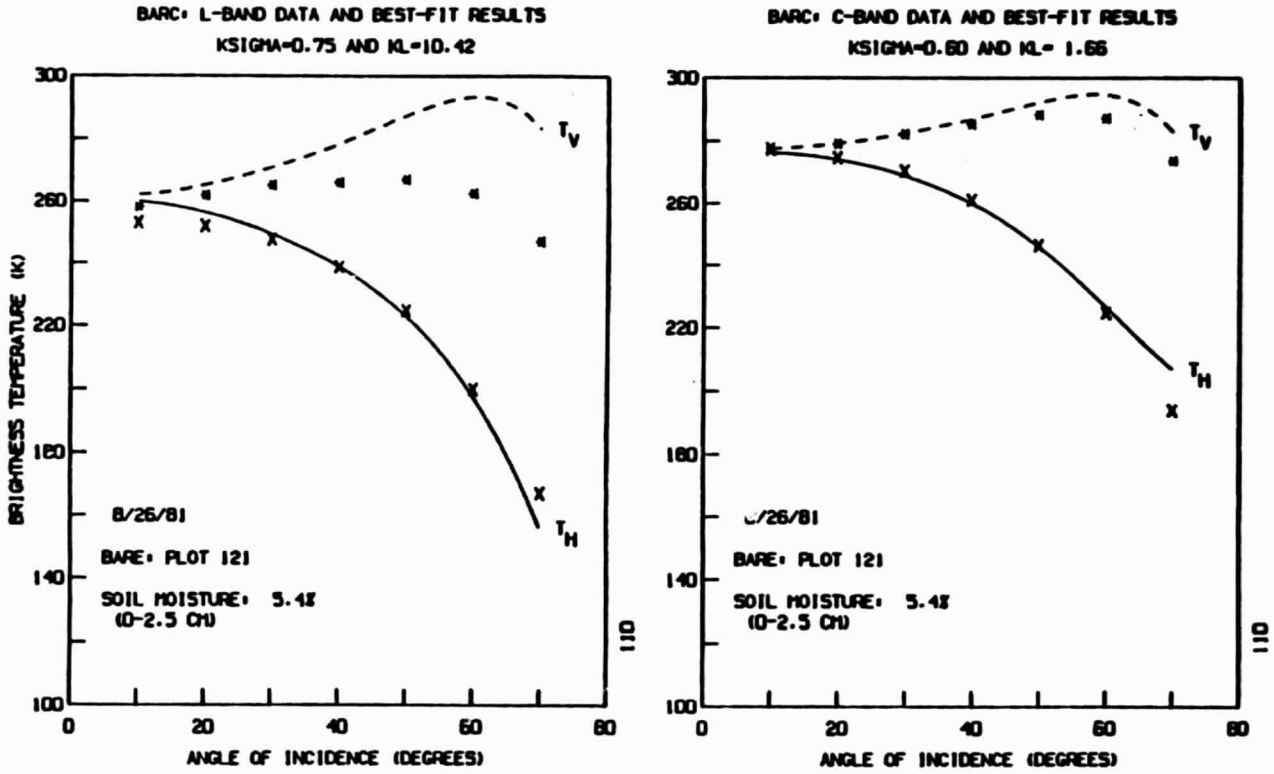
BARC: L-BAND DATA AND BEST-FIT RESULTS
KSIGMA=0.75 AND KL=10.42
BRIGHTNESS TEMPERATURE (K)
300
260
220
180
140
100
0
20
40
60
80
ANGLE OF INCIDENCE (DEGREES)
T_V
T_H
8/26/81
BARE: PLOT 121
SOIL MOISTURE: 5.4%
(0-2.5 CM)
BARC: C-BAND DATA AND BEST-FIT RESULTS
KSIGMA=0.80 AND KL= 1.66
ANGLE OF INCIDENCE (DEGREES)
T_V
T_H
BARE: PLOT 121
SOIL MOISTURE: 5.4%
(0-2.5 CM)

Figure B-10

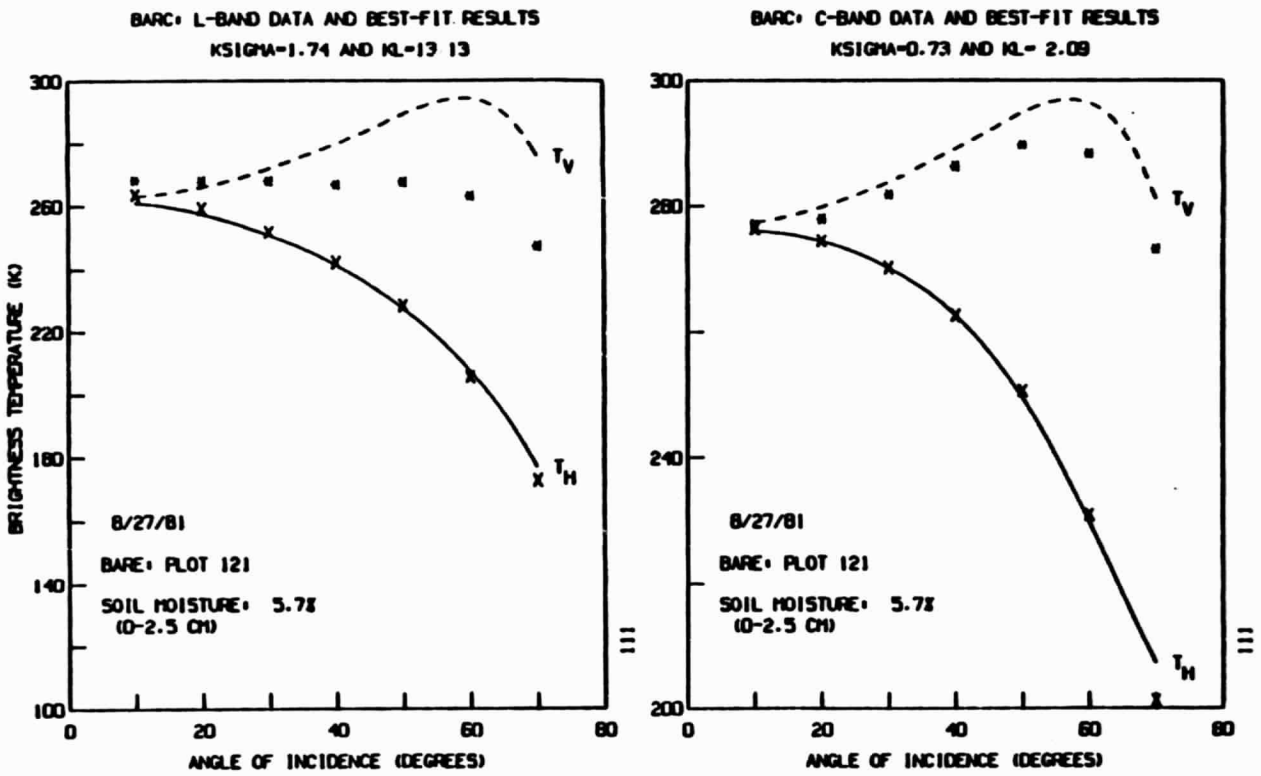
BARC: L-BAND DATA AND BEST-FIT RESULTS
KSIGMA=1.74 AND KL=13 13
BRIGHTNESS TEMPERATURE (K)
300
260
220
180
140
100
0
20
40
60
80
ANGLE OF INCIDENCE (DEGREES)
T_V
T_H
8/27/81
BARE: PLOT 121
SOIL MOISTURE: 5.7%
(0-2.5 CM)
BARC: C-BAND DATA AND BEST-FIT RESULTS
KSIGMA=0.73 AND KL= 2.09
300
280
240
200
0
20
40
60
80
ANGLE OF INCIDENCE (DEGREES)
T_V
T_H
8/27/81
BARE: PLOT 121
SOIL MOISTURE: 5.7%
(0-2.5 CM)

Figure B-11

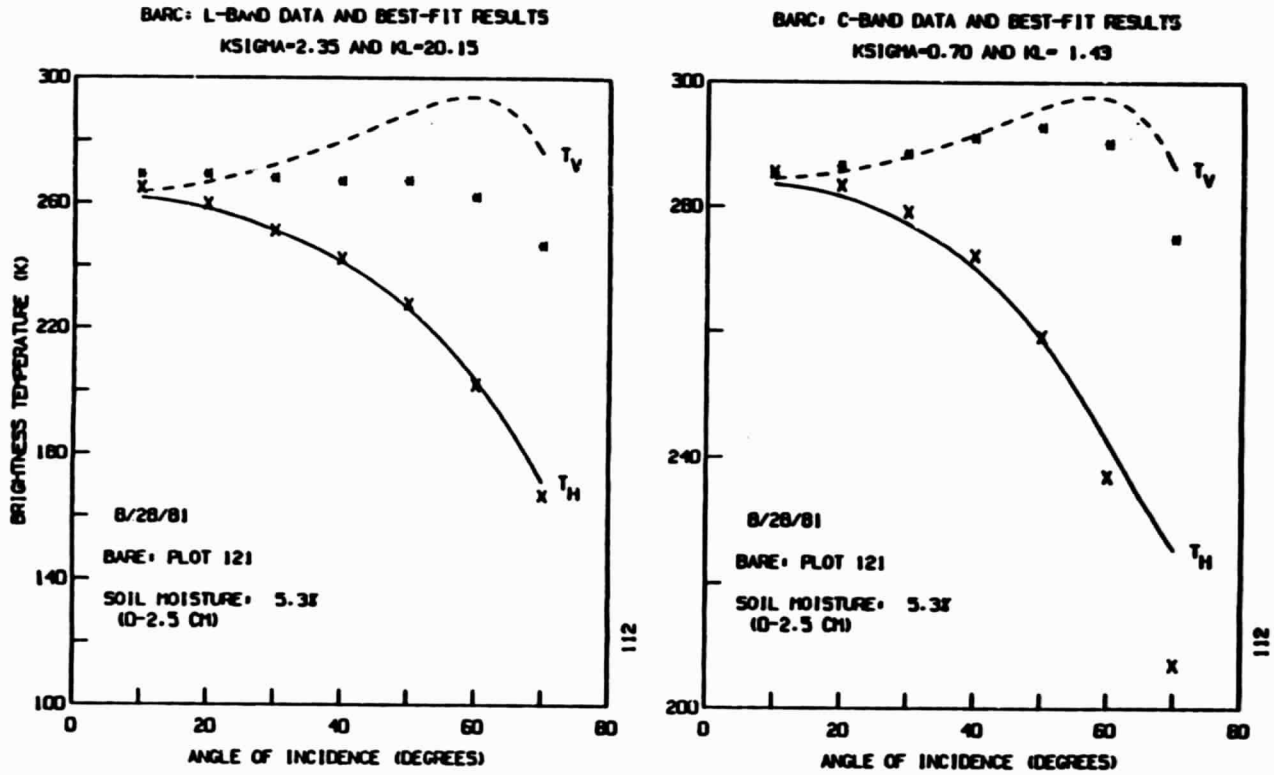
BARC: L-BAND DATA AND BEST-FIT RESULTS
KSIGMA=2.35 AND KL=20.15
BRIGHTNESS TEMPERATURE (K)
ANGLE OF INCIDENCE (DEGREES)
T_V
T_H
8/28/81
BARE: PLOT 121
SOIL MOISTURE: 5.3%
(0-2.5 CM)
112
BARC: C-BAND DATA AND BEST-FIT RESULTS
KSIGMA=0.70 AND KL= 1.43
ANGLE OF INCIDENCE (DEGREES)
T_V
T_H
8/28/81
BARE: PLOT 121
SOIL MOISTURE: 5.3%
(0-2.5 CM)
112

Figure B-12

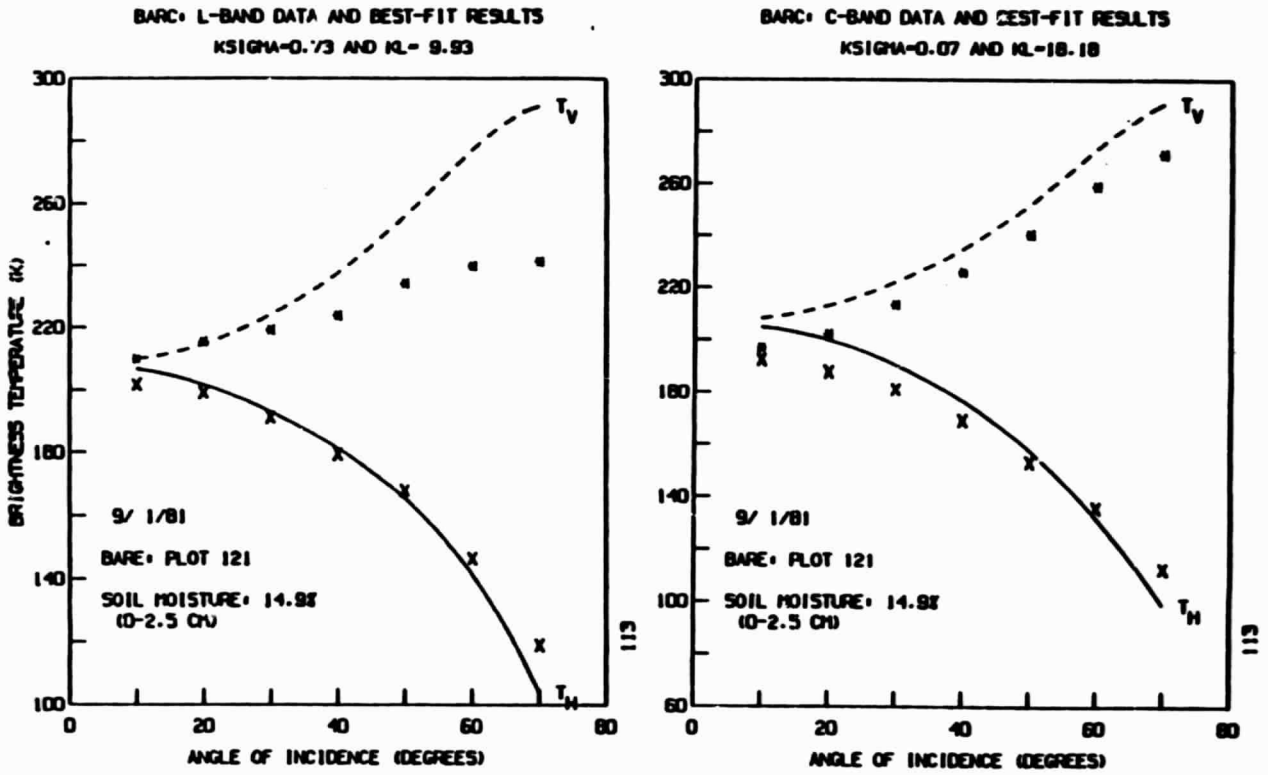
BARC: L-BAND DATA AND BEST-FIT RESULTS
KSIGMA=0.73 AND KL= 9.93
BARC: C-BAND DATA AND BEST-FIT RESULTS
KSIGMA=0.07 AND KL=18.18
BRIGHTNESS TEMPERATURE (K)
ANGLE OF INCIDENCE (DEGREES)
T_V
T_H
9/ 1/81
BARE: PLOT 121
SOIL MOISTURE: 14.9%
(0-2.5 CM)
113

Figure B-13

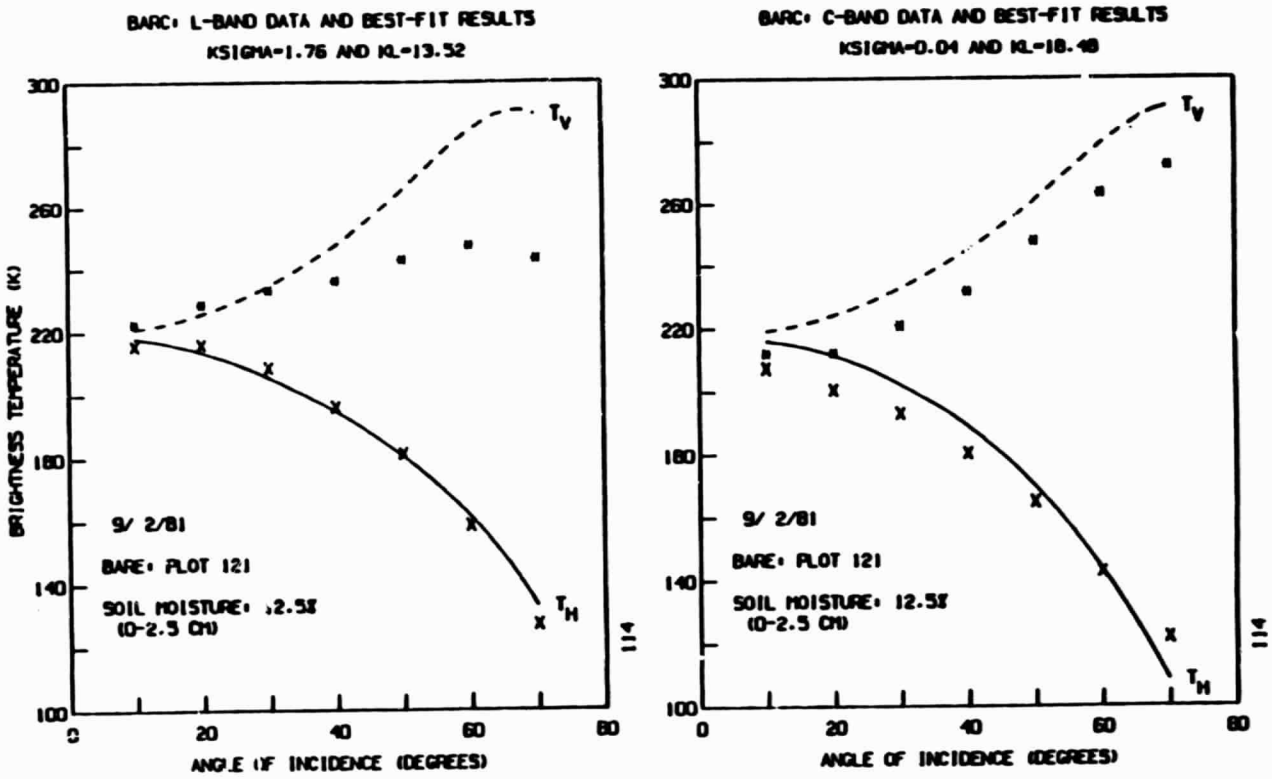
BARC: L-BAND DATA AND BEST-FIT RESULTS
KSIGMA=1.76 AND KL=13.52
BARC: C-BAND DATA AND BEST-FIT RESULTS
KSIGMA=0.04 AND KL=18.48
BRIGHTNESS TEMPERATURE (K)
ANGLE OF INCIDENCE (DEGREES)
T_V
T_H
9/ 2/81
BARE: PLOT 121
SOIL MOISTURE: 12.5%
(0-2.5 CM)
100
140
180
220
260
300
0
20
40
60
80
114

Figure B-14

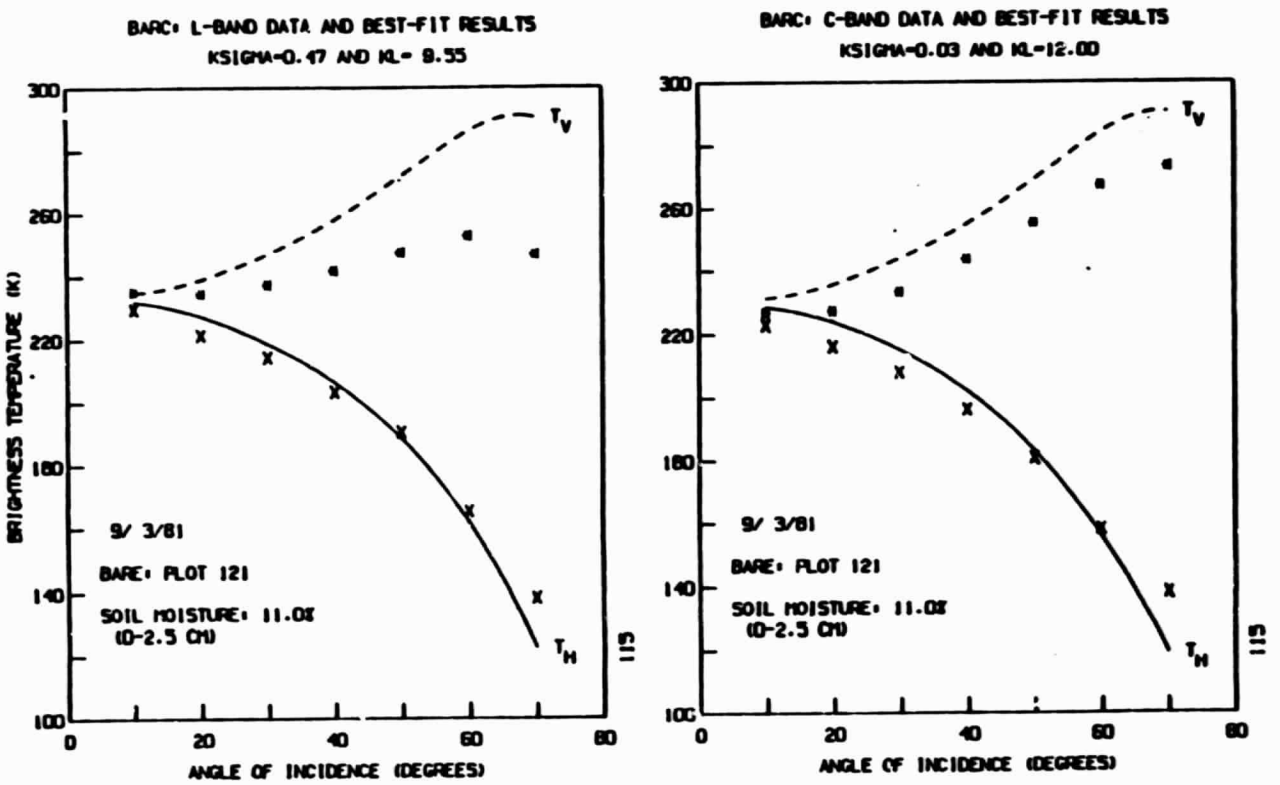
BARC: L-BAND DATA AND BEST-FIT RESULTS
KSIGMA=0.47 AND KL= 8.55
BRIGHTNESS TEMPERATURE (K)
300
260
220
180
140
100
0
20
40
60
80
ANGLE OF INCIDENCE (DEGREES)
T_V
T_H
9/ 3/81
BARE: PLOT 121
SOIL MOISTURE: 11.0%
(0-2.5 CM)
511
BARC: C-BAND DATA AND BEST-FIT RESULTS
KSIGMA=0.03 AND KL=12.00
300
260
220
180
140
100
0
20
40
60
80
ANGLE OF INCIDENCE (DEGREES)
T_V
T_H
9/ 3/81
BARE: PLOT 121
SOIL MOISTURE: 11.0%
(0-2.5 CM)
115

Figure B-15

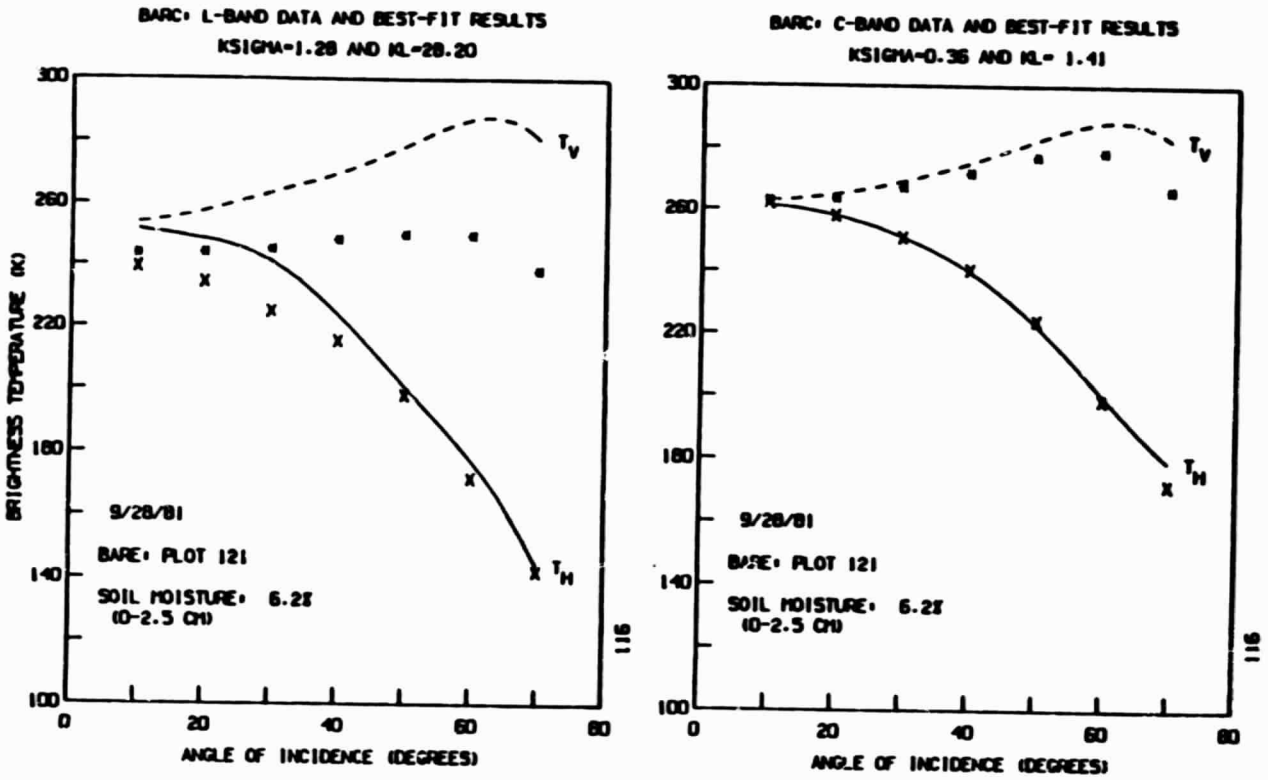
BARC: L-BAND DATA AND BEST-FIT RESULTS
KSIGMA=1.28 AND KL=28.20
BRIGHTNESS TEMPERATURE (K)
ANGLE OF INCIDENCE (DEGREES)
T_V
T_H
9/28/81
BARE: PLOT 121
SOIL MOISTURE: 6.2%
(0-2.5 CM)
BARC: C-BAND DATA AND BEST-FIT RESULTS
KSIGMA=0.36 AND KL= 1.41
ANGLE OF INCIDENCE (DEGREES)
T_V
T_H
9/28/81
BARE: PLOT 121
SOIL MOISTURE: 6.2%
(0-2.5 CM)

Figure B-16

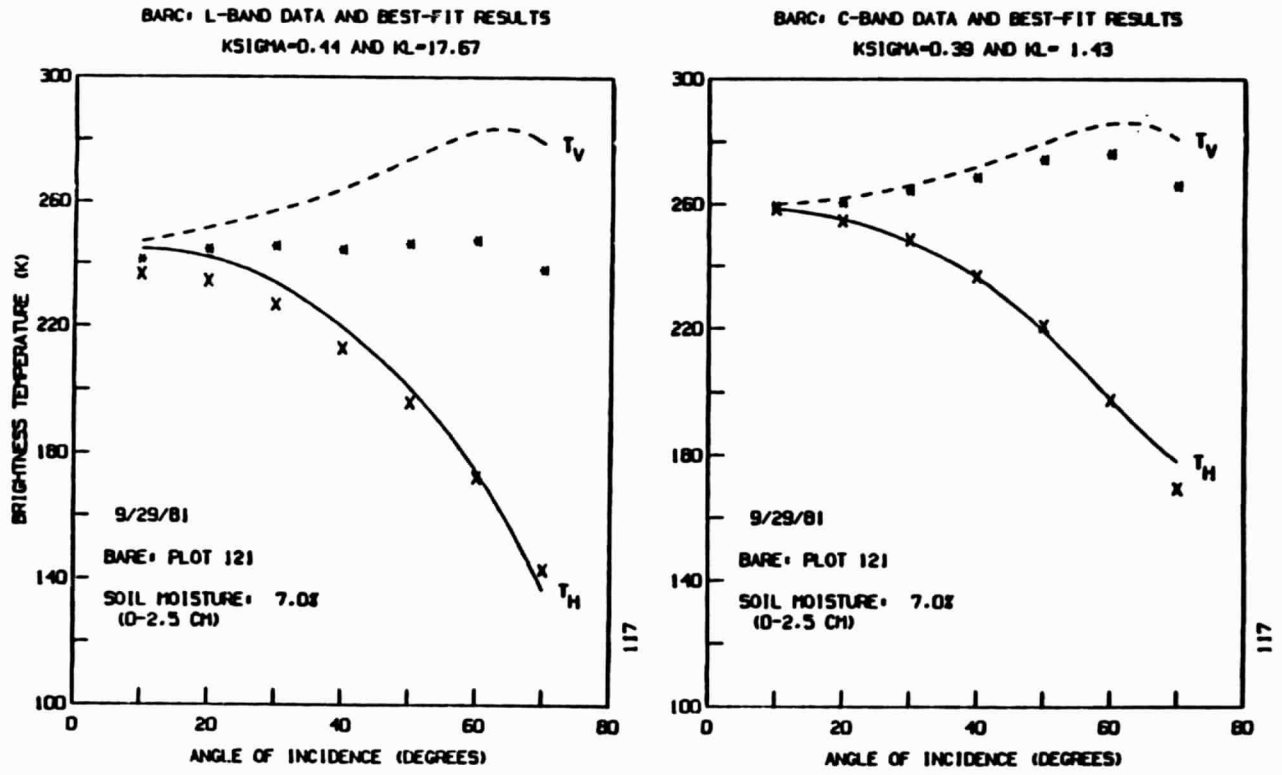
BARC: L-BAND DATA AND BEST-FIT RESULTS
KSIGMA=0.44 AND KL=17.67
BRIGHTNESS TEMPERATURE (K)
300
260
220
180
140
100
0
20
40
60
80
ANGLE OF INCIDENCE (DEGREES)
T_V
T_H
9/29/81
BARE: PLOT 121
SOIL MOISTURE: 7.0%
(0-2.5 CM)
117
BARC: C-BAND DATA AND BEST-FIT RESULTS
KSIGMA=0.39 AND KL= 1.43
300
260
220
180
140
100
0
20
40
60
80
ANGLE OF INCIDENCE (DEGREES)
T_V
T_H
9/29/81
BARE: PLOT 121
SOIL MOISTURE: 7.0%
(0-2.5 CM)
117

Figure B-17

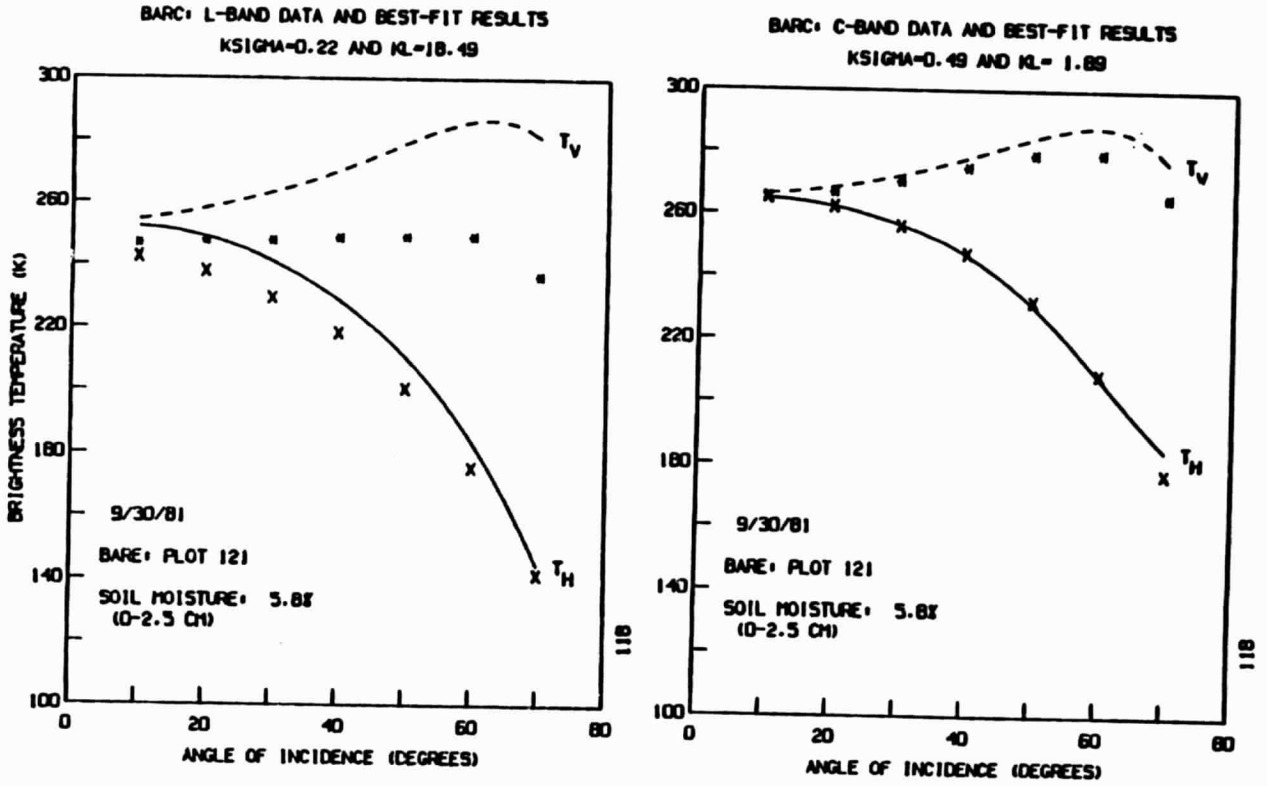
BARC: L-BAND DATA AND BEST-FIT RESULTS
KSIGMA=0.22 AND KL=18.49
BRIGHTNESS TEMPERATURE (K)
ANGLE OF INCIDENCE (DEGREES)
T_V
T_H
9/30/81
BARE: PLOT 121
SOIL MOISTURE: 5.8%
(0-2.5 CM)
BARC: C-BAND DATA AND BEST-FIT RESULTS
KSIGMA=0.49 AND KL= 1.89
ANGLE OF INCIDENCE (DEGREES)
T_V
T_H
9/30/81
BARE: PLOT 121
SOIL MOISTURE: 5.8%
(0-2.5 CM)

Figure B-18

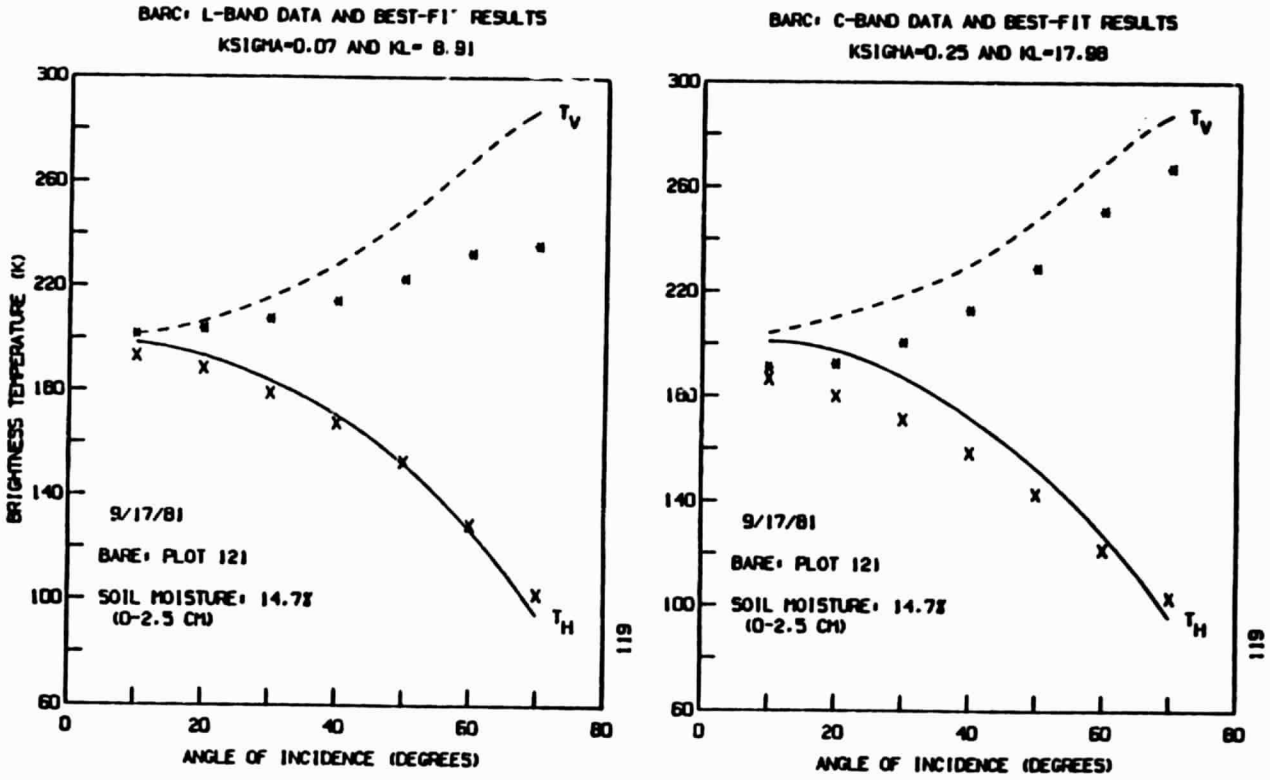
BARC: L-BAND DATA AND BEST-FIT RESULTS
KSIGMA=0.07 AND KL= 8.91
BRIGHTNESS TEMPERATURE (K)
300
260
220
180
140
100
60
0
20
40
60
80
ANGLE OF INCIDENCE (DEGREES)
T_V
T_H
9/17/81
BARE: PLOT 121
SOIL MOISTURE: 14.7%
(0-2.5 CM)
119
BARC: C-BAND DATA AND BEST-FIT RESULTS
KSIGMA=0.25 AND KL=17.98
300
260
220
180
140
100
60
0
20
40
60
80
ANGLE OF INCIDENCE (DEGREES)
T_V
T_H
9/17/81
BARE: PLOT 121
SOIL MOISTURE: 14.7%
(0-2.5 CM)
119

Figure B-19

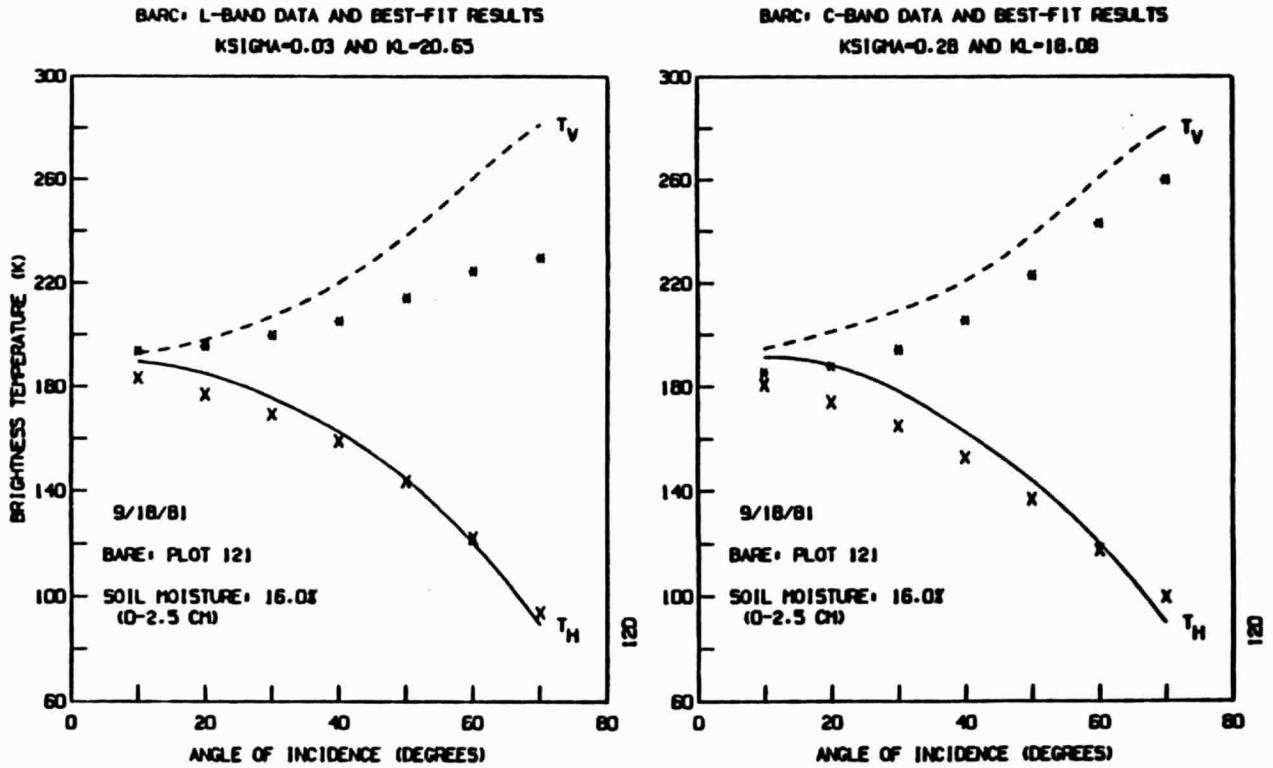
BARC: L-BAND DATA AND BEST-FIT RESULTS
KSIGMA=0.03 AND KL=20.65
BARC: C-BAND DATA AND BEST-FIT RESULTS
KSIGMA=0.28 AND KL=18.08
BRIGHTNESS TEMPERATURE (K)
ANGLE OF INCIDENCE (DEGREES)
T_V
T_H
9/18/81
BARE: PLOT 121
SOIL MOISTURE: 16.0%
(0-2.5 CM)
300
260
220
180
140
100
60
0
20
40
60
80
120

Figure B-20

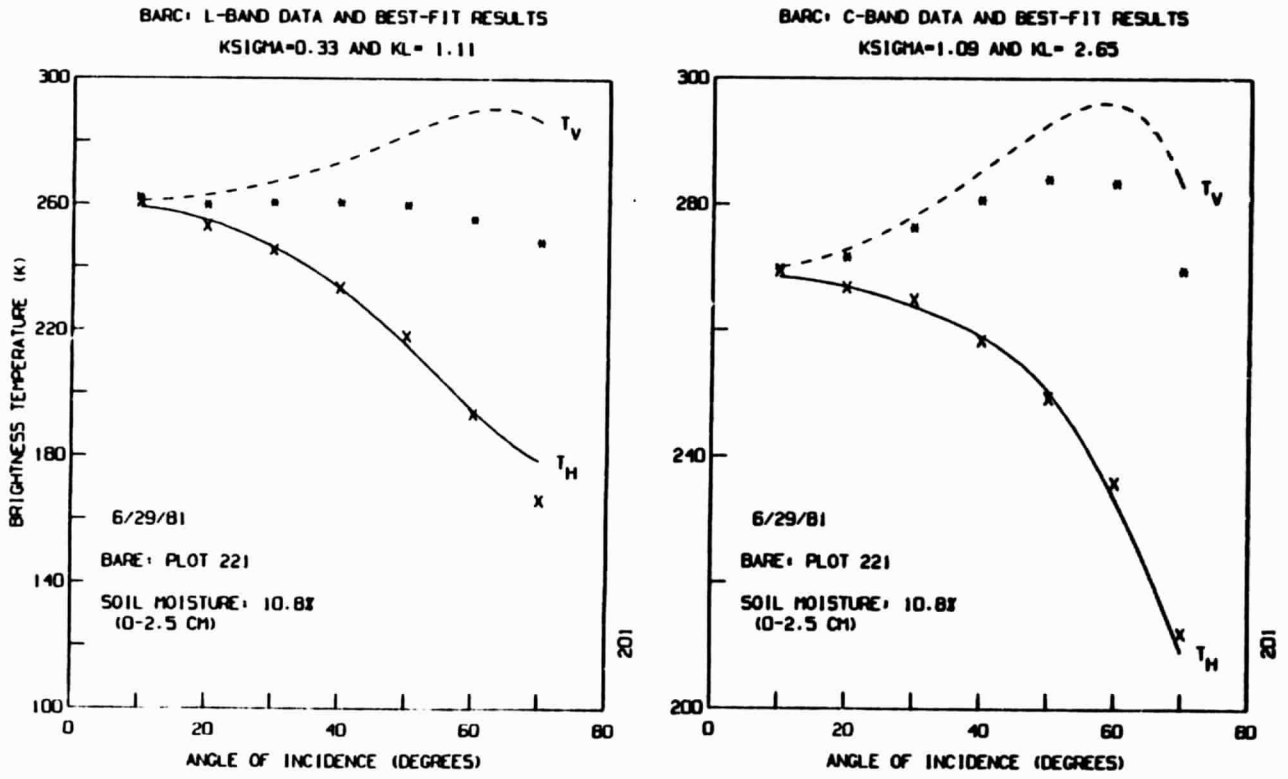
BARC: L-BAND DATA AND BEST-FIT RESULTS
KSIGMA=0.33 AND KL= 1.11
BRIGHTNESS TEMPERATURE (K)
300
260
220
180
140
100
0
20
40
60
80
ANGLE OF INCIDENCE (DEGREES)
T_V
T_H
6/29/81
BARE: PLOT 221
SOIL MOISTURE: 10.8%
(0-2.5 CM)
201
BARC: C-BAND DATA AND BEST-FIT RESULTS
KSIGMA=1.09 AND KL= 2.65
300
280
240
200
0
20
40
60
80
ANGLE OF INCIDENCE (DEGREES)
T_V
T_H
6/29/81
BARE: PLOT 221
SOIL MOISTURE: 10.8%
(0-2.5 CM)
201

Figure B-21

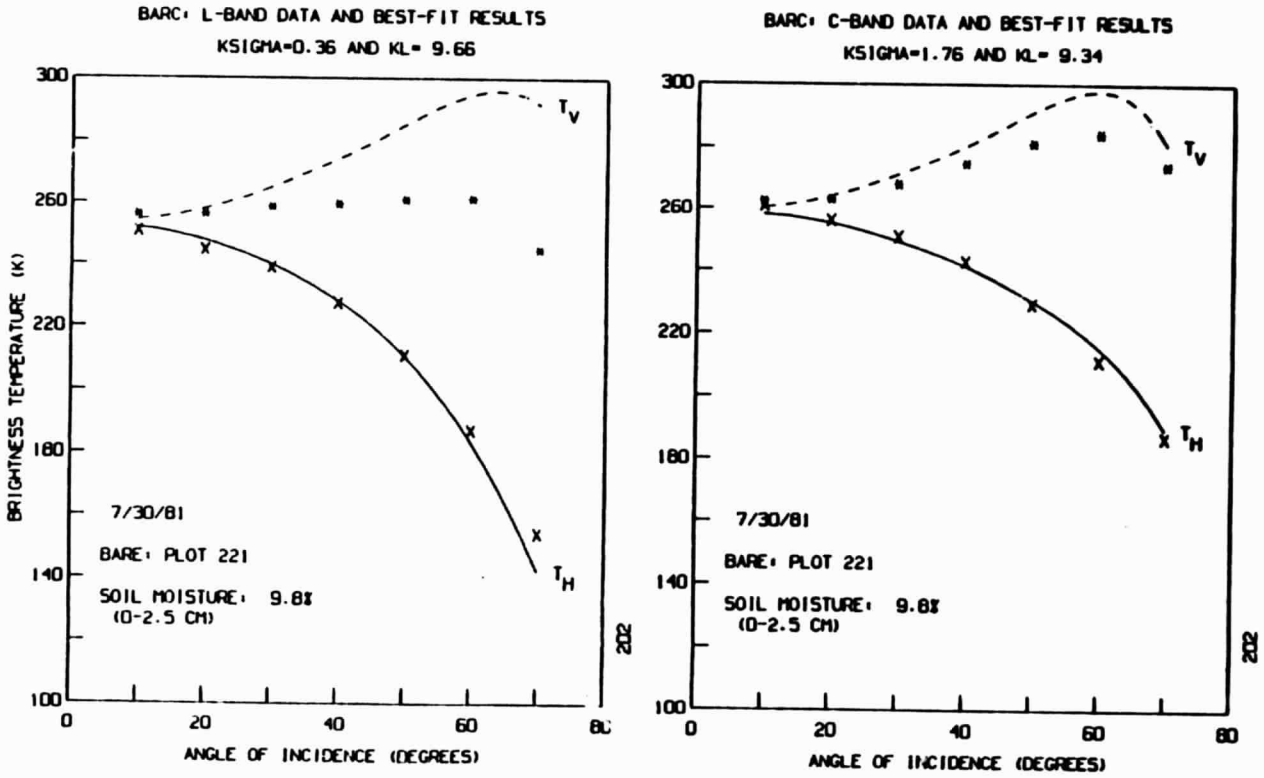
BARC: L-BAND DATA AND BEST-FIT RESULTS
KSIGMA=0.36 AND KL= 9.66
BRIGHTNESS TEMPERATURE (K)
300
260
220
180
140
100
0
20
40
60
80
ANGLE OF INCIDENCE (DEGREES)
T_V
T_H
7/30/81
BARE: PLOT 221
SOIL MOISTURE: 9.8%
(0-2.5 CM)
202
BARC: C-BAND DATA AND BEST-FIT RESULTS
KSIGMA=1.76 AND KL= 9.34
300
260
220
180
140
100
0
20
40
60
80
ANGLE OF INCIDENCE (DEGREES)
T_V
T_H
7/30/81
BARE: PLOT 221
SOIL MOISTURE: 9.8%
(0-2.5 CM)
202

Figure B-22

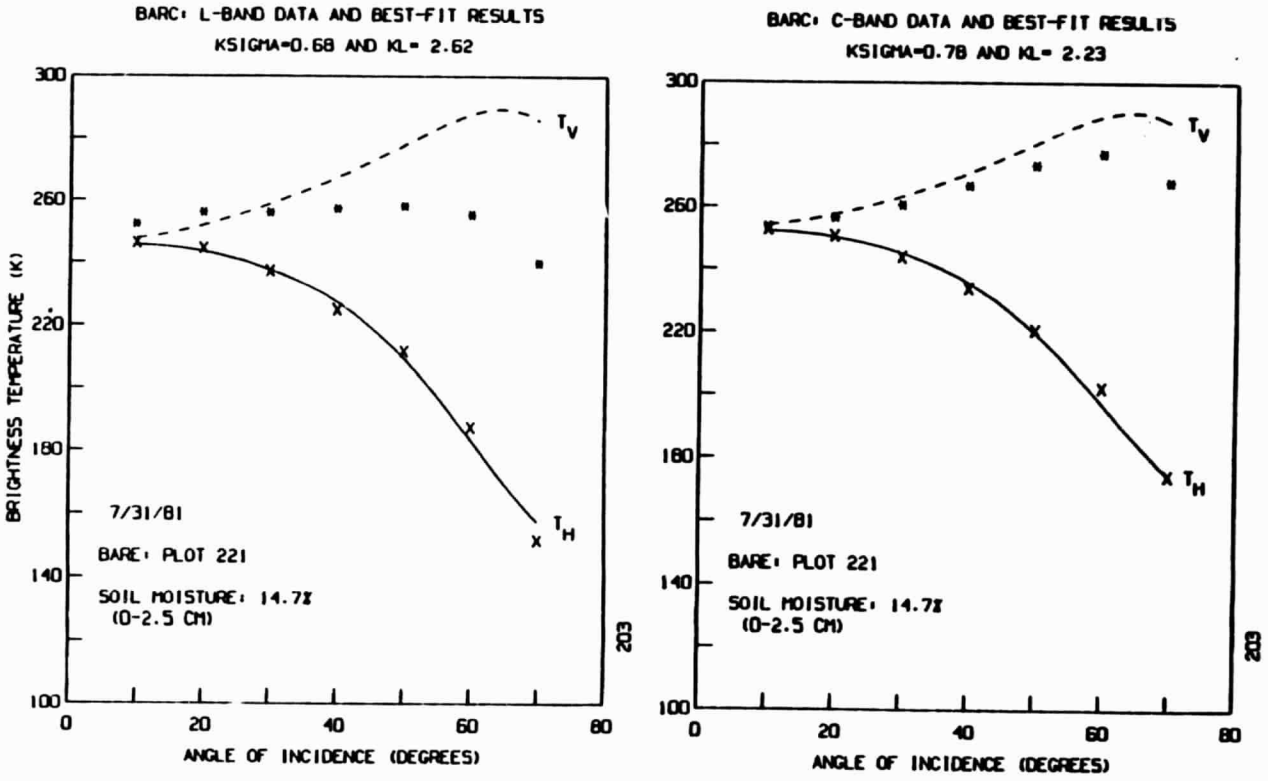
BARC: L-BAND DATA AND BEST-FIT RESULTS
KSIGMA=0.68 AND KL= 2.62
BRIGHTNESS TEMPERATURE (K)
300
260
220
180
140
100
0
20
40
60
80
ANGLE OF INCIDENCE (DEGREES)
T_V
T_H
7/31/81
BARE: PLOT 221
SOIL MOISTURE: 14.7%
(0-2.5 CM)
203
BARC: C-BAND DATA AND BEST-FIT RESULTS
KSIGMA=0.78 AND KL= 2.23
300
260
220
180
140
100
0
20
40
60
80
ANGLE OF INCIDENCE (DEGREES)
T_V
T_H
7/31/81
BARE: PLOT 221
SOIL MOISTURE: 14.7%
(0-2.5 CM)
203

Figure B-23

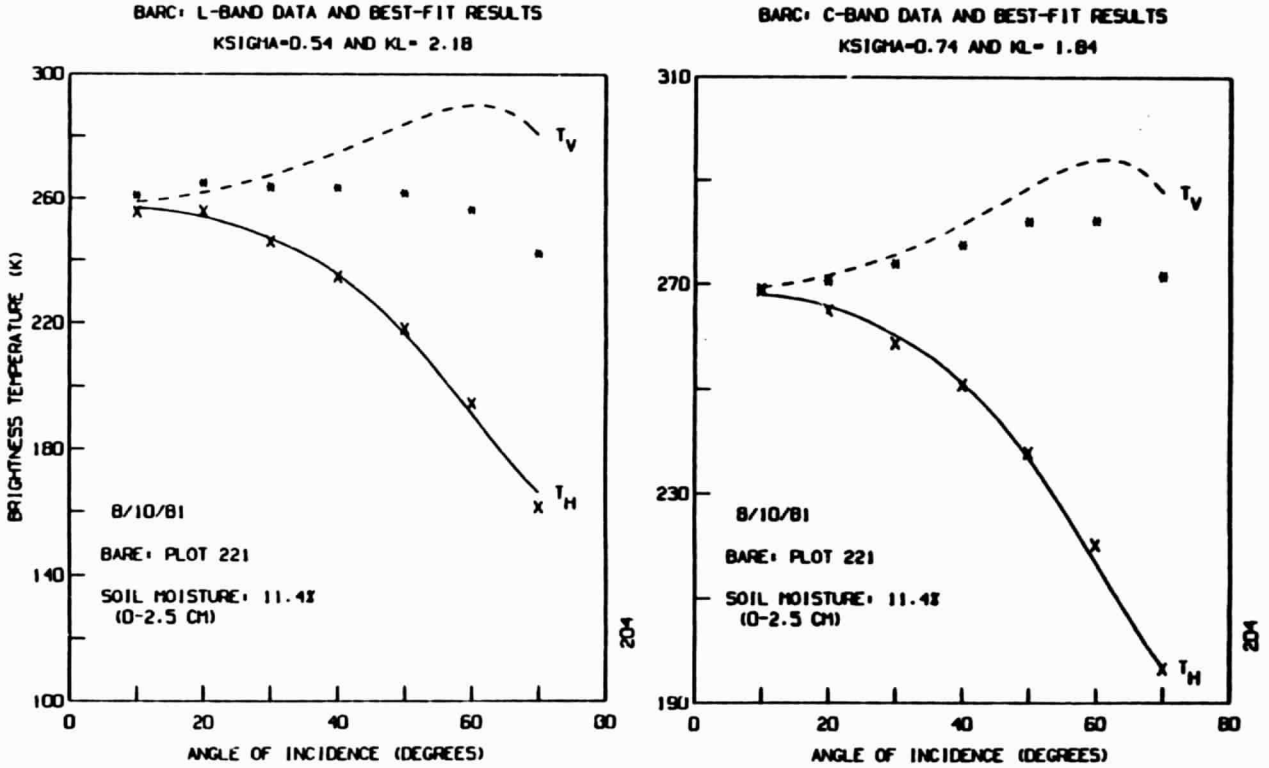
BARC: L-BAND DATA AND BEST-FIT RESULTS
KSIGMA=0.54 AND KL= 2.18
BRIGHTNESS TEMPERATURE (K)
300
260
220
180
140
100
0
20
40
60
80
ANGLE OF INCIDENCE (DEGREES)
T_V
T_H
8/10/81
BARE: PLOT 221
SOIL MOISTURE: 11.4%
(0-2.5 CM)
204
BARC: C-BAND DATA AND BEST-FIT RESULTS
KSIGMA=0.74 AND KL= 1.84
310
270
230
190
0
20
40
60
80
ANGLE OF INCIDENCE (DEGREES)
T_V
T_H
8/10/81
BARE: PLOT 221
SOIL MOISTURE: 11.4%
(0-2.5 CM)
204

Figure B-24

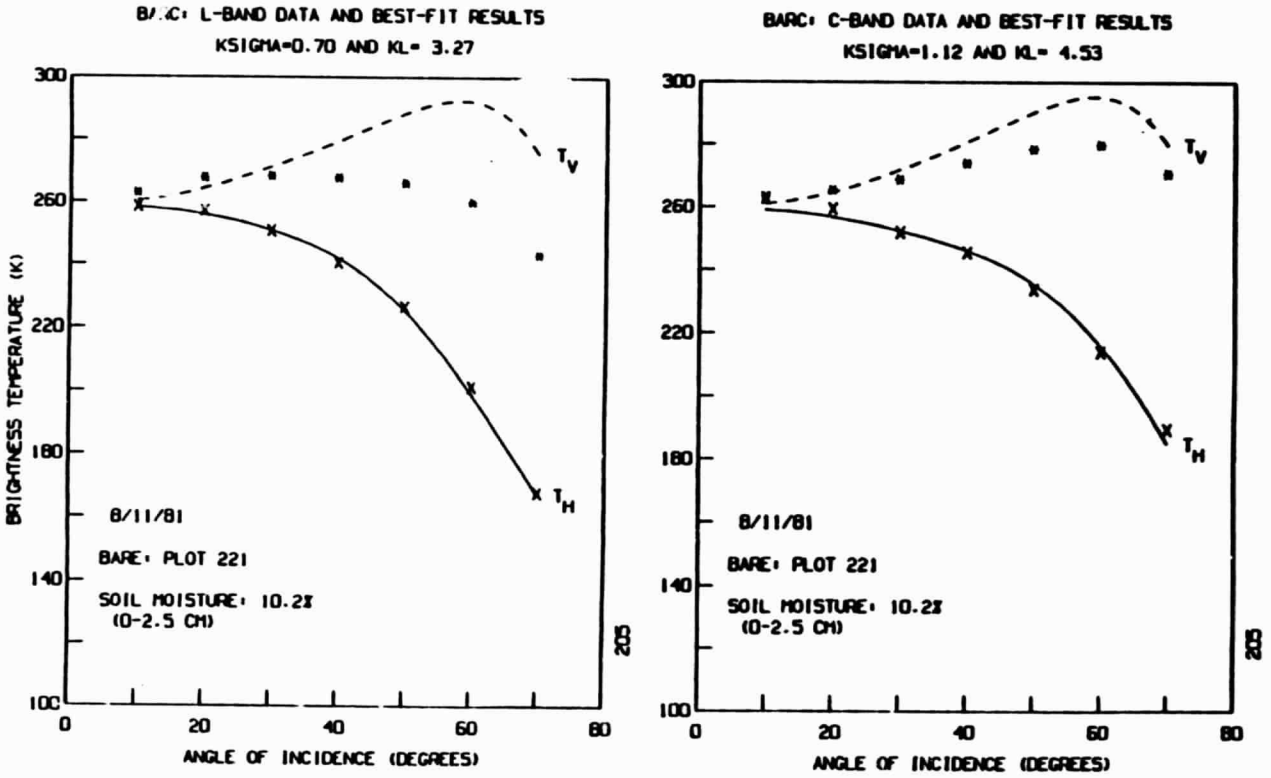
BARC: L-BAND DATA AND BEST-FIT RESULTS
KSIGMA=0.70 AND KL= 3.27
BRIGHTNESS TEMPERATURE (K)
300
260
220
180
140
100
0
20
40
60
80
ANGLE OF INCIDENCE (DEGREES)
T_V
T_H
8/11/81
BARE: PLOT 221
SOIL MOISTURE: 10.2%
(0-2.5 CM)
205
BARC: C-BAND DATA AND BEST-FIT RESULTS
KSIGMA=1.12 AND KL= 4.53
300
260
220
180
140
100
0
20
40
60
80
ANGLE OF INCIDENCE (DEGREES)
T_V
T_H
8/11/81
BARE: PLOT 221
SOIL MOISTURE: 10.2%
(0-2.5 CM)
205

Figure B-25

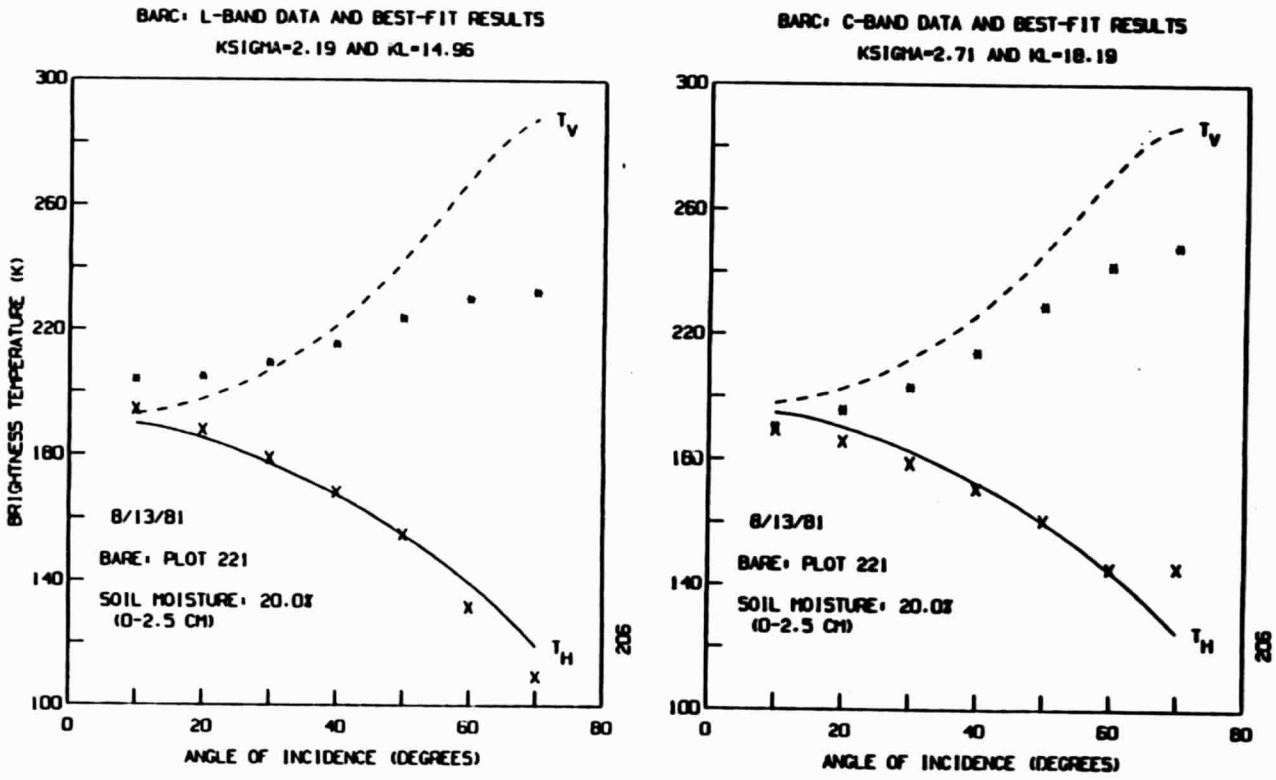
BARC: L-BAND DATA AND BEST-FIT RESULTS
KSIGMA=2.19 AND KL=14.96
BRIGHTNESS TEMPERATURE (K)
ANGLE OF INCIDENCE (DEGREES)
T_V
T_H
8/13/81
BARE: PLOT 221
SOIL MOISTURE: 20.0%
(0-2.5 CM)
BARC: C-BAND DATA AND BEST-FIT RESULTS
KSIGMA=2.71 AND KL=18.19
ANGLE OF INCIDENCE (DEGREES)
T_V
T_H
8/13/81
BARE: PLOT 221
SOIL MOISTURE: 20.0%
(0-2.5 CM)

Figure B-26

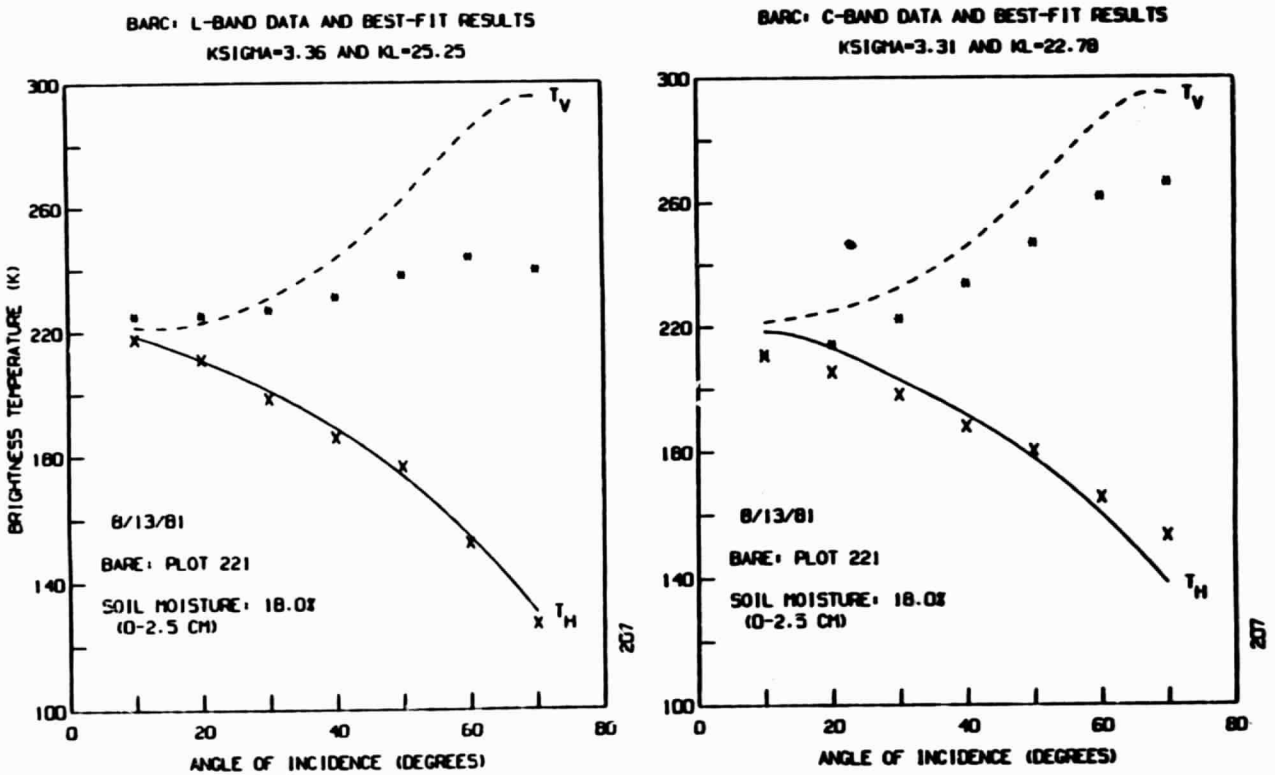
BARC: L-BAND DATA AND BEST-FIT RESULTS
KSIGMA=3.36 AND KL=25.25
BRIGHTNESS TEMPERATURE (K)
300
260
220
180
140
100
0
20
40
60
80
ANGLE OF INCIDENCE (DEGREES)
T_V
T_H
8/13/81
BARE: PLOT 221
SOIL MOISTURE: 18.0%
(0-2.5 CM)
207
BARC: C-BAND DATA AND BEST-FIT RESULTS
KSIGMA=3.31 AND KL=22.78
300
260
220
180
140
100
0
20
40
60
80
ANGLE OF INCIDENCE (DEGREES)
T_V
T_H
8/13/81
BARE: PLOT 221
SOIL MOISTURE: 18.0%
(0-2.5 CM)
207

Figure B-27

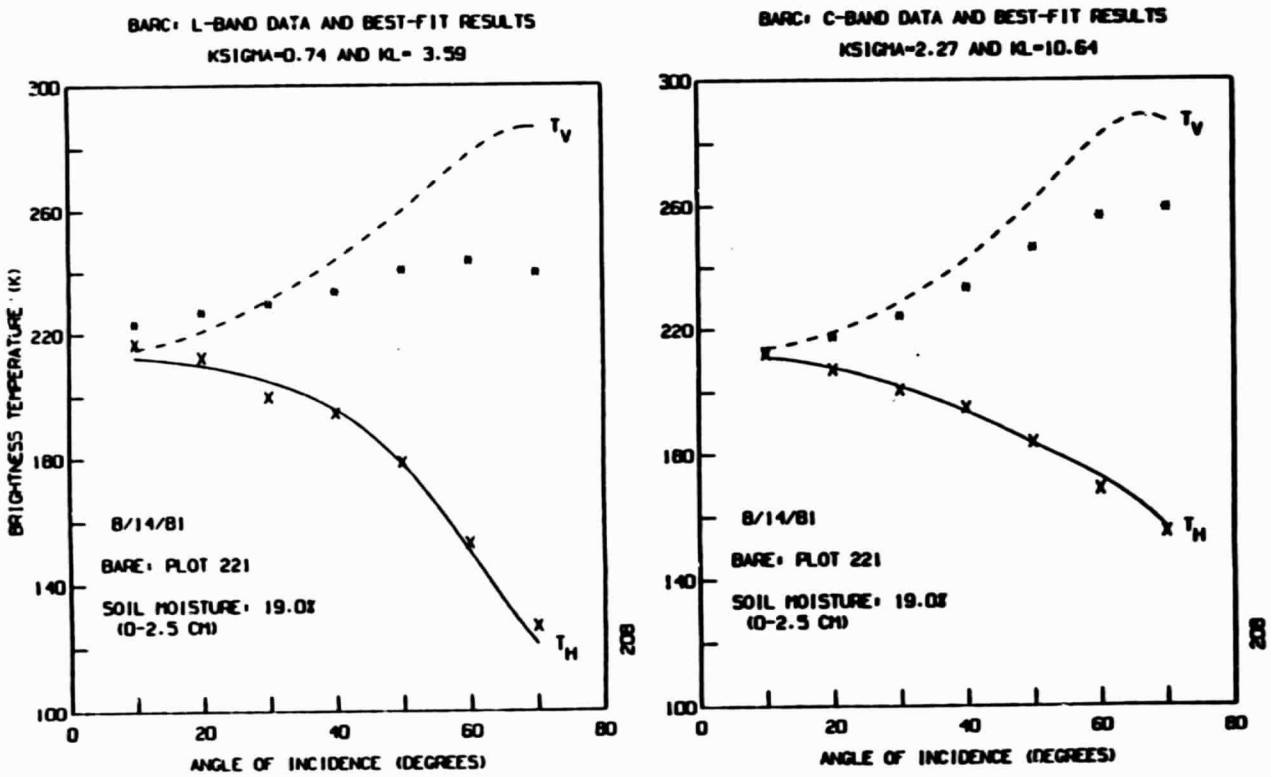
BARC: L-BAND DATA AND BEST-FIT RESULTS
KSIGMA=0.74 AND KL= 3.59
BRIGHTNESS TEMPERATURE (K)
300
260
220
180
140
100
0
20
40
60
80
ANGLE OF INCIDENCE (DEGREES)
T_V
T_H
8/14/81
BARE: PLOT 221
SOIL MOISTURE: 19.0%
(0-2.5 CM)
208
BARC: C-BAND DATA AND BEST-FIT RESULTS
KSIGMA=2.27 AND KL=10.64
300
260
220
180
140
100
0
20
40
60
80
ANGLE OF INCIDENCE (DEGREES)
T_V
T_H
8/14/81
BARE: PLOT 221
SOIL MOISTURE: 19.0%
(0-2.5 CM)
208

Figure B-28

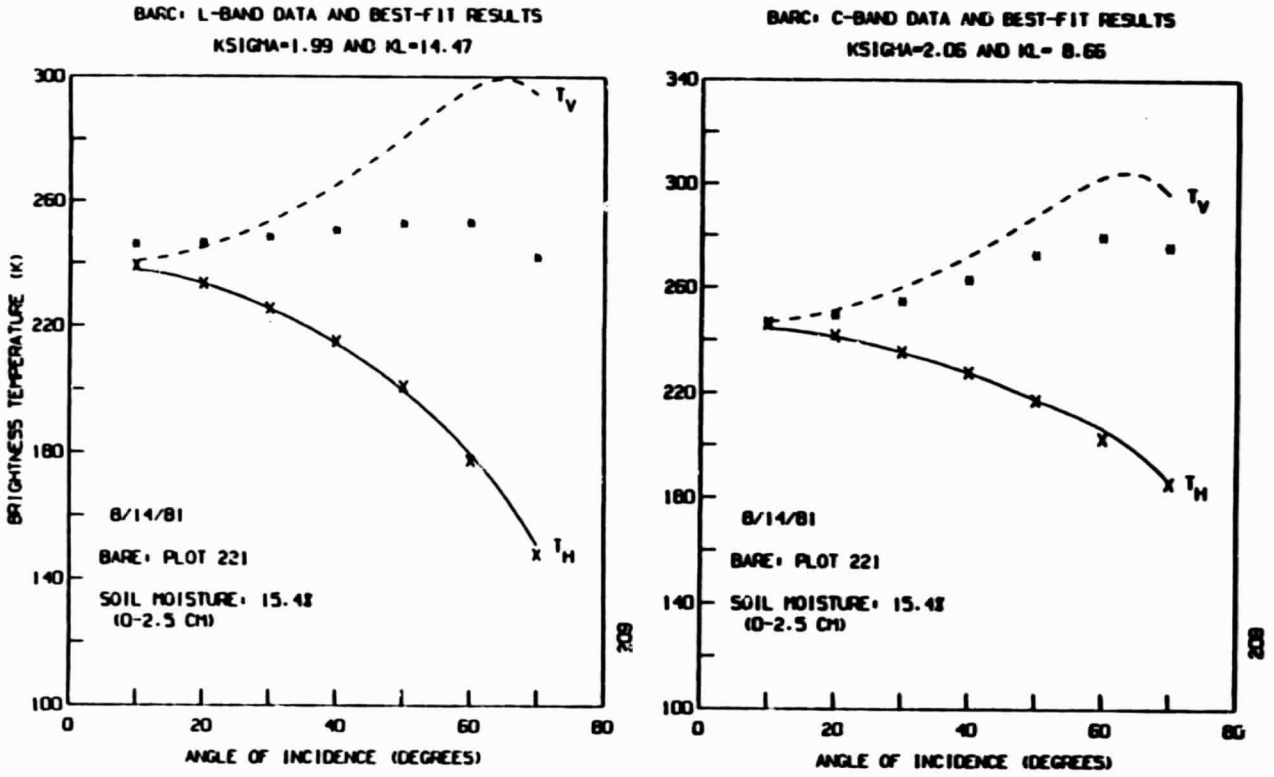
BARC: L-BAND DATA AND BEST-FIT RESULTS
KSIGMA=1.99 AND KL=14.47
BRIGHTNESS TEMPERATURE (K)
300
260
220
180
140
100
0
20
40
60
80
ANGLE OF INCIDENCE (DEGREES)
T_V
T_H
8/14/81
BARE: PLOT 221
SOIL MOISTURE: 15.4%
(0-2.5 CM)
BARC: C-BAND DATA AND BEST-FIT RESULTS
KSIGMA=2.06 AND KL= 8.66
340
300
260
220
180
140
100
0
20
40
60
80
ANGLE OF INCIDENCE (DEGREES)
T_V
T_H
8/14/81
BARE: PLOT 221
SOIL MOISTURE: 15.4%
(0-2.5 CM)

Figure B-29

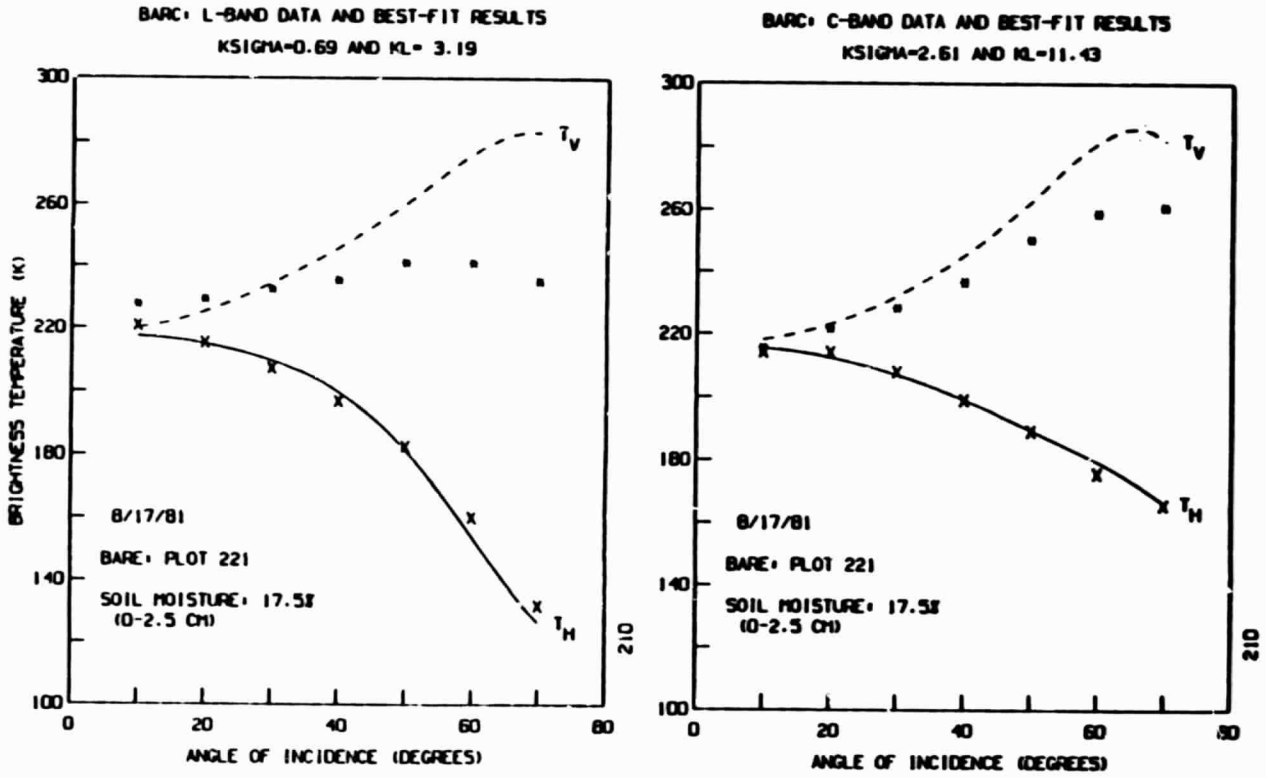
BARC: L-BAND DATA AND BEST-FIT RESULTS
KSIGMA=0.69 AND KL= 3.19
BARC: C-BAND DATA AND BEST-FIT RESULTS
KSIGMA=2.61 AND KL=11.43
BRIGHTNESS TEMPERATURE (K)
ANGLE OF INCIDENCE (DEGREES)
T_V
T_H
8/17/81
BARE: PLOT 221
SOIL MOISTURE: 17.5%
(0-2.5 CM)
300
260
220
180
140
100
0
20
40
60
80
210

Figure B-30

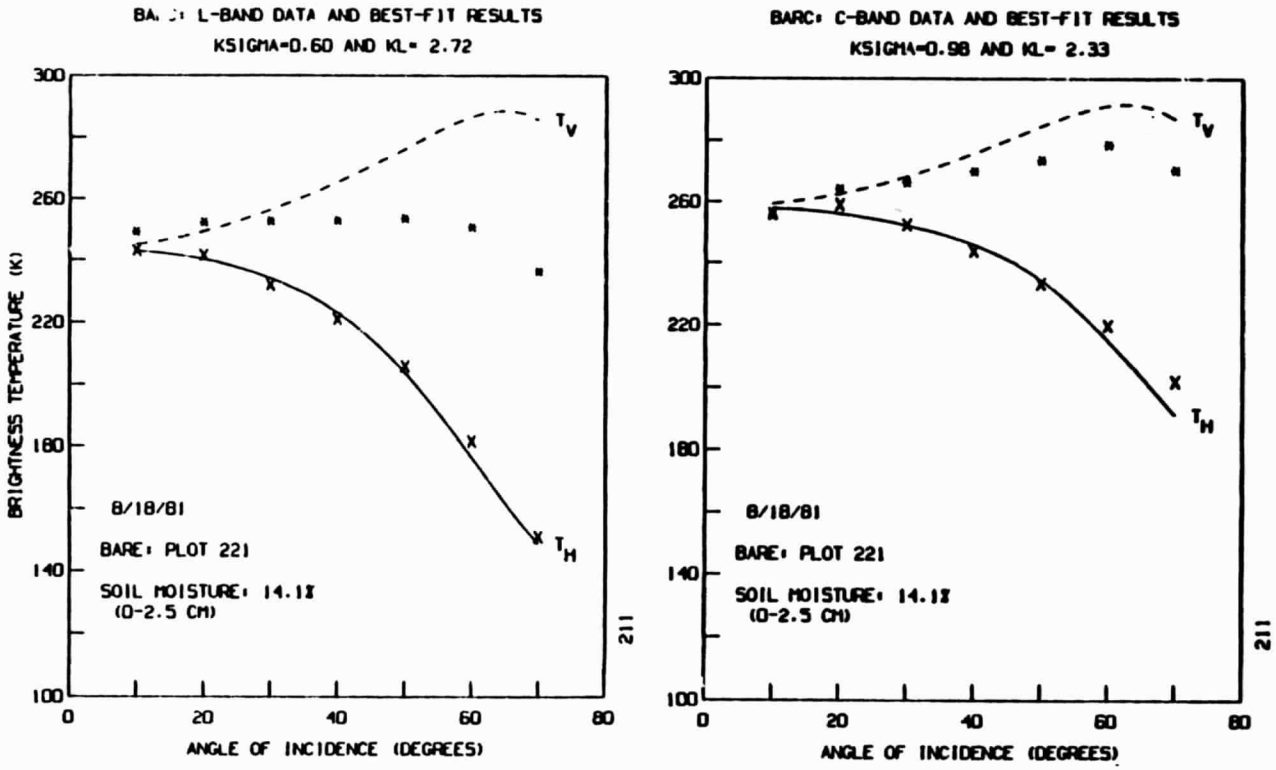
BA : L-BAND DATA AND BEST-FIT RESULTS
KSIGMA=0.60 AND KL= 2.72
BRIGHTNESS TEMPERATURE (K)
300
260
220
180
140
100
0
20
40
60
80
ANGLE OF INCIDENCE (DEGREES)
T_V
T_H
8/18/81
BARE: PLOT 221
SOIL MOISTURE: 14.1%
(0-2.5 CM)
211
BARC: C-BAND DATA AND BEST-FIT RESULTS
KSIGMA=0.98 AND KL= 2.33
300
260
220
180
140
100
0
20
40
60
80
ANGLE OF INCIDENCE (DEGREES)
T_V
T_H
8/18/81
BARE: PLOT 221
SOIL MOISTURE: 14.1%
(0-2.5 CM)
211

Figure B-31

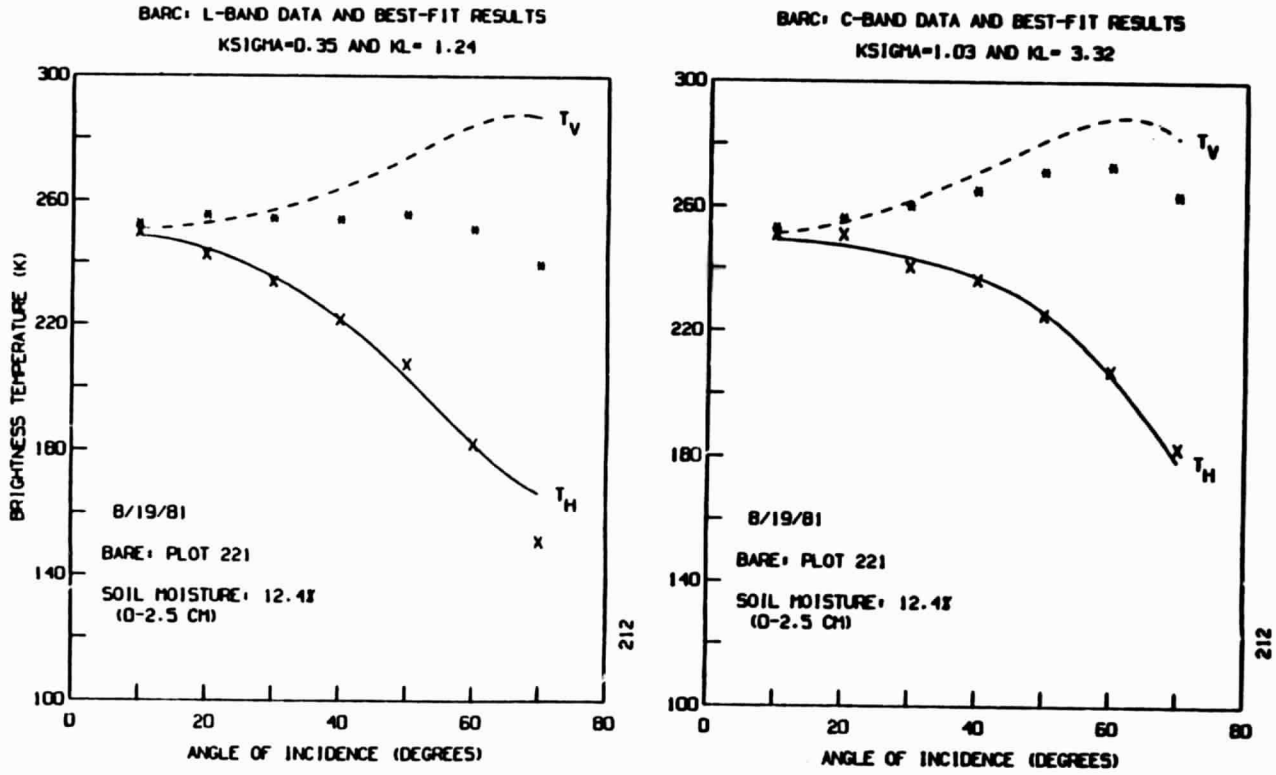
BARC: L-BAND DATA AND BEST-FIT RESULTS
KSIGMA=0.35 AND KL= 1.24
BRIGHTNESS TEMPERATURE (K)
300
260
220
180
140
100
0
20
40
60
80
212
T_V
T_H
8/19/81
BARE: PLOT 221
SOIL MOISTURE: 12.4%
(0-2.5 CM)
ANGLE OF INCIDENCE (DEGREES)
BARC: C-BAND DATA AND BEST-FIT RESULTS
KSIGMA=1.03 AND KL= 3.32
300
260
220
180
140
100
0
20
40
60
80
212
T_V
T_H
8/19/81
BARE: PLOT 221
SOIL MOISTURE: 12.4%
(0-2.5 CM)
ANGLE OF INCIDENCE (DEGREES)

Figure B-32

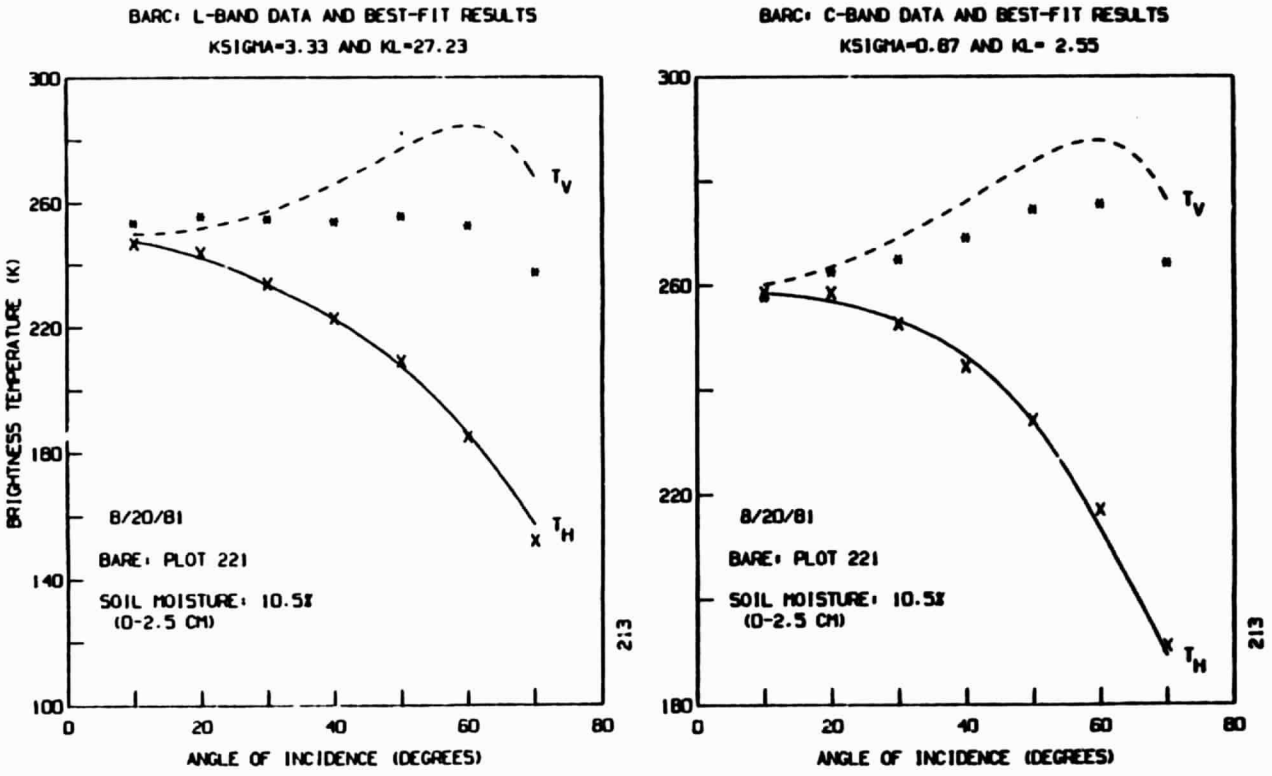
BARC: L-BAND DATA AND BEST-FIT RESULTS
KSIGMA=3.33 AND KL=27.23
BRIGHTNESS TEMPERATURE (K)
300
260
220
180
140
100
0
20
40
60
80
ANGLE OF INCIDENCE (DEGREES)
T_V
T_H
8/20/81
BARE: PLOT 221
SOIL MOISTURE: 10.5%
(0-2.5 CM)
213
BARC: C-BAND DATA AND BEST-FIT RESULTS
KSIGMA=0.87 AND KL= 2.55
300
260
220
180
0
20
40
60
80
ANGLE OF INCIDENCE (DEGREES)
T_V
T_H
8/20/81
BARE: PLOT 221
SOIL MOISTURE: 10.5%
(0-2.5 CM)
213

Figure B-33

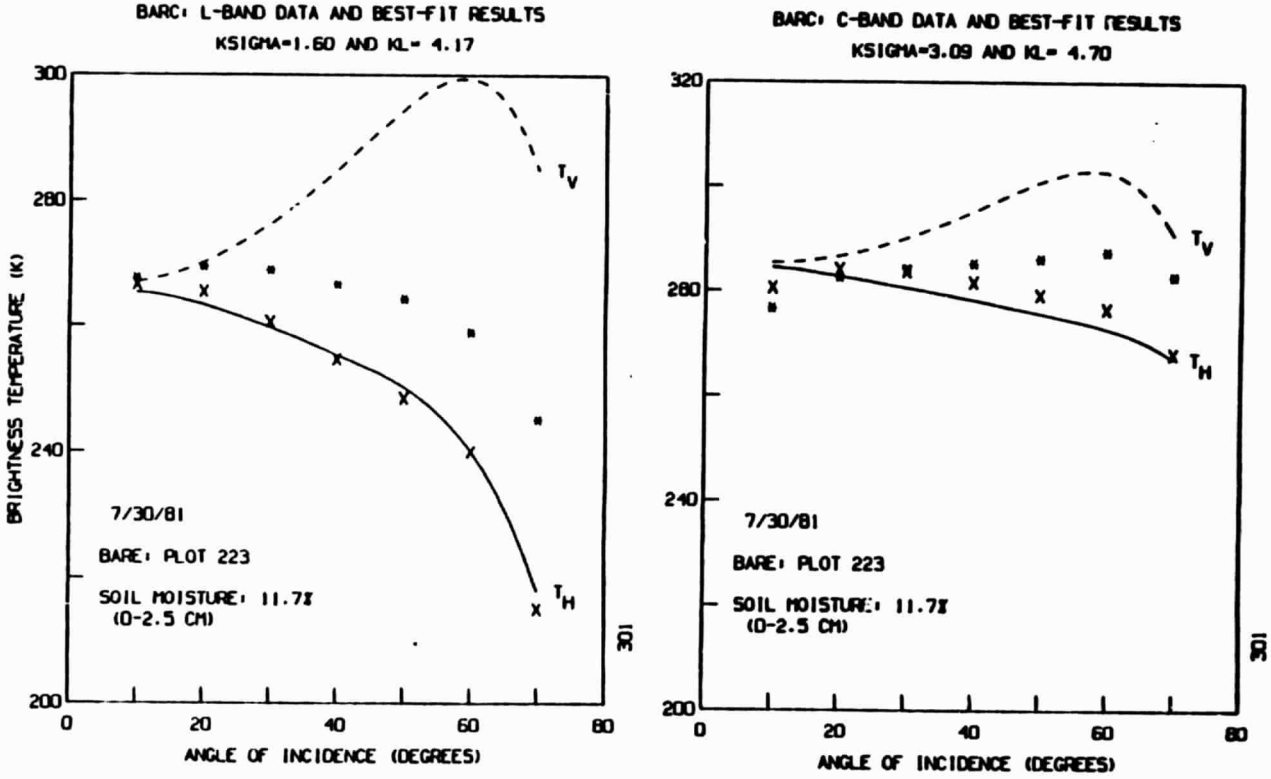
BARC: L-BAND DATA AND BEST-FIT RESULTS
KSIGMA=1.60 AND KL= 4.17
BRIGHTNESS TEMPERATURE (K)
300
280
240
200
0
20
40
60
80
ANGLE OF INCIDENCE (DEGREES)
T_V
T_H
7/30/81
BARE: PLOT 223
SOIL MOISTURE: 11.7%
(0-2.5 CM)
301
BARC: C-BAND DATA AND BEST-FIT RESULTS
KSIGMA=3.09 AND KL= 4.70
320
280
240
200
0
20
40
60
80
ANGLE OF INCIDENCE (DEGREES)
T_V
T_H
7/30/81
BARE: PLOT 223
SOIL MOISTURE: 11.7%
(0-2.5 CM)
301

Figure B-34

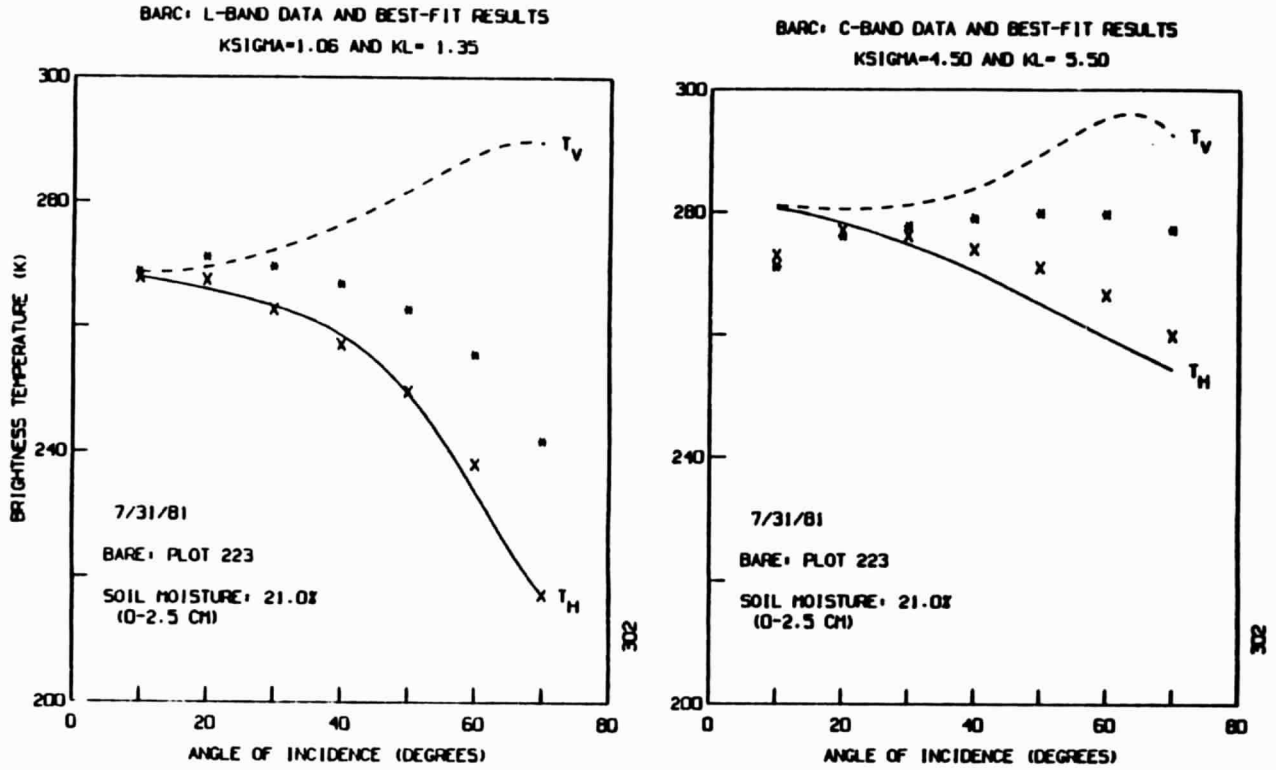
BARC: L-BAND DATA AND BEST-FIT RESULTS
KSIGMA=1.06 AND KL= 1.35
BRIGHTNESS TEMPERATURE (K)
300
280
240
200
0
20
40
60
80
ANGLE OF INCIDENCE (DEGREES)
T_V
T_H
7/31/81
BARE: PLOT 223
SOIL MOISTURE: 21.0%
(0-2.5 CM)
302
BARC: C-BAND DATA AND BEST-FIT RESULTS
KSIGMA=4.50 AND KL= 5.50
300
280
240
200
0
20
40
60
80
ANGLE OF INCIDENCE (DEGREES)
T_V
T_H
7/31/81
BARE: PLOT 223
SOIL MOISTURE: 21.0%
(0-2.5 CM)
302

Figure B-35

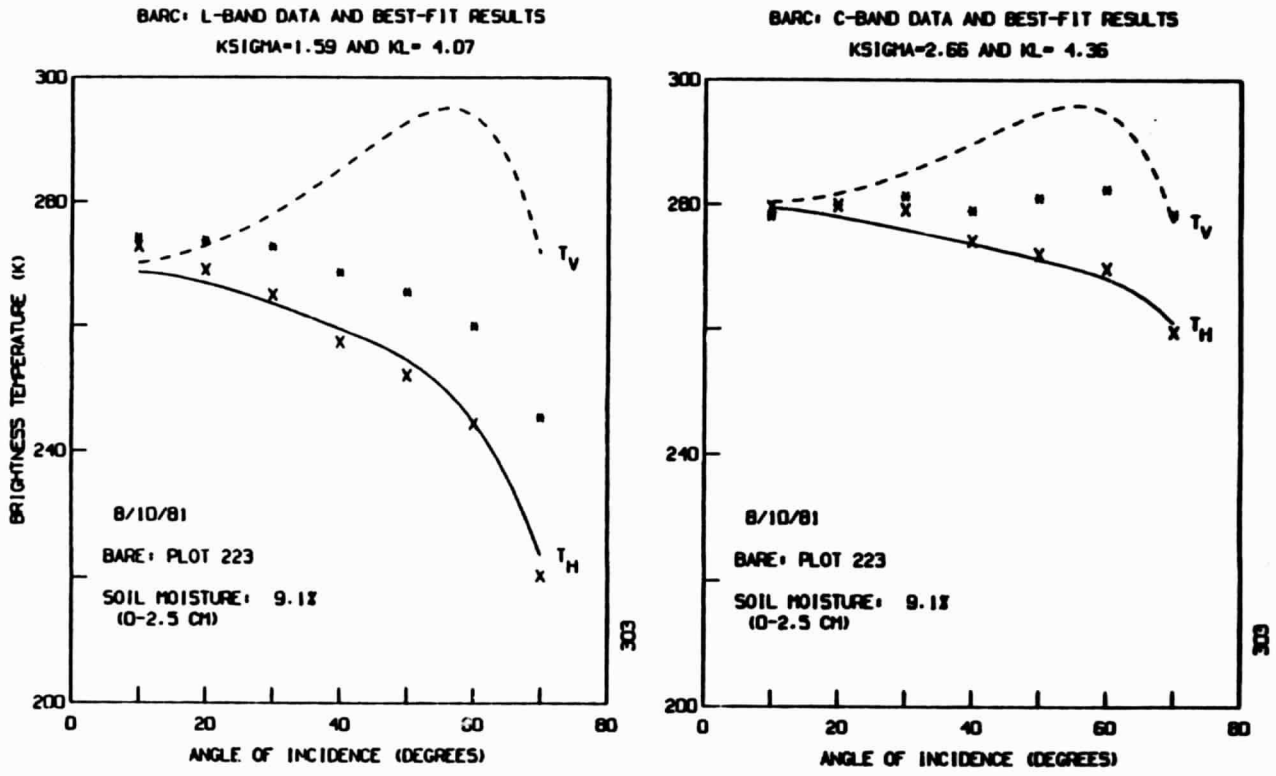
BARC: L-BAND DATA AND BEST-FIT RESULTS
KSIGMA=1.59 AND KL= 4.07
BRIGHTNESS TEMPERATURE (K)
300
280
240
200
0
20
40
60
80
ANGLE OF INCIDENCE (DEGREES)
T_V
T_H
8/10/81
BARE: PLOT 223
SOIL MOISTURE: 9.1%
(0-2.5 CM)
303
BARC: C-BAND DATA AND BEST-FIT RESULTS
KSIGMA=2.66 AND KL= 4.36
300
280
240
200
0
20
40
60
80
ANGLE OF INCIDENCE (DEGREES)
T_V
T_H
8/10/81
BARE: PLOT 223
SOIL MOISTURE: 9.1%
(0-2.5 CM)
303

Figure B-36

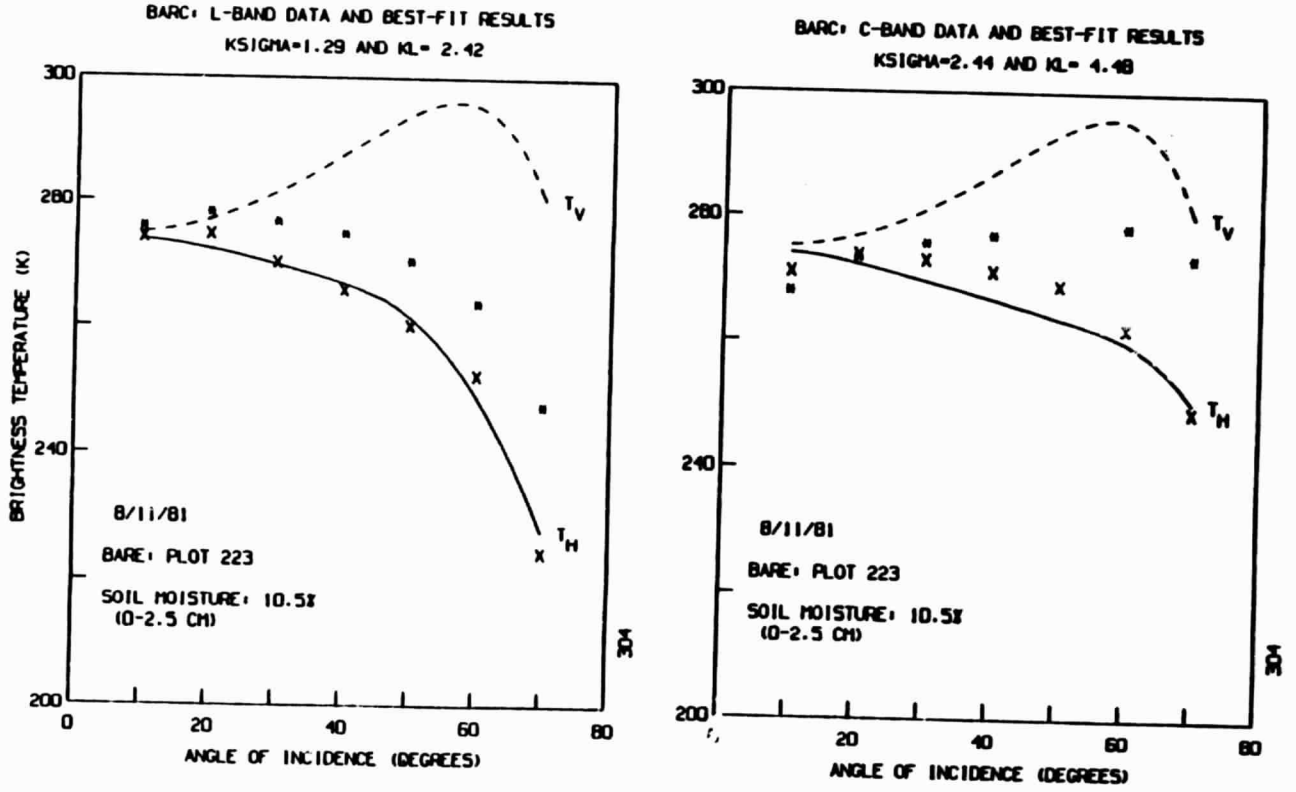
BARC: L-BAND DATA AND BEST-FIT RESULTS
KSIGMA=1.29 AND KL= 2.42
BRIGHTNESS TEMPERATURE (K)
300
280
240
200
0
20
40
60
80
ANGLE OF INCIDENCE (DEGREES)
T_V
T_H
8/11/81
BARE: PLOT 223
SOIL MOISTURE: 10.5%
(0-2.5 CM)
304
BARC: C-BAND DATA AND BEST-FIT RESULTS
KSIGMA=2.44 AND KL= 4.48
300
280
240
200
20
40
60
80
ANGLE OF INCIDENCE (DEGREES)
T_V
T_H
8/11/81
BARE: PLOT 223
SOIL MOISTURE: 10.5%
(0-2.5 CM)
304

Figure B-37

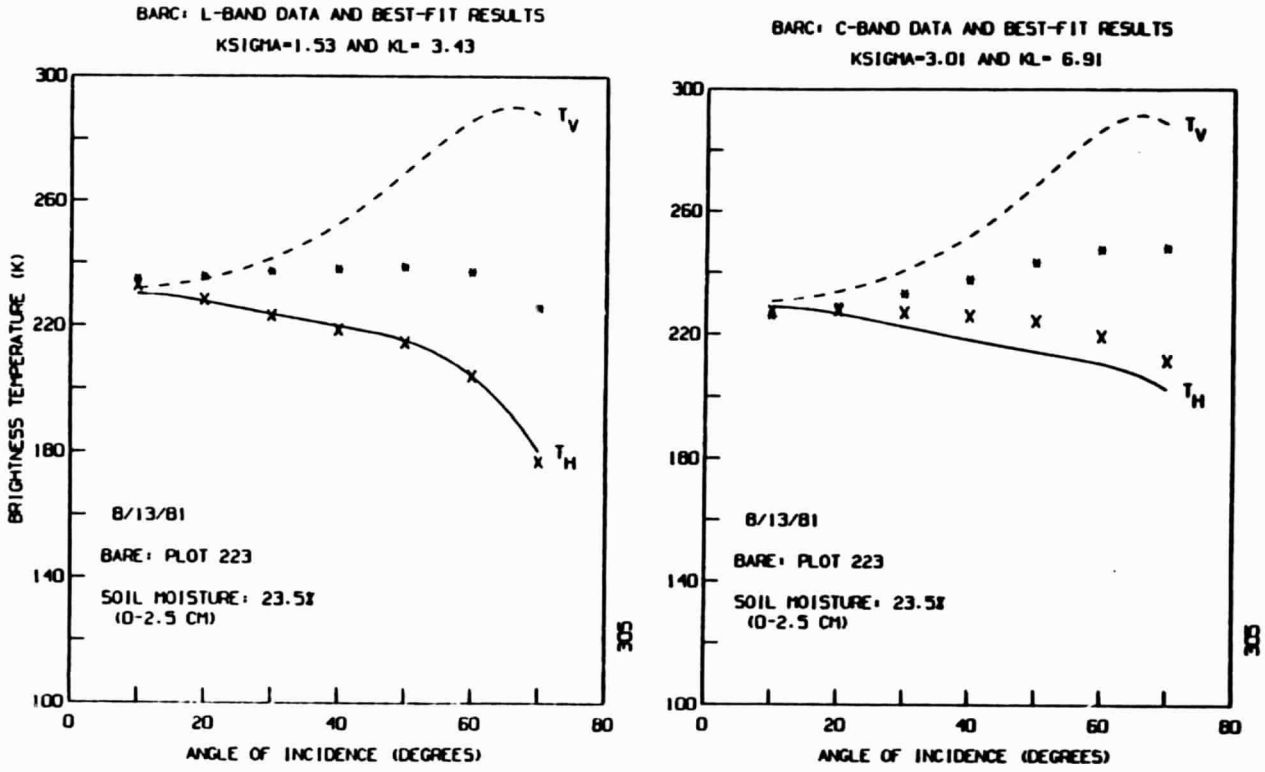
BARC: L-BAND DATA AND BEST-FIT RESULTS
KSIGMA=1.53 AND KL= 3.43
BRIGHTNESS TEMPERATURE (K)
300
260
220
180
140
100
0
20
40
60
80
ANGLE OF INCIDENCE (DEGREES)
T_V
T_H
8/13/81
BARE: PLOT 223
SOIL MOISTURE: 23.5%
(0-2.5 CM)
305
BARC: C-BAND DATA AND BEST-FIT RESULTS
KSIGMA=3.01 AND KL= 6.91
300
260
220
180
140
100
0
20
40
60
80
ANGLE OF INCIDENCE (DEGREES)
T_V
T_H
8/13/81
BARE: PLOT 223
SOIL MOISTURE: 23.5%
(0-2.5 CM)
305

Figure B-38

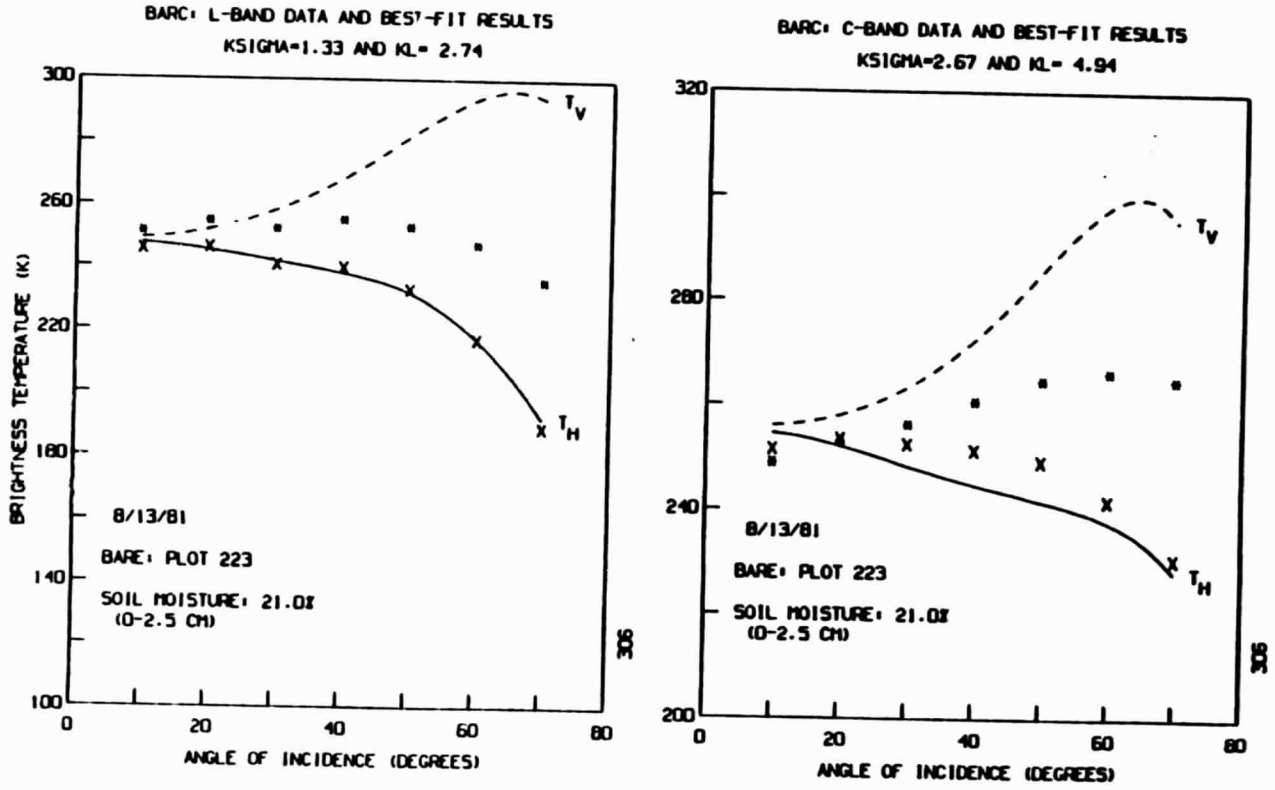
BARC: L-BAND DATA AND BEST-FIT RESULTS
KSIGMA=1.33 AND KL= 2.74
BRIGHTNESS TEMPERATURE (K)
300
260
220
180
140
100
0
20
40
60
80
ANGLE OF INCIDENCE (DEGREES)
T_V
T_H
8/13/81
BARE: PLOT 223
SOIL MOISTURE: 21.0%
(0-2.5 CM)
305
BARC: C-BAND DATA AND BEST-FIT RESULTS
KSIGMA=2.67 AND KL= 4.94
320
280
240
200
0
20
40
60
80
ANGLE OF INCIDENCE (DEGREES)
T_V
T_H
8/13/81
BARE: PLOT 223
SOIL MOISTURE: 21.0%
(0-2.5 CM)
305

Figure B-39

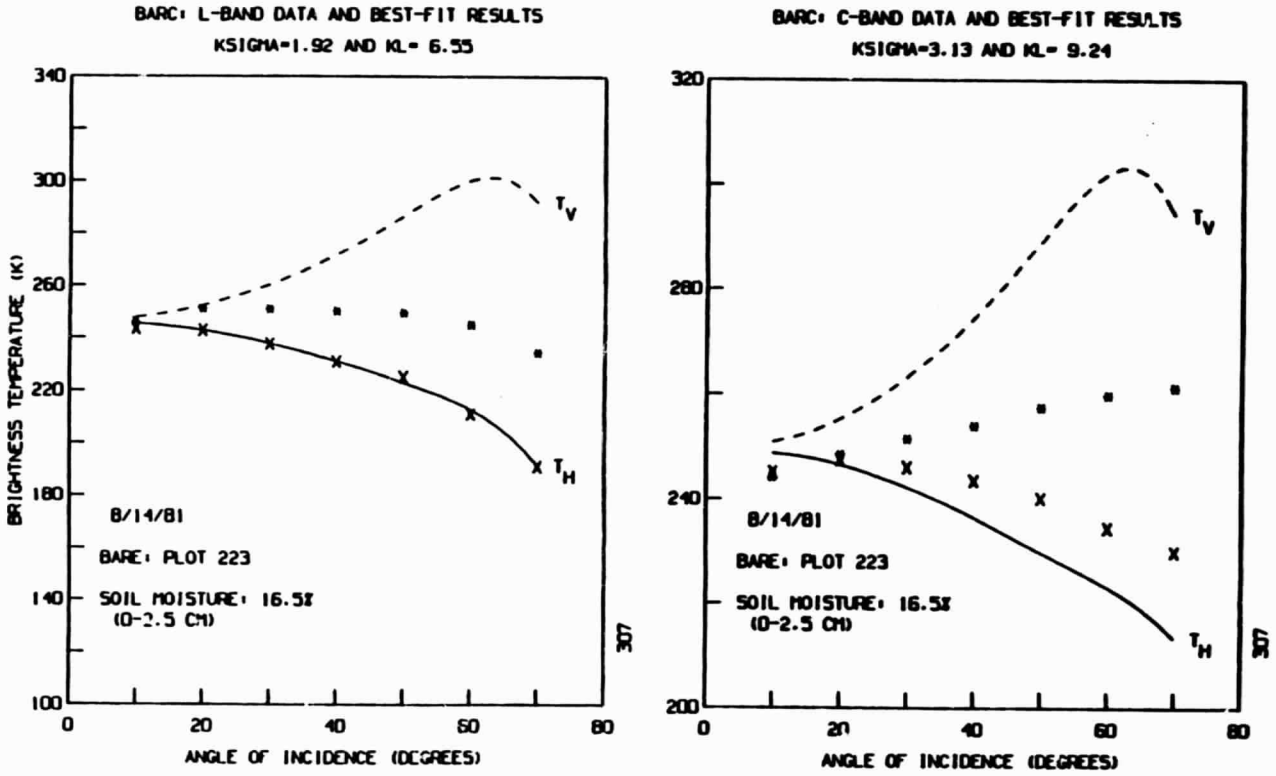
BARC: L-BAND DATA AND BEST-FIT RESULTS
KSIGMA=1.92 AND KL= 6.55
BRIGHTNESS TEMPERATURE (K)
340
300
260
220
180
140
100
0
20
40
60
80
ANGLE OF INCIDENCE (DEGREES)
T_V
T_H
8/14/81
BARE: PLOT 223
SOIL MOISTURE: 16.5%
(0-2.5 CM)
307
BARC: C-BAND DATA AND BEST-FIT RESULTS
KSIGMA=3.13 AND KL= 9.24
320
280
240
200
0
20
40
60
80
ANGLE OF INCIDENCE (DEGREES)
T_V
T_H
8/14/81
BARE: PLOT 223
SOIL MOISTURE: 16.5%
(0-2.5 CM)
307

Figure B-40

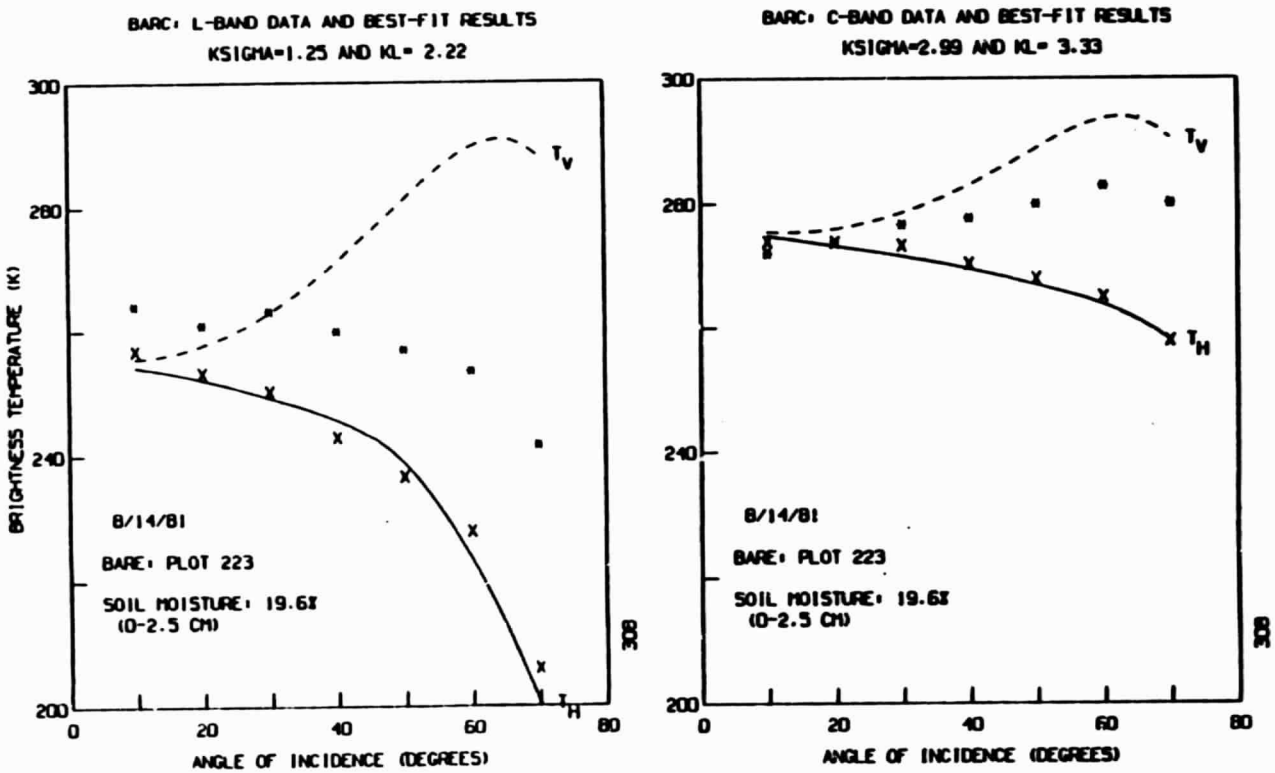
BARC: L-BAND DATA AND BEST-FIT RESULTS
KSIGMA=1.25 AND KL= 2.22
BRIGHTNESS TEMPERATURE (K)
300
280
240
200
0
20
40
60
80
ANGLE OF INCIDENCE (DEGREES)
T_V
T_H
8/14/81
BARE: PLOT 223
SOIL MOISTURE: 19.6%
(0-2.5 CM)
308
BARC: C-BAND DATA AND BEST-FIT RESULTS
KSIGMA=2.99 AND KL= 3.33
300
280
240
200
0
20
40
60
80
ANGLE OF INCIDENCE (DEGREES)
T_V
T_H
8/14/81
BARE: PLOT 223
SOIL MOISTURE: 19.6%
(0-2.5 CM)
308

Figure B-41

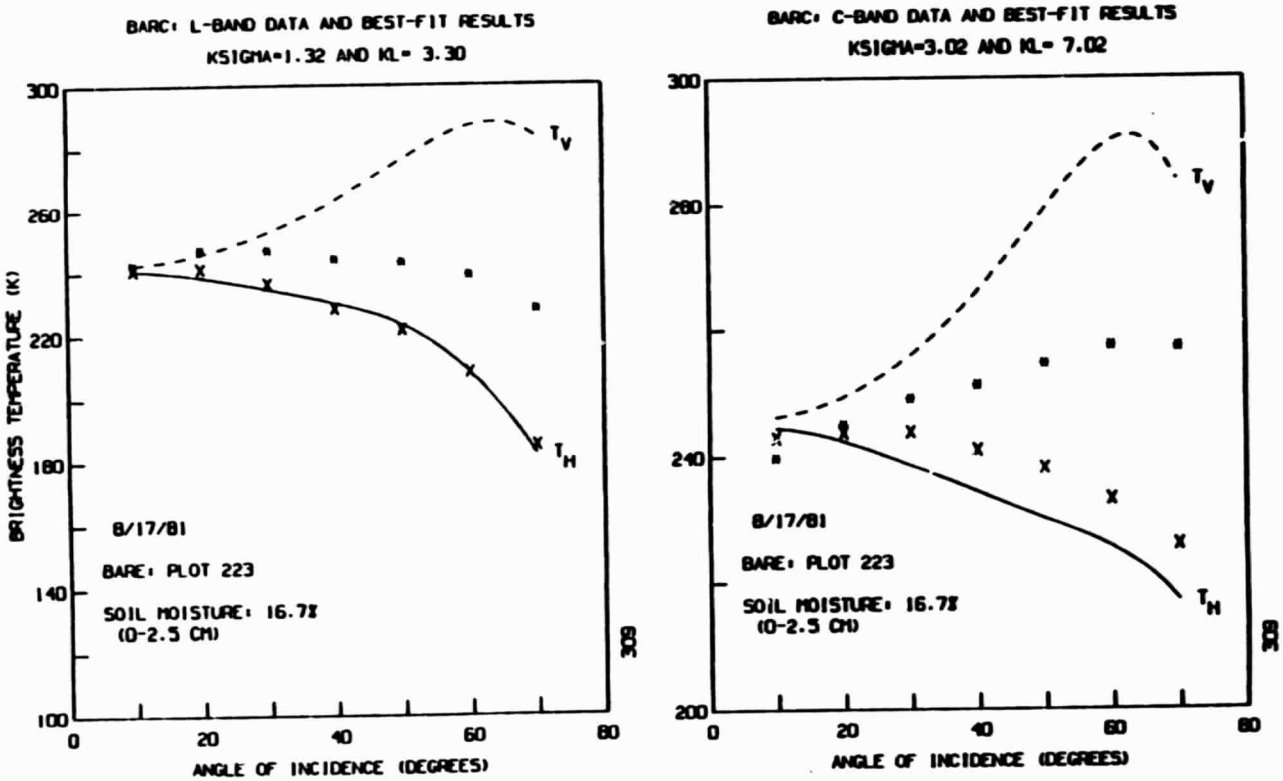
BARC: L-BAND DATA AND BEST-FIT RESULTS
KSIGMA=1.32 AND KL= 3.30
BRIGHTNESS TEMPERATURE (K)
300
260
220
180
140
100
0
20
40
60
80
ANGLE OF INCIDENCE (DEGREES)
T_V
T_H
8/17/81
BARE: PLOT 223
SOIL MOISTURE: 16.7%
(0-2.5 CM)
BARC: C-BAND DATA AND BEST-FIT RESULTS
KSIGMA=3.02 AND KL= 7.02
300
280
240
200
0
20
40
60
80
ANGLE OF INCIDENCE (DEGREES)
T_V
T_H
8/17/81
BARE: PLOT 223
SOIL MOISTURE: 16.7%
(0-2.5 CM)

Figure B-42

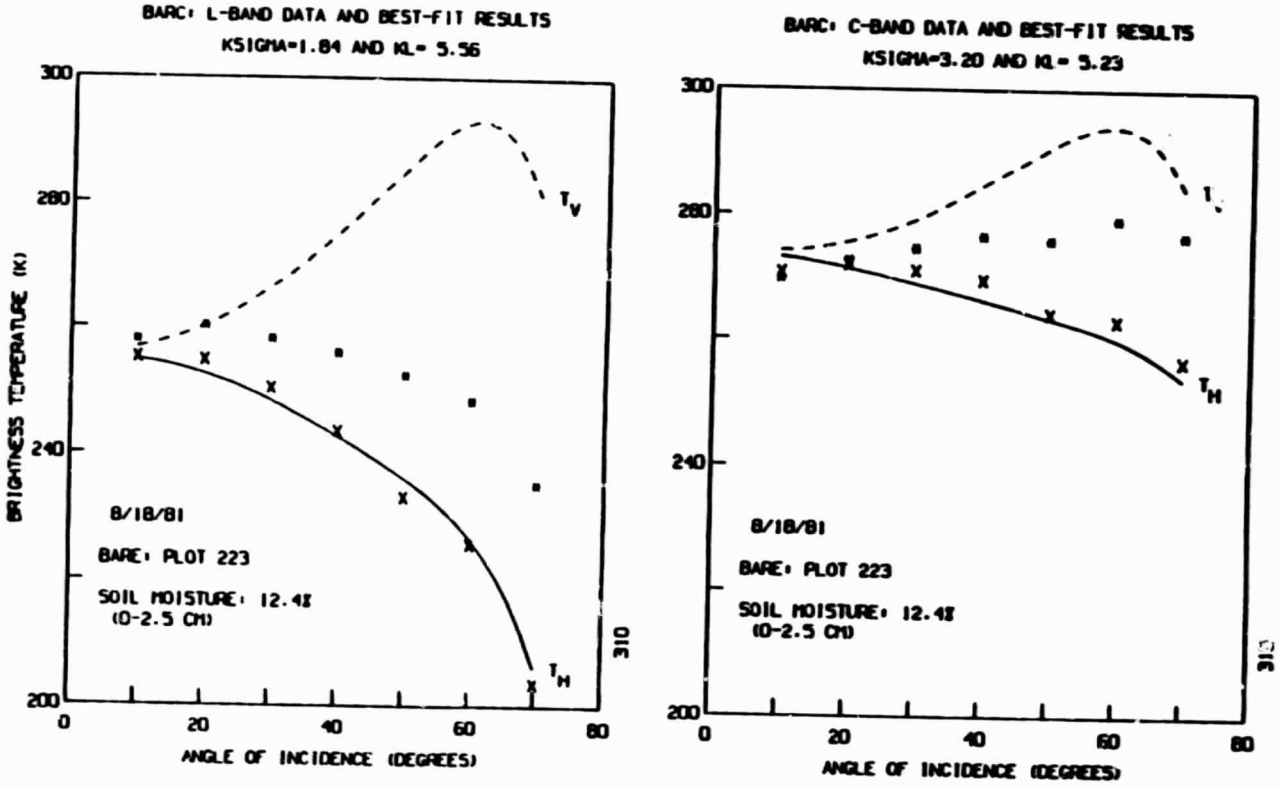
BARC: L-BAND DATA AND BEST-FIT RESULTS
KSIGMA=1.84 AND KL= 5.56
BRIGHTNESS TEMPERATURE (K)
300
280
240
200
0
20
40
60
80
310
T_V
T_H
8/18/81
BARE: PLOT 223
SOIL MOISTURE: 12.4%
(0-2.5 CM)
ANGLE OF INCIDENCE (DEGREES)
BARC: C-BAND DATA AND BEST-FIT RESULTS
KSIGMA=3.20 AND KL= 5.23
300
280
240
200
0
20
40
60
80
T_V
T_H
8/18/81
BARE: PLOT 223
SOIL MOISTURE: 12.4%
(0-2.5 CM)
ANGLE OF INCIDENCE (DEGREES)

Figure B-43

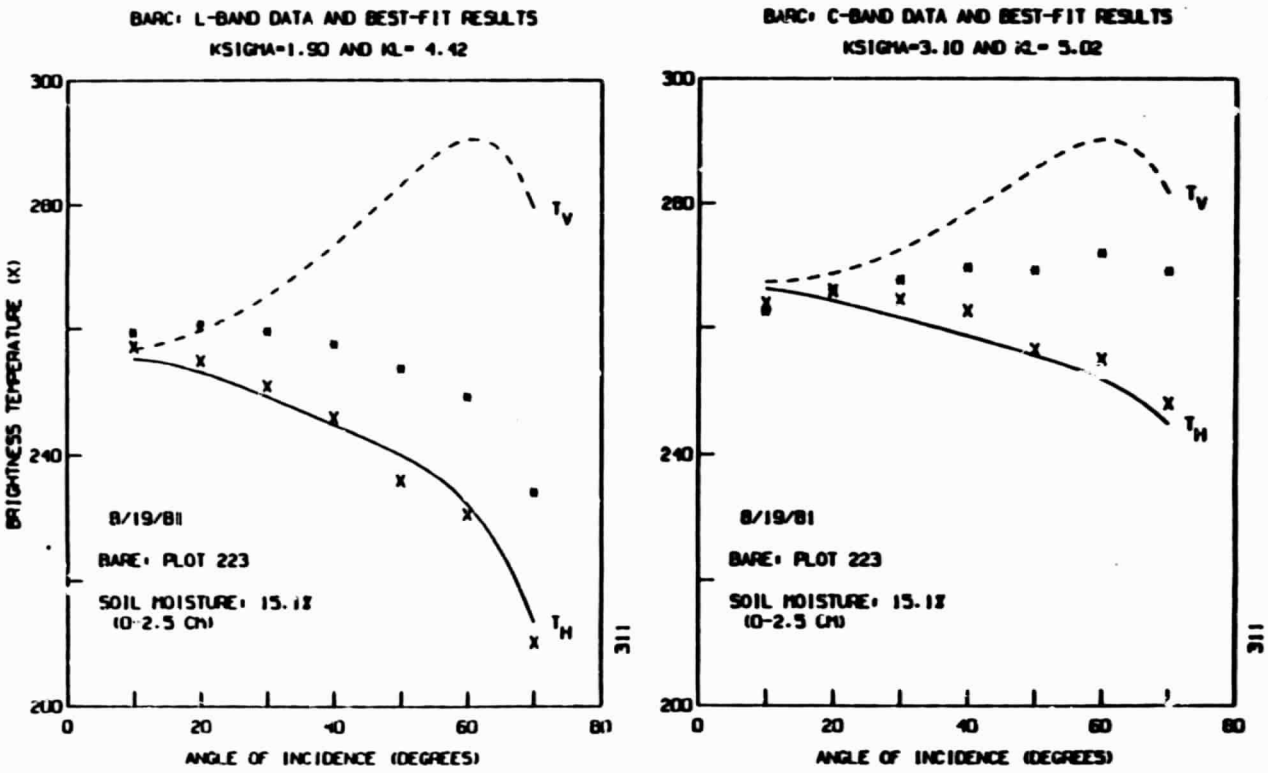
BARC: L-BAND DATA AND BEST-FIT RESULTS
KSIGMA=1.90 AND KL= 4.42
BARC: C-BAND DATA AND BEST-FIT RESULTS
KSIGMA=3.10 AND KL= 5.02
BRIGHTNESS TEMPERATURE (K)
300
280
240
200
0
20
40
60
80
ANGLE OF INCIDENCE (DEGREES)
T_V
T_H
8/19/81
BARE: PLOT 223
SOIL MOISTURE: 15.1%
(0-2.5 CM)
311

Figure B-44

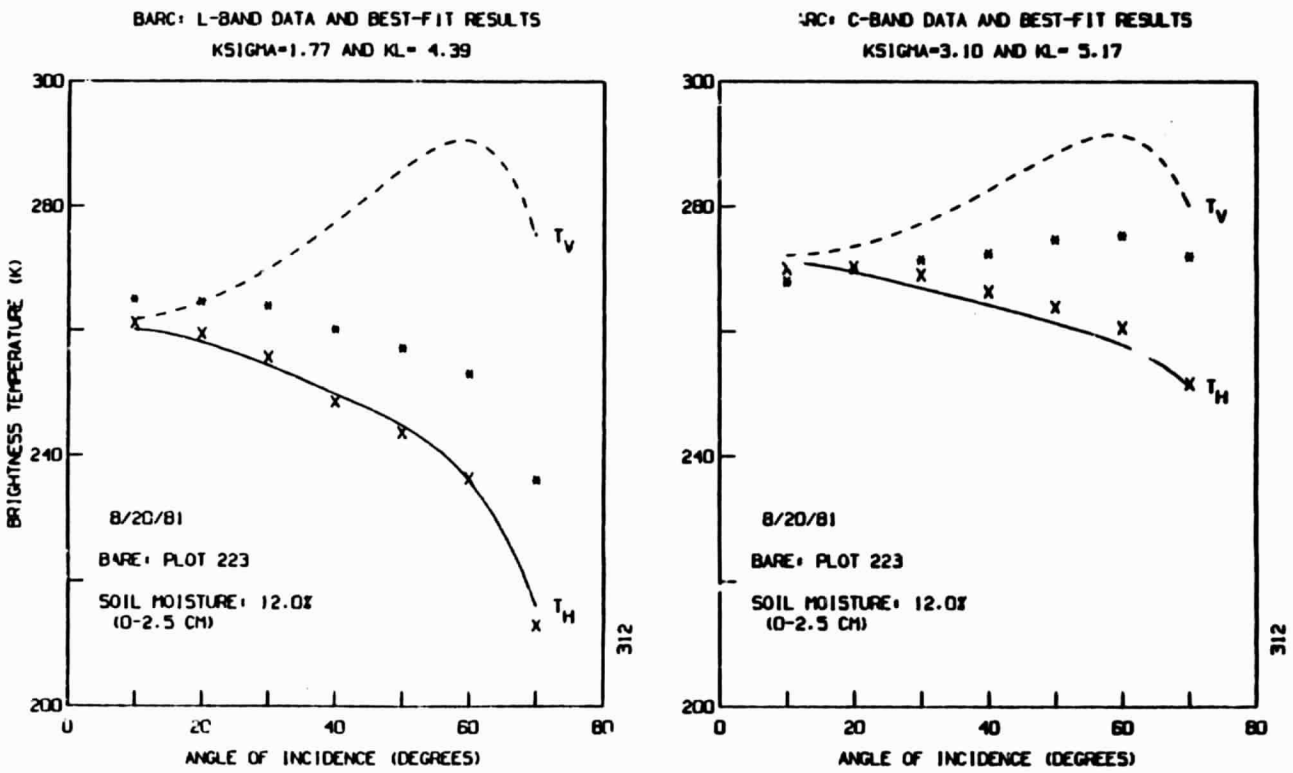
BARC: L-BAND DATA AND BEST-FIT RESULTS
KSIGMA=1.77 AND KL= 4.39
BRIGHTNESS TEMPERATURE (K)
300
280
240
200
0
20
40
60
80
ANGLE OF INCIDENCE (DEGREES)
T_V
T_H
8/20/81
BARE: PLOT 223
SOIL MOISTURE: 12.0%
(0-2.5 CM)
312
BARC: C-BAND DATA AND BEST-FIT RESULTS
KSIGMA=3.10 AND KL= 5.17
300
280
240
200
0
20
40
60
80
ANGLE OF INCIDENCE (DEGREES)
T_V
T_H
8/20/81
BARE: PLOT 223
SOIL MOISTURE: 12.0%
(0-2.5 CM)
312

Figure B-45

REFERENCES

1. Stogryn, A., "Electromagnetic Scattering from Rough Finitely Conducting Surfaces," Radio Sci., vol. 2, pp. 415-428, 1967

2. Fung, A. K. and H. J. Eom, "An Approximate Model for Backscattering and Emission from Land and Sea" paper presented at the International Geoscience and Remote Sensing Symposium, IEEE Geosci and Remote Sensing Soc., Washington, D. C., June 1981 (also TR SM-K1-0409, Remote Sensing Lab., University of Kansas)

3. Fung, A. K. and H. J. Eom, "Note on the Kirchhoff Rough Surface Solution in Backscattering," Radio Sci., vol. 16, pp. 229-302, 1981

4. Semyonov, B., "Approximate Computation of Scattering of Electromagnetic Waves by Rough Surface Contours," Radio Engineering and Electronic Phys., vol. 11, pp. 1179-1187, 1966

5. Ulaby, F. T., R. K. Moore, and A. K. Fung, Microwave Remote Sensing: Active and Passive, vol. 2, Addison-Wesley Publishing Company, Reading, Massachusetts, 1982

6. Mo, T., T. J. Schmugge, and T. J. Jackson, "Calculations of Radar Backscattering Coefficient of Vegetation-Covered Soils," Remote Sensing of Environment, 15, pp. 119-133, 1984

7. Mo, T., B. J. Chcudhury, T. J. Schmugge, J. R. Wang, and T. J. Jackson, "A model for Microwave Emission from Vegetation-Covered Fields," J. Geophys. Res., 87, pp. 11229-11237, 1982

8. Mo, T. and T. J. Schmugge, "Monte Carlo Simulation of the Effect of Soil Moisture Variation on the Microwave Emission from Soils," IEEE Trans. Geosci. Remote Sensing, vol. GE-21, pp. 473-479, 1983

9. Mo, T., B. J. Blanchard, and T. J. Schmugge, "Effects of Vegetation Canopy on the Radar Backscattering Coefficient," NASA Technical Memorandum 85070, 1983

10. Tsang, L. and R. W. Newton, "Microwave Emission from Soils with Rough Surfaces," J. Geophys. Res. vol. 11, pp. 9017-9024, 1982

11. Tsan, L., "Thermal Emission of Nonspherical Particles," Radio Sci., vol. 19, pp. 966-974, 1984

12. Tsang, L. and J. A. Kong, "Thermal Microwave Emission from Half-space Random Media," Radio Sci., vol. 11, pp. 599-609, 1976

13. Tsang, L., A. J. Blanchard, R. W. Newton, and J. A. Kong, "A Simple Relation Between Active and Passive Microwave Remote Sensing Measurements of Earth Terrain," IEEE Trans. Geosci. and Remote Sensing, GE-20, pp. 482-485, 1982

14. Chuang, S. L. and J. A. Kong, "Wave Scattering from a Periodic Dielectric Surface for a General Angle of Incidence," Radio Sci., vol. 17, pp. 545-557, 1982

15. Fung, A. K. and H. J. Eom, "Coherent Scattering of a Spherical Wave from an Irregular Surface," IEEE Trans., Antennas and Propagation, vol. AP-31, pp. 68-72, 1983

16. Wilheit, T. T., "Radiative Transfer in a Plane Stratified Dielectric," IEEE Trans. Geoscience Electron., GE-16, pp. 138-143, 1978

17. Wang, J., T Jackson, E. Engman, W. Gould, J. Fuchs, W. Glazer, P. O'Neill, T. Schmugge, and J. McMurtrey, "Microwave Radiometer Experiment of Soil Moisture Sensing at BARC Test Site During Summer 1981," NASA Technical Memorandum 86056, 1984

18. Beckmann, P. and A. Spizzichino, The Scattering of Electromagnetic Waves from Rogh Surfaces, MacMillan, New Yor, 1963

19. Peake, W. H., "Interaction of Electromagnetic Waves with Some Natural Surfaces," IEEE Trans. Antennas Propagate., vol. AP-7, Special suppl., pp. S324-S329, 1959

20. Beckmann, P., "Shadowing of Random Rough Surface," IEEE Trans. Antennas Propagate., vol. AP-13, pp. 384-388, 1965

21. Brocklman, R. A. and T. Hagors, "Note on the Effect of Shadowing on the Backscattering of Waves from a Random Rough Surface," IEEE Trans. Antennas Propagate., vol. AP-14, pp. 621-626, 1966

22. Wagner, R. J., "Shadowing of Randomly Rough Surfaces," J. Acoust. Soc. Am. vol. 41, pp. 138-147, 1967

23. Lynch, P. J. and R. J. Wagner, "Rough-Surface Scattering: Shadowing, Multiple Scatter, and Energy Conservation," J. Math. Phys., vol. 11, pp. 3032-3042, 1970

24. Wang, J. R., P. E. O'Neill, T. J. Jackson, and E. T. Engman, "Multifrequency Measurements of the Effects of Soil Moisture, Soil Texture, and Surface Roughness," IEEE Trans. Geosci. Remote Sensing, GE-21, pp. 44-51, 1983

25. Wang, J. R. and T. J. Schmugge, "An empirical model for the complex dielectric permittivity of soils as a function of water content," IEEE Trans. Geosci. Remote Sensing, vol. GE-18, pp. 288-295, 1980